Trail of nucleotides and the traits of ADP/ATP-binding inside the subunits A and B of the archaeal energy producer A1AO ATP synthase

Kumar, Anil

2009

Kumar, A. (2009). Trail of nucleotides and the traits of ADP/ATP-binding inside the subunits A and B of the archaeal energy producer A1AO ATP synthase. Doctoral thesis, Nanyang Technological University, Singapore.

https://hdl.handle.net/10356/40160

https://doi.org/10.32657/10356/40160

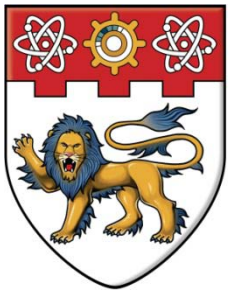

NANYANG TECHNOLOGICAL UNIVERSITY

The trail of nucleotides and the traits of ADP/ATP-binding inside the subunits A and B of the archaeal energy producer A_1A_O ATP synthase

ANIL KUMAR

SCHOOL OF BIOLOGICAL SCIENCES

2009

The trail of nucleotides and the traits of ADP/ATP-binding inside the subunits A and B of the archaeal energy producer A_1A_O ATP synthase

ANIL KUMAR

SCHOOL OF BIOLOGICAL SCIENCES

A thesis submitted to the Nanyang Technological University in partial fulfillment of the requirement for the degree of Doctor of Philosophy

2009

Acknowledgements

This research work is by far one of the most significant scientific accomplishments in my life and it would have been impossible without the following people, who supported me and had belief in me.

First and foremost, I want to express my wholehearted gratitude to my mentor and research advisor Associate Professor Gerhard Grüber, for his expert guidance and motivation throughout my research work. I am grateful to him for his invaluable support and also for introducing me to the wonderful and interesting field of molecular motor proteins. I wish to continue developing some of his great qualities as a disciplined scientist and as an observant and humble person.

I would also like to express my sincere thanks to Mr. Ingmar Schäfer for initiating the project and also for training me in molecular biology techniques during the early days of my PhD. He has been instrumental in training me in learning the protein purification procedures and crystallization techniques. I am indebted to Dr. Asha and Dr. Sony for training me in the field of protein crystallography. I am very thankful for their time and patience in explaining the concepts to me. I am thankful to Dr. Hunke for assistance in experiments and educating me in the basic concepts of FCS technique. I am also thankful to Dr. Biuković and Raj for fruitful discussions and suggestions. I owe very special thanks to my colleagues Shovan, Vikeram, Rishi, Priya, Yew Kwang, Neelu, Hema, Sandip, Phat and Jubi and to all my friends at NTU. I want to thank them for all their help, support, interest and valuable hints.

I gratefully acknowledge the financial support rendered by the Nanyang Technological University of Singapore in the form of Research Scholarship. I am also grateful to the academic and technical staffs at the School of Biological Sciences who have helped me in one way or the other in my research work. I wish to express my sincere appreciation and thanks to the staff at beamline 13B1,13C1 and 12B2 at NSRRC (National Synchrotron Radiation Research Center) Taiwan and beamline BL26B2 at SPring-8 RIKEN, Japan for their help in data collection. I would also wish to acknowledge A*STAR BMRC (06/1/22/19/467) for the research support granted.

Above all, I want to thank my family, which continuously supported me at all times. I thank my parents for teaching me the value of education at a young age and instilled in me a

desire for higher education. I wish to thank my brothers for their love and support. Words cannot express the love, encouragement and unequivocal support I received from my wife Rupali without whose constant help and support, my PhD. research work would have remained a daydream. The loving family environment and support I enjoyed from all my family members was greatly instrumental in providing me the tranquility and enthusiasm to pursue my research with a piece of mind.

To dear mummy, papa and guddu for your unconditional love!

List of figures

Introduction

Materials and methods

Results

Discussion

List of tables

Abbreviations

A-ATP synthase	Archaeal ATP synthase
ADP	Adenosine diphosphate
AMPPNP	Adenosine 5′-(β,γ-imido) triphosphate
ATP	Adenosine triphosphate
Å	Ångstrøm
BSA	Bovine Serum Albumin
CNS	Crystallography and NMR system
DTT	Dithiothreitol
E. coli	*Escherichia coli*
EDTA	Ethylenediaminetetraacetic acid
FCS	Fluorescence Correlation Spectroscopy
FPLC	Fast Protein Liquid Chromatography
IPTG	Iopropyl-β-D-thiogalactoside
ITC	Isothermal Titration Calorimetry
Kb	Kilo base pairs
kDa	Kilo-Dalton
M	Molar
M. mazei Gö1	*Methanosarcina mazei* Gö1
NTA	Nitrilotriacetic acid
NBD-Cl	4-chloro-7-nitrobenzofurazan
PAGE	Polyacrylamide Gel Electrophoresis
PCR	Polymerase Chain Reaction
PDB	Protein Data Bank
Pefabloc^{SC}	(4-(2-Aminoethyl)benzenesulfonylfluoride)
PMSF	Phenylmethylsulfonyl fluoride
P. horikoshii	*Pyrococcus horikoshii*
RMSD	Root Mean Square Deviation
SDS	Sodium Dodecyl Sulfate
TCEP	Tris(2-carboxyethyl) phosphine
Tris	Tris-(hydroxymethyl) aminomethane

Abstract

Archaea are microorganisms which thrive under extreme environmental conditions. These organisms are placed at the bottom of the evolutionary tree of life and retain some of the efficient energy conserving mechanisms. Archaeal A_1A_O ATP synthases (A-ATP synthases) are a separate class of energy converters, synthesizing adenosine triphosphate (ATP) by means of ion gradient-driven phosphorylation. These enzymes possess the unique capability to couple ATP synthesis to the transport of both, H^+ and Na^+ ions. An A-ATP synthase is composed of a total of nine subunits in the stoichiometry of A_3:B_3:C:D:E:F:H_2:*a*:c_x. Adenosine triphosphate is synthesized in the A_3B_3 headpiece of the A_1 domain, and the energy provided for this process is transmitted to the membrane-bound A_O domain. The energy coupling between the A_3B_3 hexamer and the A_O sector occurs via the stalk subunits C, D and F. In the intact A-ATP synthase, the A-B dimer interface in the A_3B_3 hexamer is the nucleotide binding site, wherein subunit A and B are catalytic and non-catalytic/regulatory subunits, respectively. Recently, the structures of subunit A from thermophilic archaea *Pyrococcus horikoshii* OT3 and subunit B from a methanogenic archaea *Methanosarcina mazei* Gö1 have been determined in the absence of nucleotides (Maegawa *et al*. 2006; Schäfer *et al*., 2006). In an attempt to understand the nucleotide binding and catalytic mechanism, crystal structures of subunit A from *P. horikoshii* OT3 are determined and presented in complex with a phosphate analog-, AMPPNP- and ADP to resolutions of 2.47 Å and 2.4 Å, respectively (Kumar *et al*., 2009a). In these structures, the nucleotides are bound near the phosphate binding P-loop region ($_{234}$GPFGSGKT$_{241}$). A comparison of the nucleotide bound structures highlights the conformational changes in S238A, T241 and T243. In order to understand the role of P-loop residues, Ala mutants of F236, S238, G239, K240 and T241 were constructed. The nucleotide binding affinities of wild type subunit A (WT) and its P-loop mutants were determined by Isothermal Titration Calorimetry (ITC), which indicated that Mg-ADP binds more tightly when compared to Mg-ATP. The order of binding affinity is WT > T241A > S238A, wherein G239A and K240A do not bind either nucleotides. The structure of S238A mutant determined at 2.4 Å resolution, highlighted major conformational changes in the P-loop region, which is now in a relatively relaxed state similar to that of the related β-subunit of the F-ATP synthase (Kumar *et al*., 2009a). Structure comparison of the nucleotide bound forms of subunit A with subunit β of bovine mitochondrial F_1-ATPases have shown differential binding for the phosphate group, which could be explained by the distinct P-loop conformations in the two.

Although, nucleotide binding subunit B from A-ATP synthases, does not possess the consensus glycine rich P-loop sequence, the evidence for nucleotide binding capacity came from photoaffinity labeling experiments and fluorescence correlation spectroscopic (FCS) experiments, which showed that subunit B from *M. mazei* Gö1 binds to nucleotide analogues with lower affinity compared to subunit A (Schäfer *et al*., 2006). Here a residue, R416 was mutated to tryptophan in the adenine binding pocket and tryptophan fluorescence quenching experiments have shown that the mutated residue (R416) is in close vicinity to the proposed nucleotide binding site. FCS experiments using smaller sized nucleotide analogues showed preferential binding of ATP in subunit B. A protocol developed for co-crystallization helped in getting two ATP bound structures of R416W mutant of subunit B with ATP bound at different positions (Kumar *et al*., 2009b; Manimekalai *et al*., 2009). The nucleotide bound structures are termed as transient-I and transient-II, respectively. In transient-I structure the ATP molecule is bound near the helix-turn-helix motif of the C-terminal domain of chain A, while ATP is bound near the P-loop region in transient-II. Tryptophan fluorescence quenching experiments using A373W and F149W in transient-I and transient-II structures, provide experimental evidence for the significance of these binding sites. Upon N-terminal superposition of the transient structures I and II with R416W nucleotide free structure, the C-terminal domains of of the transient structures I and II are rotated by 6.0º and 5.8°, indicating that ATP binding has led to a conformational change on the C-terminal domain. The transient structures represent trapped transition positions of the nucleotide while on its way to the actual binding site, enabling to propose a model for the possible entry route of nucleotide into A-ATP synthases.

References:

Kumar, A., Manimekalai, M. S. S., Balakrishna, A. M., Jeyakanthan J. and Grüber, G. (2009a). Nucleotide binding states of subunit A of A-ATP synthase and the implication of P-loop switch in evolution. *J. Mol. Biol.*, **396**, 301-320.

Kumar, A., Manimekalai, M. S. S., Balakrishna, A. M., Hunke, C., Sewald, N. and Grüber, G. (2009b). Spectroscopic and crystallographic studies of the mutant R416W give insight into the nucleotide binding traits of subunit B of the A_1A_O ATP synthase. *PROTEINS: Structure, Function and Bioinformatics* **75**, 807-819.

Maegawa, Y., Morita, H., Iyaguchi, D., Yao, M., Watanabe, N., and Tanaka, I. (2006). Structure of the catalytic nucleotide-binding subunit A of A-type ATP synthase from *Pyrococcus horikoshii* reveals a novel domain related to the peripheral stalk. *Acta Cryst.* D **62**: 483-488.

Schäfer, I., Bailer, S. M., Düser, M. G., Börsch, M., Ricardo, A. B., Stock, D. and Grüber, G. (2006). Crystal structure of the archaeal A_1A_O ATP synthase subunit B from *Methanosarcina mazei* Gö1: Implications of nucleotide-binding differences in the major A_1A_O subunits A and B. *J. Mol. Biol.* **358,** 725-740.

1. Introduction

1.1 Archaea

Archaea are primitive microorganisms and belongs to an altogether different kingdom which is located near to the root of evolutionary tree and have evolved separately during the course of evolution (WOESE et al., 1990; SCHÄFER *et al*., 1999). A comparison of 16S ribosomal RNA sequences indicate that archaea are related to each other but not to eubacteria or the eukaryotes (MÜLLER and GRÜBER, 2003) (Figure 1.1). The members of this class thrive at extreme environmental conditions of high temperatures (above 80 ºC) and tolerate very high salt concentrations and extreme pH ranges (MÜLLER and GRÜBER, 2003; MÜLLER *et al*., 2005). The phylogenic position and the adaptability to withstand extreme environmental conditions indicate that archaea possess some of the most simple and robust energy conserving mechanisms. This is highlighted by the fact that these organisms possess unique metabolic pathways which utilize low energy substrates. However, they employ a vast variety of energy transducing mechanisms including respiration, anaerobic respiration with nitrate, fermentation, anaerobic photorespiration, sodium motive methyl transfer reactions and membrane bound proton reducing hydrogenases (SCHÄFER *et al*., 1999; MÜLLER *et al*., 2005).

Figure 1.1. The tree of life showing relationships among members from three kingdoms of life (WOESE *et al*., 1990; LEWALTER *et al.*, 2006).

Based on biochemical properties and physiology, archaea are classified into three distinct groups; these are, Crenaarchaeota (thermophiles and thermoacidophiles), Euryarchaeota (halophiles and methanogens) and Korarchaeota (uncultivable microbes inhabiting hot springs) (THAUER *et al*., 2008; DEPPENMEIER, 2002).

Methanogens are methane producing archaea, which are strictly anaerobic and grow by conversion of low energy substrates like atmospheric CO_2 and H_2 to methane (CH_4) (THAUER *et al*., 2008; SCHÄFER *et al*., 1999). The overall reaction for methanogenesis can be summarized as follows:

$$CO_2 + H_2 \rightarrow CH_4 + 2\ H_2O$$

It has been reported that like halophiles, methanogens are also discerningly chemiosmotic and they couple the pathway of methanogenesis to the generation of two primary ion gradients: sodium (Na^+) and hydrogen (H^+) ions, across the plasma membrane (DEPPENMEIER *et al*., 2002). These electrochemical ion gradients have both electrical and chemical components, contributed by Na^+ and H^+ and therefore, can be represented by following equation:

$$\Delta\mu_{ion+} = F\,\Delta\Psi - 2.2303\,RT\log([ion^+_{inside}]/\,[ion^+_{Outside}])$$

Where $\Delta\mu_{ion+}$ is the electrochemical potential, F is the Faraday constant (96500 J V^{-1} mol^{-1}), $\Delta\Psi$ is the membrane potential, R is the gas constant (8.303 J mol^{-1} K^{-1}) and T is the temperature in Kelvin. The electrochemical potential of hydrogen or sodium ions is build up across membrane either by redox systems along the electron transport system located along the membranes (ETS), or by methyl transfer reactions (SCHÄFER *et al.,* 1999). The potential energy thus stored in the transmembrane electro-chemical gradient across the membrane can be utilized to drive the synthesis of adenosine triphosphate (ATP) from adenosine diphosphate (ADP) and inorganic phosphate (Pi) by a membrane bound ATP synthase (Figure 1.2). The ATP synthesis is tightly coupled with the influx of ions along their poteintial difference across the membrane. The number of protons required and the magnitude of electro-chemical gradient $\Delta\mu_{ion+}$, correlate with the phosphorylation potential (THAUER *et al*., 2008). Interestingly, methanogenic archaea thrives in habitats where the partial pressure of H_2 is so low that the free energy change (ΔG) for the reduction of CO_2 and H_2 to CH_4 is well below the required energy (40 kJ/mol) needed to drive the synthesis of one mol of ATP under standard conditions. It explains the low growth yields observed in methanogens and hence give an indication about the adaptability and highly efficient energy conservation mechanisms adopted by these organisms (THAUER *et al*., 2008). Because these organisms are rooted close to the origin of the tree of life, these unusual mechanisms are considered to have developed very early in the history of life and, therefore, may represent first energy-conserving mechanisms. Unlike bacteria and eukaryotic cells, there is lack of detailed information about the metabolic pathways and energy transduction methods present in methanogens. Hence it was not clear until recently, how exactly the energy currency adenosine tri-phosphate is being synthesized in this class of organisms (THAUER *et al*., 2008; MÜLLER *et al*., 2005; SCHÄFER *et al*., 1999).

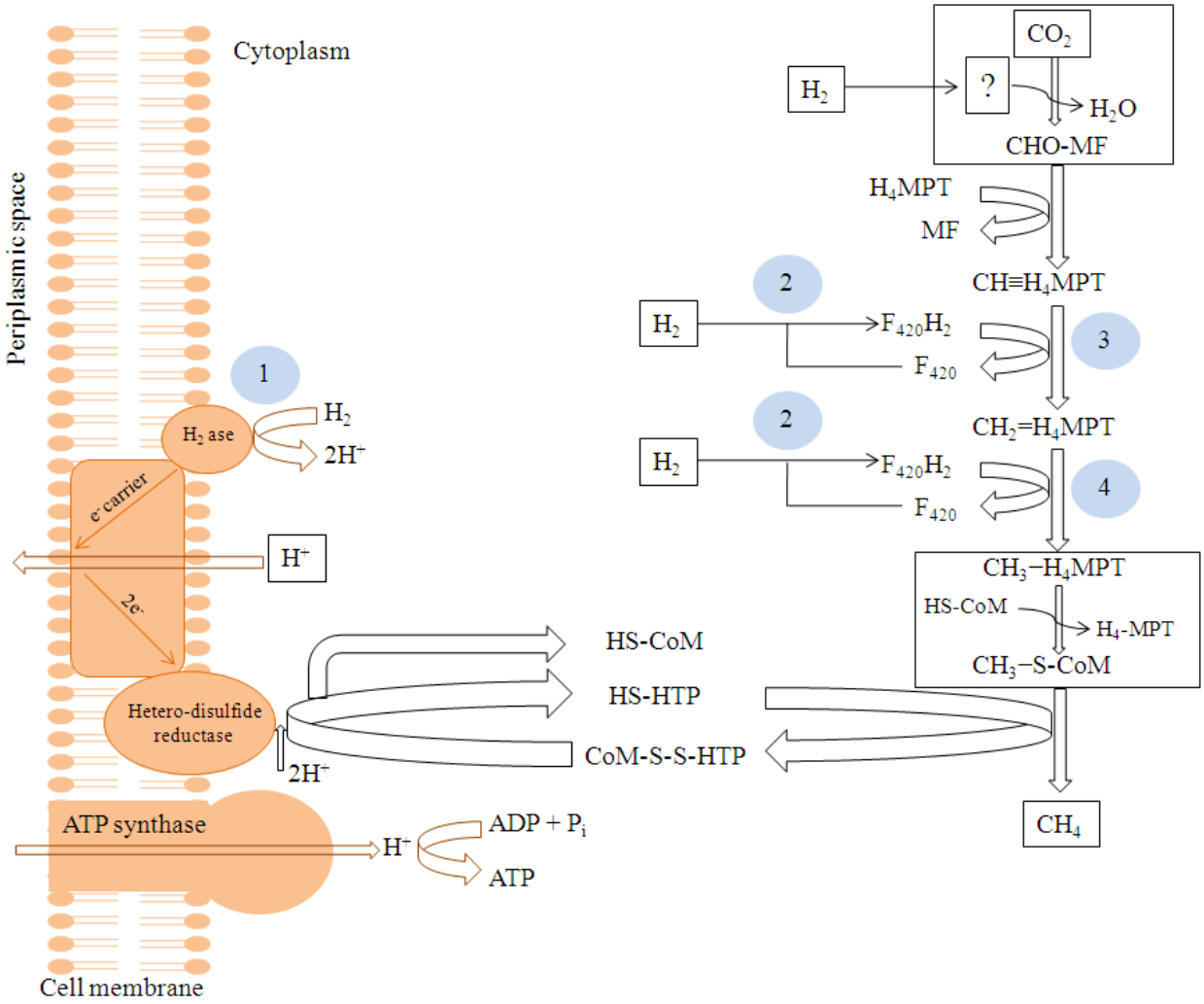

Figure 1.2. A schematic overview of methanogenesis process in archaea. A H_2-dependent disulfide reductase system participates in energy transduction from CO_2 and H_2. The figure is modified according to FERRY *et al.*, (1993).

1.2 ATP synthase

ATP synthases are membrane bound enzyme found in archaea, eubacteria, lower eukaryotes (yeast) and higher eukaryotes (plants, and animals). In most of the organisms the primary function of the enzyme is to synthesize the energy currency ATP from adenosine di-phosphate (ADP) and inorganic phosphate (P_i). Apart from synthesizing ATP, these enzymes may act as primary ion pumps, utilized to establish transmembrane ion motive force at the expense of ATP hydrolysis. It is believed that these enzymes accounts for 95 % of the total ATP synthesized in living organisms. The energy required for the synthesis process is derived from the ion electrochemical potential difference generated across plasma membrane by respiration or photosynthesis processes (MITCHELL *et al.*, 1961). The ATP synthase family can be divided into two major subfamilies: the F-ATP synthases and the archaeal A-ATP synthases. The members of the two subfamilies are evolutionarily related and based on sequence, structural and

functional attributes, it is believed that the two subfamilies have originated from a common ancestor during the course of evolution (NELSON, 1992; HILARIO and GOGARTEN, 1998; CROSS and MÜLLER, 2004). A unique feature of the F- and A-ATP synthases is that they are rotary molecular motor enzymes. The processes of ATP synthesis at the water soluble catalytic headpiece and ion translocation at across the hydrophobic pore channel complex are coupled via a rotational motion of a central stalk domain.

Archaeal A_1A_O	**Bacterial F_1F_O**
A	**β**
B	**α**
C	**–**
D	**γ**
E	**–**
F	**ε**
–	**δ**
H	**b**
a	**a**
c	**c**

Table 1.1. Subunit composition of the bacterial F_1F_O ATP Synthase and the archaeal A_1A_O ATP synthase (MÜLLER and GRÜBER, 2003).

1.3 F-ATP synthases

F_1F_O ATP synthases are the most extensively studied enzymes among the family of ATP synthases and most of the current knowledge about ATP synthases is garnered through the structural and functional studies on this class of the enzyme. The F-ATP synthases are found in the plasma membrane of bacteria, thylakoid membrane of chloroplasts in plants and inner membranes of mitochondria in animals and plants (CAPALDI *et al.*, 2002). These enzymes are large macromolecular complex of molecular weight of the order of 550-600 kDa and are composed of eight subunits in prokaryotes (eubacteria) and about 14-18 subunits in eukaryotic cells (CAPALDI *et al.*, 2002). The overall architecture of the F-ATP synthases is composed of a water soluble F_1 domain and a membrane bound F_O domain wherein, the F_1 part consists of five subunits in the stoichiometry of α_3:β_3:γ:δ:ε. The F_O sector in its simplest form is made up of subunits *a*, *b*, *c* in the stoichiometry 1:2:9-15 and is responsible for pumping the protons across the membrane (STOCK *et al.*, 2000). The F_1 and F_O part are connected by a central stalk which consists of subunits γδε, wherein the γ subunit protrudes inside the $\alpha_3\beta_3$ hexamer. The first crystal structure was obtained for the $\alpha_3\beta_3\gamma$ sector of the catalytic F_1 domain of the F-ATP

synthase enzyme at 2.8 Å resolution from bovine heart mitochondria (ABRAHAMS *et al*., 1994). In the structure, most of the subunit γ structure was disordered and could not be assigned. The structure of $\alpha_3\beta_3$ and half γ subunit from *E. coli was* solved at 4.4 Å resolution (HAUSRATH and GRUBER, 1999). It showed the additional alpha-helical regions within the gamma subunit and suggested that the gamma subunit traverses the full length of the stalk and links the F_1 and F_O parts and also makes significant contacts with the *c* subunit ring of F_O domain. The findings paved a way to conduct the classic rotation experiment done by Yoshida and Kinosita, which proved the 360 º rotational movement of the γ subunit with respect to α and β (NOJI *et al*., 1997). The yeast F_1 domain structure has recently been determined at 2.8 Å resolution and have complete structure for the entire F_1 domain (KABALEESWARAN *et al*., 2006). The structure of bovine mitochondrial complex determined at 2.4 Å and 2.0 Å are the most complete structures for the F_1 catalytic domain and the central stalk subunits (γδε) (GIBBONS *et al*., 2000; MENZ *et al*., 2001) (Figure 1.3A and B). The cenral stalk (γδε) constitutes the rotary element during the enzymes catalytic mechanism. The α_3:β_3 head piece of the F_1 domain is the catalytic center and is made up of catalytic subunit β and non-catalytic subunit α, arranged in an alternating fasion to constitute a pseudohexameric α_3:β_3 sector. The nucleotide binding sites are located at the interface of the subunits β and α (Figure 1.4A and B). ATP synthesis / hydrolysis events occur at the $\alpha_3\beta_3$ sector and the energy provided for or released is transferred to the F_O domain via central stalk subunits. Several experimental evidences have now shown that the F-ATP synthase is indeed a rotary motor enzyme (DIEZ *et al*., 2004; DUNCAN *et al*., 1995; NISHIO *et al*., 2002; NOJI *et al*., 1997; SABBERT *et al*., 1996; ZHOU *et al*., 1997), wherein the proton translocation along the interface of subunits *c* and *a* of the F_O domain drives rotation of the ring of *c* subunits along with central stalk subunits γ and ε, against the catalytic α_3:β_3 domain. The proton gradient induced rotation of the γδε subunits inside the α_3:β_3 hexamer facilitates the binding of the substrates (Mg-ADP and inorganic phosphate) at the catalytic sites and subsequent release of the product (ATP). During the rotational events, the peripheral stalk, made up of the δ and *b* subunits maintain the F_1 and F_O domains in the correct spatial arrangement for energy coupling to occur. The ‘‘binding change’’ model of cooperative catalysis proposed by Paul D. Boyer in 1993 states, that the synthesis or hydrolysis of ATP occurs on the three catalytic sites in a sequential manner. All the three catalytic binding sites undergo a series of conformational changes in steps of 120˚.

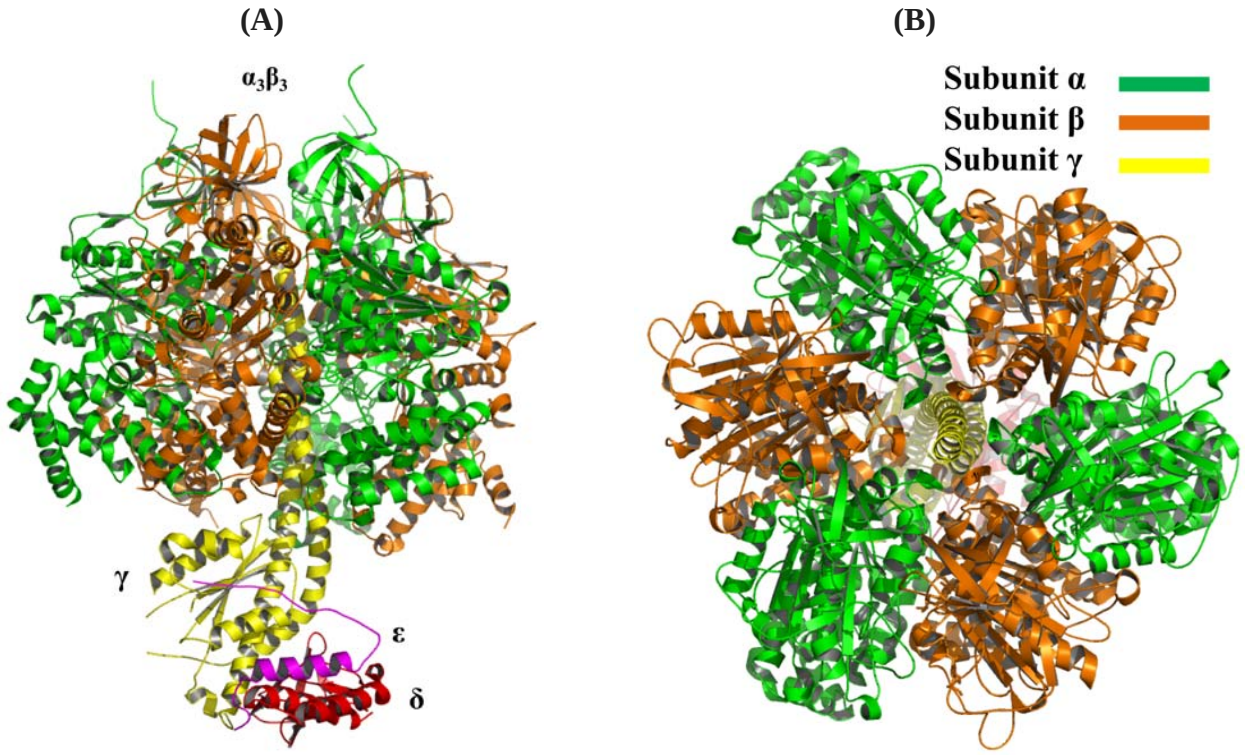

Figure 1.3. Crystal structure of the bovine heart mitochondrial F_1 ATPase showing the subunits α, β, γ, ε and δ (PDB: 1E79) (GIBBONS *et al.*, 2000). (A) Side view showing the pseudohexagonal arrangement of subunits α and β arranged in alternating fashion; top view (B). Nucleotide binding sites are located at the α-β dimer interface region.

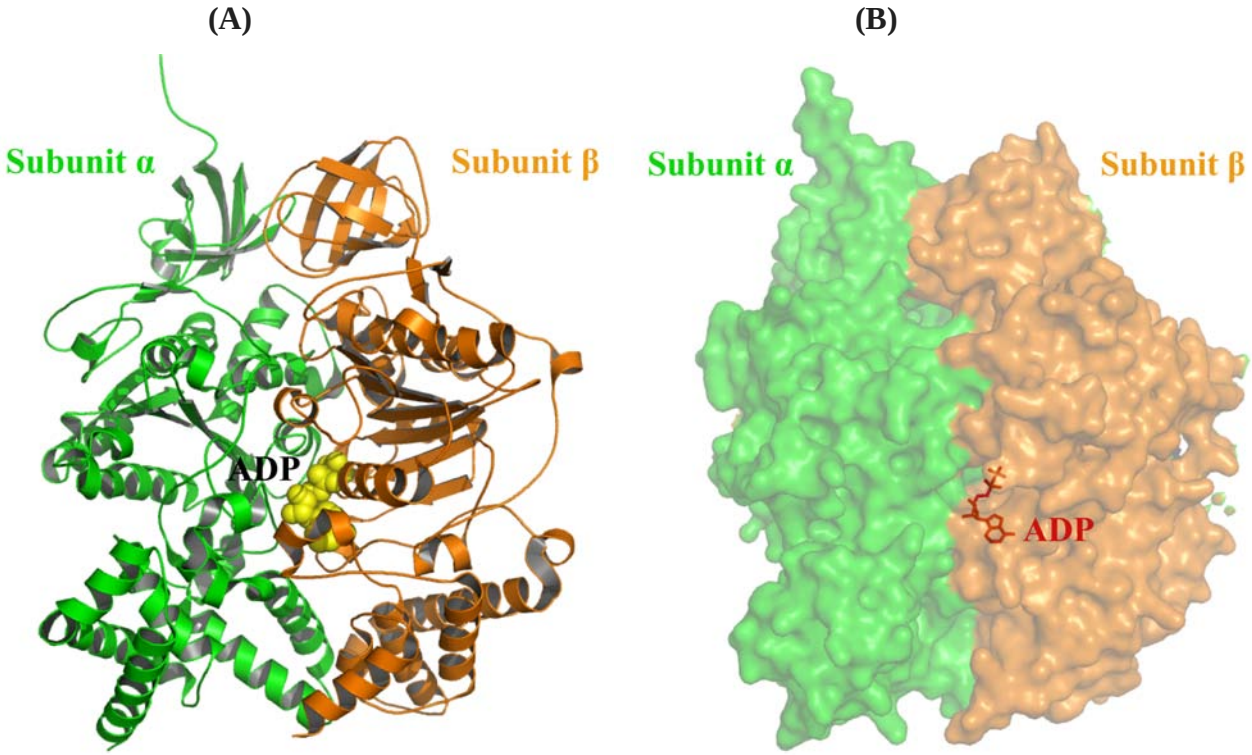

Figure 1.4. Crystal structures of the bovine heart mitochondrial F_1 ATPase showing the α-β dimer interface (PDB: 1E79) (GIBBONS *et al.*, 2000). (A) A cartoon representation of the interface region, showing bound ADP molecule as spheres (yellow). (B) Surface diagram highlighting the ADP position in the dimer interface.

According to the model, the nucleotide binding sites can be either in a tight (T), loose (L), or open (O) state, and inter-conversion of these states is coupled to the translocation of protons (or ions) through the proton conducting membrane embedded F_O domain of the enzyme (ABRAHAMS, *et al*., 1994). Recently available structures have revealed that the maximum turnover of ATP hydrolysis in F_1 ATPase occurs only with all three catalytic sites filled with nucleotide (WEBER and SENIOR, 1997; MENZ *et al*., 2001). This finding is in contrast to previous proposals and models, where one of the catalytic β subunit was required to be in an open conformation during the course of catalysis (ABRAHAMS, *et al*., 1994).

1.4 Nucleotide binding in catalytic $\alpha_3\beta_3$ domain and subsequent conformational changes

The major nucleotide binding subunits α and β display significant similarity at the level of the primary structures, and the available crystal structures showed that this is also true for the tertiary structures of these subunits. The overall structure of each α and β subunit is made up of three domains: an N-terminal β barrel, an intermediate domain containing α helices, and β sheet and an α-helical C-terminal domain. The nucleotide binding sites, are located at the interfaces of the α and β subunits (Figure 1.5). Therefore, a total of six nucleotide binding sites are formed by amino acid residues from both the α and β subunits. Although, the catalytic nucleotide binding sites are mostly located on the β subunits, some contribution comes from the α subunits. The non-catalytic ones are mostly formed from α subunit residues with some contribution from the adjacent β subunits. ATP synthesis or hydrolysis is catalyzed in the nucleotide binding sites that are located mostly on the β subunits, at the interface to the α subunits (ABRAHAMS *et al*., 1994), wherein function of the non-catalytic nucleotide binding sites is not clearly understood yet. Each nucleotide binding site has an adenine binding pocket and a glycine rich phosphate binding loop with the well known P-loop or Walker A motif GXXXXGKT/S and also a GER sequence (WALKER *et al*., 1982). The residues from the P-loop provide stabilizing interactions to the phosphate moiety of nucleotide molecule while the glutamate residue of the GER sequence is believed to stabilize the penta-coordinated transition intermediate of the γ phosphate during catalytic events. The glutamate residue is believed to ligand through its carboxyl oxygens to a specific water molecule positioned appropriately to make nucleophilic attack at the γ-phosphate of the ATP molecule (ABRAHAMS *et al*., 1994). The mutagenesis of the conserved glutamate has very large impairing effects on catalysis (SENIOR and AL-SHAWI, 1992; PARK *et al*., 1994), reducing hydrolysis rates by three or more orders of magnitude most likely by abolishment of the transition-state stabilization (NADANACIVA *et al*., 1999); however, no significant effects occur on Mg-ATP or Mg-ADP binding (LÖBAU *et al*., 1997). In the reported

crystal structures of the mitochondrial F_1 domain, all three non-catalytic nucleotide binding sites are occupied by magnesium-nucleotide (non-hydrolyzable ATP analogue, AMPPNP, or ADP) and the structure of these non-catalytic α/β interfaces shows slight variation among the three sites. On the other hand, it showed that the three catalytic nucleotide binding sites can exist in different states. In the first high resolution structure of the F_1 domain, out of three β catalytic sites, two were occupied by Mg-ADP.AlF_4 and remaining one was occupied by Mg-ADPSO_4 (MENZ *et al*., 2001). All the binding sites on α subunits were occupied by ADP.SO_4. The respective structural superposition of the β subunits of the F_1 structure with nucleotide bound on all the catalytic sites with the native F_1 structure, defined the three different states (MENZ *et al*., 2001; ABRAHAMS *et al*., 1994). These are 'closed state' with strong affinity for nucleotides, 'half-closed state' with intermediate affinity and 'open state' with low affinity for nucleotides. Superposition of the β_{DP} (ADP) and β_{TP} (AMPPNP) subunits from native F_1 structure with ADP.AlF_4 bound β subunits showed that they adopt similar closed conformation and had very little structural differences. On the other hand nucleotide free empty β subunit from native structure represents the low affinity 'open' state. Upon N-terminal superposition it was found quite different, the nucleotide binding pocket had huge structural changes and the entire C-terminal domain was rotated and shifted downward by about 33 º. In the ADP.AlF_4 structure, the β_E subunit binds ADP and SO_4 and adopts 'half-closed' conformation (β_{ADP+Pi}) that is intermediate between 'closed' and 'open' states. Upon N-terminal superposition, the C-terminal of the β_{ADP+Pi} is related to the 'open' conformation by 16 º and to the closed conformation by a rotation of 23 º (MENZ *et al*., 2001). Again, the structure of the α subunits had very little variation among the three copies present in the complex. Despite the presence of three copies of each of the α and β subunits, the F_1 displays a significant degree of asymmetry which is probably due to the differential interaction of the three α/β pairs with the single copy γ subunit and the different occupancy of the nucleotide binding sites. This structural asymmetry is not only an interesting consequence of the sequential catalysis, but it probably also provides a mechanism for interaction with only one copy of the peripheral stalk forming δ subunit. This asymmetry in the catalytic β subunits, however, is only seen in structures in which Mg-nucleotides were included in the crystallization setups. In the absence of either nucleotides or magnesium, perfect three-fold symmetry is observed as has been noted for the structure of the nucleotide-free $\alpha_3\beta_3$ catalytic sector of the thermophilic bacterium PS3 (SHIRAKIHARA *et al*., 1997) and the F_1-ATPase from rat liver mitochondria (BIANCHET *et al*., 1998), which was crystallized with ATP, but no magnesium.

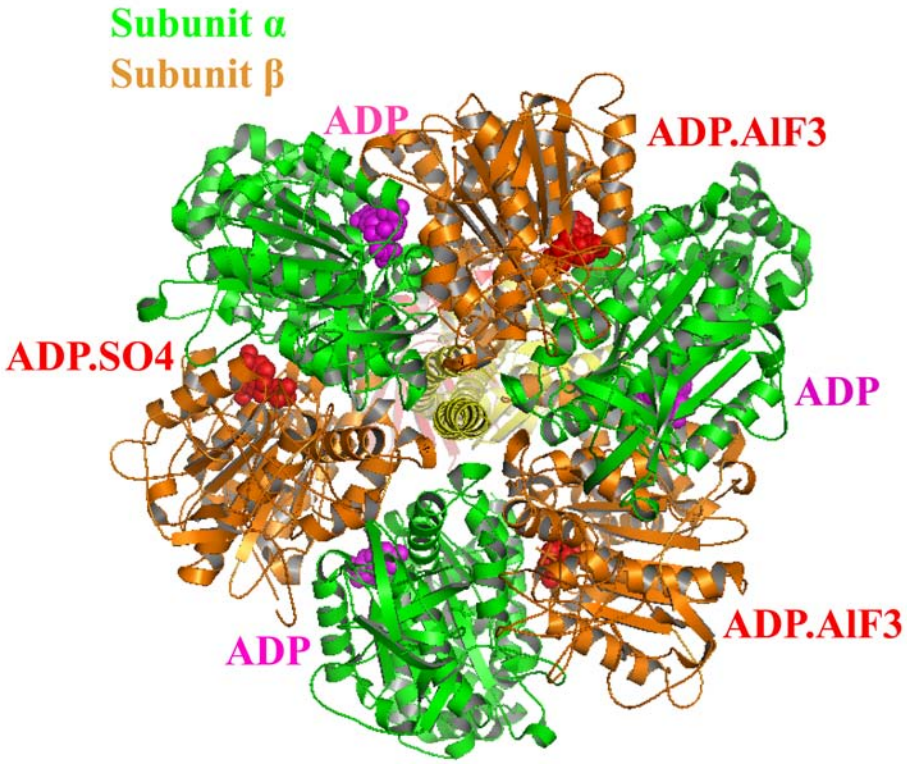

Figure 1.5. Structure of the bovine heart mitochondrial F_1 ATPase showing all the nucleotide binding sites occupied with nucleotides and SO_4 (MENZ *et al*., 2001). The nucleotides are bound at the interface of α-β dimer and are shown as spheres (magenta); bound nucleotides in α and β are shown in magenta and red color, respectively.

1.5 A_1A_O ATP synthases

Archae bacteria possess a unique class of ATP synthase enzyme designated as A_1A_O ATP synthases. Very limited structural information is available about this class of ATP synthase. The primary structure of the archaeal ATP synthases is similar to that of the eukaryotic V-ATPases, but their function as an ATP synthase is more similar to that of the F-ATP synthases. Sequence and structural comparison studies of individual subunits have shown that the archaeal A_1A_O ATP synthase share properties with both bacterial F-ATP synthases and eukaryotic V-ATPases. This indicates that the A-ATP synthase have evolved as a separate class of ATPases/synthases. Recently the structure of an intact A-ATP synthase was determined by electron microscopy of single particles at a resolution of 1.8 nm from a methanogenic bacteria *Methanocaldococcus jannaschii* (COSKUN *et al*., 2004b). Figure 1.6 shows a toplogical model of A_1A_O ATP synthase from *M. jannaschii* (GRÜBER and MARSHANSKY, 2008). A-ATP synthase from *M. jannaschii* is composed of total nine subunits (A, B, C, D, E, F, H, a, and c), in the stoichiometry of (A_3:B_3:C:D:E:F:H_2:a:c_x) (BIUKOVIĆ *et al*., 2007). Among different members of archaea the stoichiometry of subunit c is found to be variable. Like the related bacterial F-ATP synthase (α_3:β_3:γ:δ:ε:a:b_2:c_x) (WEBER *et al*., 2003) and the eukaryotic V-ATPase (A_3:B_3:C:D:E_x:F:G_2:H:a:d:c_x:c_x':c_x'') (FORGAC *et al*., 2000), it is composed of a water soluble

A_1 headpiece (A_3:B_3), which is attached to membrane-embedded ion-translocating part known as A_O (consists of subunits a and c), via a central stalk and two peripheral stalks (MÜLLER and GRÜBER, 2003). The head domain consists of nucleotide binding subunits A and B arranged in a pseudo-hexagonal fashion (COSKUN *et al.*, 2002; COSKUN *et al.*, 2004a; COSKUN *et al.*, 2004b; GRÜBER *et al.*, 2008). The subunits C, D and F, constitute the central stalk part and the peripheral stalks are formed by the subunits H and *a*, respectively. ATP is synthesized or hydrolyzed on the A_1 headpiece, which consists of an A_3:B_3 domain, and the energy provided for or released during this process is transmitted to the membrane-bound A_O domain. The energy coupling between the two active domains occurs via the stalk sector (MÜLLER and GÜRBER, 2003). In the intact A_1A_O ATP synthase, subunit B is in close contact with the subunit A and the interface region is proposed to be the nucleotide binding site. There are a total of six nucleotide-binding sites on A_1 and they are located in the A_3:B_3 headpiece (SCHÄFER *et al*., 1999; SCHÄFER and MEYERING-VOS, 1992). Subunit A and B are considered to be as catalytic and non catalytic in function, respectively (COSKUN *et al*., 2002; COSKUN *et al*., 2004b; SCHÄFER *et al*., 2006b).

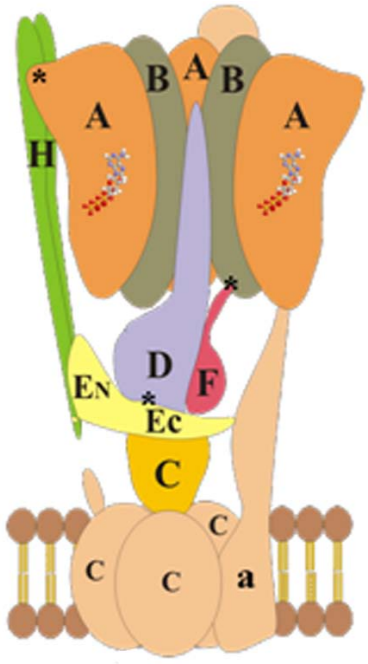

Figure 1.6. The arrangement of subunits in the A-ATP synthase (GRÜBER and MARSHANSKY, 2008). One B subunit has been removed from the A_1 headpiece to reveal subunit D. The A subunit is attached to subunit N-terminal domain (E_N) by a peripheral stalk composed of subunit H, whereby the C-terminal part of E (E_C) is in close proximity to the coupling subunit D.

1.6 Structure of subunit A from A_1A_O ATP synthase of *Pyrococcus horikoshii* OT3

The catalytic subunit A of the A_1A_O ATP synthase of *Pyrococcus horikoshii* OT3 can be divided into four major domains: an N-terminal domain (domain I (blue), residues 1-79, 110-116, 189-

199), a knob-like β–sheet structure (domain II (red), residues 117-188), a nucleotide binding α–β domain (domain III (yellow), residues 80-99, 200-437) and a C-terminal α–helical domain (domain IV (green), residues 438-588) (Figure 1.7) (MAEGAWA *et al*., 2006; KUMAR *et al*., 2009b). The N-terminal domain (domain I) is primarily made up of loops and β sheets. The domain II (residues 117-188) is flanked by N-terminal domain I and the nucleotide binding domain III, constitutes a part of the Non-Homologous Region (NHR), made up of 90 amino acids (spanning residues P122 to P210 of the subunit A of the A_1A_O ATP synthase from *P. horikoshii*) (Figure 1.7). The NHR domain is highly conserved in the nucleotide binding subunit A of A- ATP synthase and V-ATPases but the β subunits of F-ATP synthases do not possess this domain. The domain II is made up of eight β-strands, which are folded into a β-sandwich structure with two fold symmetry and according to the subunit topology model proposed for A_1A_O ATP synthase (COSKUN *et al*., 2004a; COSKUN *et al*., 2004b), it corresponds a the knob-like structure in the electron microscopy projection in the entire complex, and is located such that it protrudes towards the opposite side of the central rotor suggesting that the domain II might form a part of the peripheral stalk connecting A_1 and A_O domains in the entire A_1A_O complex. The nucleotide binding domain III in subunit A is an α/β domain comprised of residues 80-99 and 200-437 (Figure 1.7). Similar to the catalytic β subunit of F-ATP synthases, two nucleotide binding motifs, the Walker A motif ($_{234}$GPFGSGKT$_{241}$), and the Walker B motif ($_{320}$RDMGYDDVALMAD$_{331}$), are conserved in subunit A (MAEGAWA *et al*., 2006). A P-loop, is an ATP binding motif found in many nucleotide-binding proteins. The P-loop is a glycine-rich loop preceded by a β-sheet and followed by an α-helix. P-loop residues interact with the phosphate groups of the nucleotide and the Mg^{2+} ion, which coordinates the β and the γ phosphates (SARASTE and SIBBALD, 1990). These consensus sequences are found conserved in several other nucleotide binding proteins like myosin, transducin, helicases, small GTPases like Ras protein and F-ATPases (SARASTE and SIBBALD, 1990). This conservation of amino acids essential for the nucleotide binding and catalysis in the primary sequence of subunit A suggest that A-ATP synthases might employ similar catalysis mechanism as F-ATP synthases. The C-terminal α-helical domain (domain IV) spans residues 438-588 (Figure 1.7). This domain is believed to play an important role during the catalysis event when nucleotides occupy the active sites, by contacting the rotating D subunit through the amino acid sequence DALPERE (residues 482-488) in *P. horikoshii* (COSKUN *et al*., 2002). The subunit A in A_1A_O ATP synthase is also believed to interact with subunits D and/or F via this region of the domain IV (COSKUN *et al*., 2002).

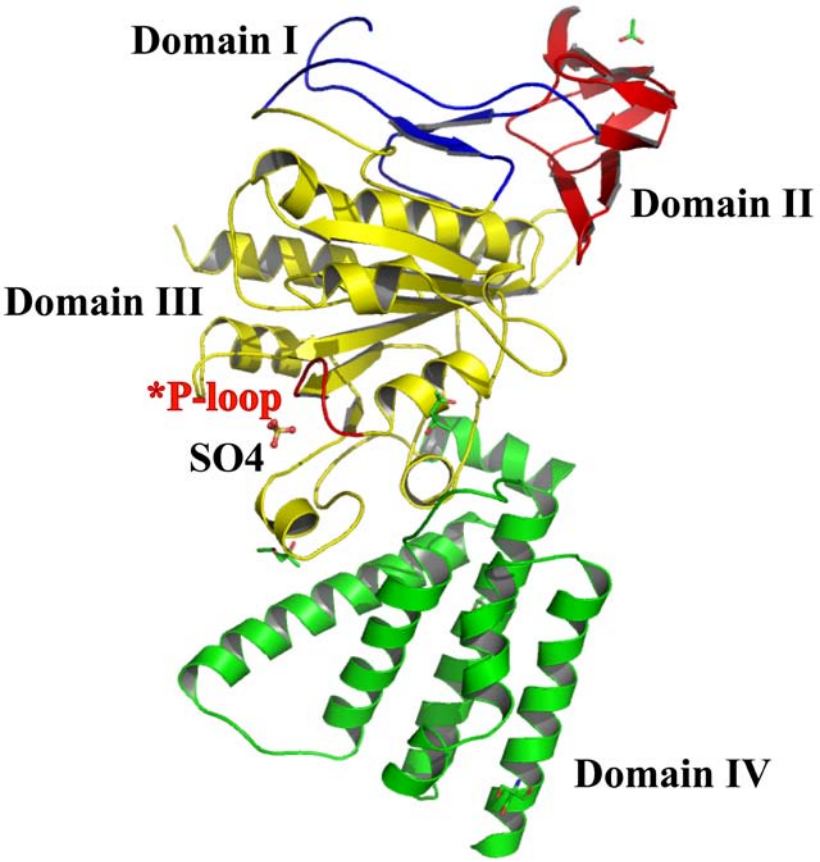

Figure 1.7. Crystal structure of the subunit A from *P. horikoshii* OT3 in complex with a phosphate analog (SO_4) (PDB: 3I72) (KUMAR *et al*., 2009b). The four domains of subunit A are labelled in different colour codes and the P-loop region ($_{234}$GPFGSGKT$_{241}$) is highlighted in red color.

1.7 Structure of subunit B from A_1A_O ATP synthase of *Methanosarcina mazei* Gö1

The crystal structure of the nucleotide binding subunit B of A-ATP synthase from *M. mazei* Gö1 is available in nucleotide free form at 1.5 Å resolution (SCHÄFER *et al*., 2006b). The overall structure of subunit B is made up of three domains, an N-terminal six-stranded β barrel (residues 13-76), an intermediate α-β domain (residues 77-358), and a C-terminal four α-helical bundle (residues 359-460) (Figure 1.8A). The intermediate α-β domain is considered to be the nucleotide binding domain. The important difference between the structures of the subunit A and B is the presence of an NHR domain which unlike subunit A is absent in subunit B. The nucleotide-binding subunit B does not have the ATP binding sequence GXXGXGKTV and a GER sequence. It is well known that most of the ATP binding proteins contain Walker A and Walker B sequences but there are examples in nature where it has been found that some ATP binding proteins do not possess these sequences, but still bind to nucleotides. Sequence alignment of subunit B from A_1A_O ATP synthase has shown that there is a conserved glycine rich motif similar to that of a P-loop sequence (GXGXGKT) but it is located 195 residues downstream of the expected site. It is at a position where it forms a loop like structure that connects the middle and C-terminal domains of subunit B (SCHÄFER *et al*., 2006b).

1.8 Nucleotide binding site in subunit B

Earlier results of photoaffinity labelling study, using a photoaffinity ATP analogue, 8-N_3-3'-biotinyl-ATP, on subunit B, showed that the azido group of the photoaffinity labeled ATP interacts with Y338 of the peptide G336-R349 of subunit B (SCHÄFER *et al*., 2006b). This residue is predicted to have a π – π interaction with the adenine ring of the incoming nucleotide. Figure 1.8A and B show a highlighted R416 residue, predicted to be conferring cation – π interaction with the adenine ring of the nucleotide.

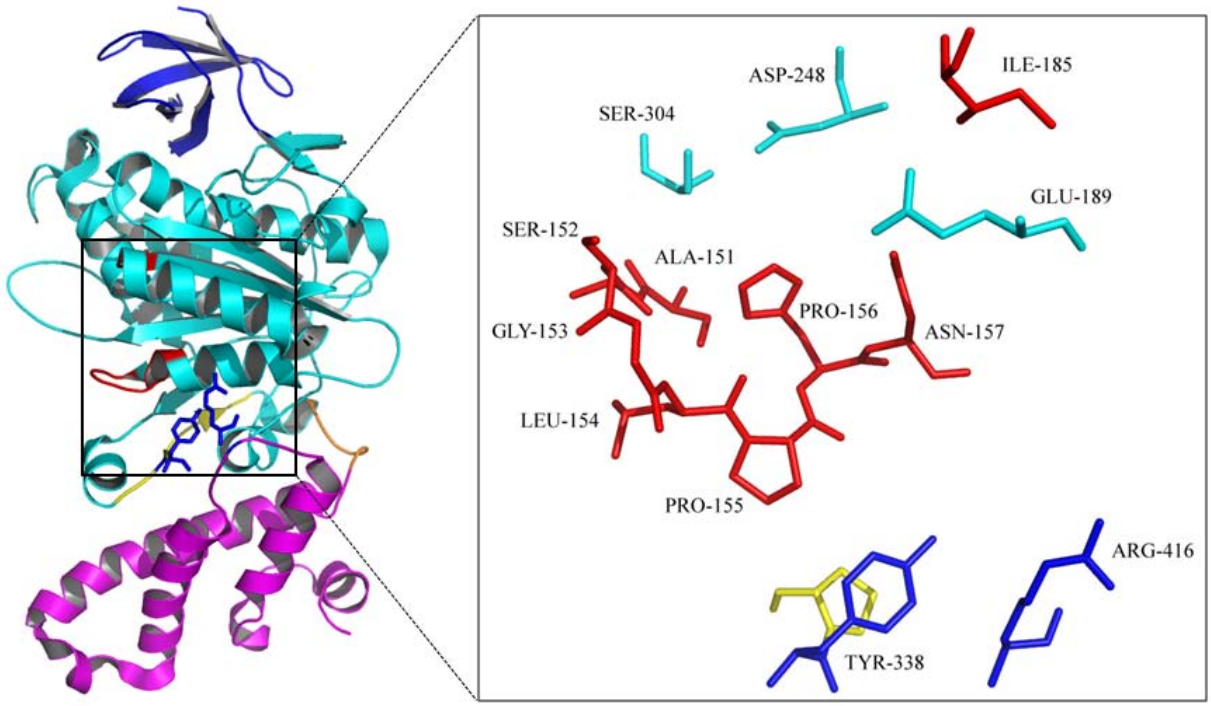

Figure 1.8. (A). Crystal structure of subunit B from A_1A_O ATP synthases from *M. mazei* Gö1 at 1.5 Å resolution (PDB: 2C61), (SCHÄFER *et al*., 2006b). The structure of subunit B consist of three domains, an N-terminal six-stranded β barrel (blue), an intermediate α-β domain (cyan), and a C-terminal four α-helical bundle (purple). (B) A zoom in window highlighting residues, considered to be important for nucleotide binding in subunit B.

The residues Y338 and R416 are believed to form the adenine binding site of the nucleotide binding pocket. Based on the results of structural alignment of subunit B with the α subunit of F-ATP synthase, it has been observed that the peptide sequence ($_{150}$SASGLPHN$_{157}$) is slightly away from the expected binding site of AT(D)P (SCHÄFER *et al*., 2006b). A conserved lysine residue in α and β subunits of the related F_1F_O ATP synthase is found to have interactions with the γ phosphate of ATP molecule (ABRAHAMS *et al*., 1996). In subunit B the H156 residue is present at corresponding position and positive charge of this H156 residue might take the role of lysine residue in the loop sequence $_{150}$SASGLPHN$_{157}$ (SCHÄFER *et al*., 2006b). The superposition of subunit B with the β subunit of F_1F_O ATP synthase has shown that both loops, formed by the peptide $_{150}$SASGLPHN$_{157}$ and $_{184}$GIT$_{186}$, are present at corresponding positions in

the structure of subunit B (SCHÄFER *et al*., 2006b). In Figure 1.9, labeled residues from subunit B are forming the peptide sequences $_{150}$SASGLPHN$_{157}$ and $_{184}$GIT$_{186}$. It shows that the adenine binding site in the wild type subunit B have aromatic Y338 and the basic R416 residues, predicted to undergo π - π stacking and cation - π interactions, respectively with the incoming nucleotide.

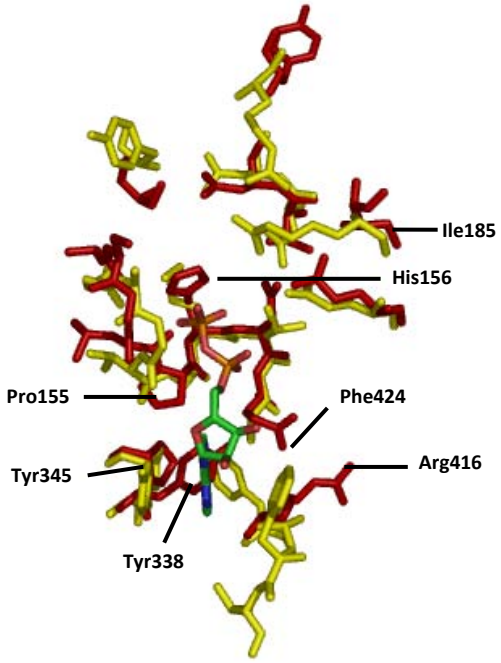

Figure 1.9. Superposed nucleotide binding pockets of subunit B from A_1A_O ATP synthase (red, PDB: 2C61) (SCHÄFER *et al*., 2006b) and β subunit from F_1F_O ATP synthase (yellow, PDB 1H8E) (MENZ *et al*., 2001) with ADP molecule (green).

In the β subunit of F-ATP synthase there is another peptide sequence GER also known as Walker B sequence, which is found to have an important role in nucleotide binding and catalysis events (ABRAHAMS *et al*., 1996). Incidently, a similar sequence $_{184}$GIT$_{186}$ is present in the structure of subunit B at a corresponding position (INATOMI *et al*., 1989). Based on multiple sequence alignment results it was found that the sequence $_{184}$GIT$_{186}$ is conserved in A_1A_O ATP synthases (INATOMI *et al*., 1989). The glutamate residue of the GER loop (Walker B sequence) of the β subunit of F-ATP synthase has been proposed to stabilize the penta-coordinated transition state during cleavage of ATP molecule and hence play a crucial role in catalysis reaction mechanism (WEBER *et al*., 1996). The importance of this glutamate residue in subunit β is highlighted by the fact that upon mutation with a glutamine residue the nucleotide binding of subunit β is drastically reduced (3-4 times reduced) (WEBER *et al*., 1996). This observation may justify the lack of catalytic activity in the α subunit of F-ATP synthase due to lack of a catalytic carboxylate group. Surprisingly, in subunit B from the V-ATPase of yeast (*Saccharomyces cerevisiae*)

possess same sequence ($_{175}$SASGLPHN$_{182}$) at corresponding position (VASILYEVA *et al*., 1997). Mutational studies of individual residues from this sequence in yeast V-ATPase have shown that the H180C or N182C mutants have about 25 % less ATPase activity and proton transport loss while mutations in S176 and P180 has led to drastic loss of ATPase activity (about 55 – 60 %) (VASILYEVA *et al*., 1997). These experimental observations indicate that GXXGXGKTV sequence does not characterize all ATP-binding sites.

1.9 Objectives of the thesis

The subunits A and B of the A_1A_O ATP synthase are major nucleotide binding subunits with catalytic and non-catalytic/regulatory functions, respectively, and the availability of high resolution structures of these subunits in nucleotide bound forms are a prerequisite to get a deeper understanding of the mode of nucleotide binding and catalysis events in the A_1 headpiece of the A-ATP synthases. So far no structures have been reported for the ligand bound forms of both these subunits from the A-ATP synthase. Therefore, the present study has focused on obtaining the nucleotide bound form of the catalytic subunit A from *Pyrococcus horikoshii* OT3 and the regulatory subunit B from *Methanosarcina mazei* Gö1 and to pin point the role of individual amino acids in the nucleotide binding pocket of the respective subunits. Mutation of key residues in the nucleotide binding pocket regions (P-loop and adenine binding region) of subunits A and B are expected to offer further insight into the nucleotide binding events. Alanine scanning of the P-loop region was planned in subunit A. Systematic substitution of important amino acids has been planned to realize the role of individual residues. Tryptophan has been used as an optical probe to facilitate spectroscopic experiments in subunit B, because it has only one W430 residue present far away from the proposed nucleotide binding site. By taking advantage of crystallographic and spectroscopic properties of the mutants, the approach was to identify the role of key amino acids and structural motifs, giving subunit A and B the capacity of being catalytic and nucleotide binding or even a catalytic/regulatory subunit, respectively.

2. Materials and methods

2.1 Materials

2.1.1 Chemicals

All the chemicals used in the current study were of at least analytical grade and were purchased from the following companies:

Buffers and salts	Sigma (St. Louis, MO, USA), USB (Sampscott, MA), Calbiochem (Darmstadt, Germany), Fluka (Sigma, Buchs Germany), Roth (Karlsruhe, Germany), Serva (Heidelberg, Germany)
Pefabloc^{SC}	BIOMOL (Hamburg, Germany)
PMSF	Sigma (St. Louis, MO, USA)
DTT	Hoefer (San Francisco, CA, USA)
LB Media	BD (Sparks, MD, USA)
Electrophoresis Chemicals (Agarose, SDS, APS etc.)	Bio-Rad (Hercules, CA, USA)
Antibiotics	Calbiochem, Sigma and Gibco (Invitrogen)
IPTG	Fermentas
BSA	GERBU (Heidelberg, Germany)
Nucleotides (ATP, ADP, AMPPNP)	Sigma (St. Louis, MO, USA)
EDA-ATP ATTO-647N	ATTO-TEC (Siegen, Germany)
EDA-ADP ATTO-647N	ATTO-TEC (Siegen, Germany)

2.1.2 Molecular biology materials

2.1.2.1 Primers

Primers	1st Base and Research Biolabs (Singapore)

2.1.2.2 Enzymes and kits

Pfu Polymerase	Fermentas (Glen Burnie, MD, USA)
NcoI, SacI, NdeI, SalI	Fermentas and New England Biolabs
T4 DNA Ligase	Fermentas and NEB
T4 Quick Ligase	Promega
CIAP	Fermentas (Glen Burnie, MD, USA)
Miniprep Plasmid Kit	Qiagen (Hilden, Germany)
Nucleobond AX mediprep Kit	MN & Co (Düren, Germany)

2.1.2.3 Vectors

pET-9d1	(GRÜBER *et al.*, 2002)
pET-22b (+)	Novagene (Darmstadt, Germany)

2.1.3 Chromatography

2.1.3.1 Ion exchange

Affinity Ni^{2+}-NTA	QIAGEN (Hilden)
RESOURCE™ Q	GE Healthcare (Uppsala, Sweden)
SOURCE™ 30Q	GE Healthcare (Uppsala, Sweden)

2.1.3.2 Gel filtration

Superdex HR 75 (10/30)	GE Healthcare (Uppsala, Sweden)
Superdex 200 HR (10/30)	GE Healthcare (Uppsala, Sweden)
PD-10 desalting column	Amersham Biosciences

2.1.3.3 Instruments and accessories

Äkta FPLC	GE Healthcare (Uppsala, Sweden)
Millex Filters (0.45 µM)	Millipore (Bradford, USA)
Syringe, needles and accessories	BD Biosceinces

2.1.3.4 Protein concentration, estimation and dialysis

Centriprep YM30	Millipore (Co-cork, Ireland)
Amicon ulta (50 kDa)	Millipore (Co-cork, Ireland)
Protein estimation: BCA Assay Kit	Pierce (Rockford, IL, USA)
Dialysis Spectra Por®CE membranes	Roth (Karlsruhe, Germany)

2.1.4 Other instrumentation

PCR Thermocycler	
Biometra T personal	Biometra
Biometra T gradient	Biormetra
Micropulser Electroporator	Bio-Rad
Ultraspec 2100 Pro Spectromphotometer	Amersham Biosciences
Sonoplus Sonicator	Bendelin
Microcal iTC200	Microcal (Northampton, UK)

2.1.5 Computer softwares

Vector NTI 10.3.0	Invitrogen
HKL2000 package	(OTWINOWSKI and MINOR, 1997)
Refmac5 (CCP4 package)	(MURSHUDOV *et al*., 1997)
MOLREP	(VAGIN and TAPLYAKOV, 1997)
PHASER	(McCOY *et al*., 2007)
CNS	(BRUNGER *et al*., 1998)
PyMOL	(DeLANO, 2001)
Coot	(EMSLEY and COWTAN, 2004)
Ramachandran plot	(RAMACHANDRAN *et al*., 1963)
PROCHECK	(LASKOWSKI *et al*., 1993)
Quantity One	(Bio-Rad)
CCP4	(1994)

2.2 Methods

2.2.1 Construction of subunit A and its mutants

The gene encoding subunit A of the A_1A_O ATP synthase from *Pyrococcus horikoshii* OT3 was amplified by PCR according to the method of Cann *et al.*, 2001, using four primers: *a* with an *NdeI* restriction site (5'-GAGGTGAGTACATATGGTGGCGAAGGGGAG-3'), *d* with a *SalI* restriction site (5'-CTTGCTCAGTCGACTCACGCCCCATACTTC-3'), *c* (5'-GGCCTTTCGG-CAGCGGTAAGACGGTGACTCAGCATCAGC) and *b* (5'-GCTGATGCTGAGTCACCGTC-TTACCGCTGCCGAAAGGCC). The DNA fragments encoding the N-terminal extein (723 nucleotides) and C-terminal extein (1044 nucleotides) were amplified by PCR from the genomic DNA of *P. horikoshii* (ATCC, JCM 9974) with the primers *a*-*b* and *c*-*d*, respectively. Two separate PCR reactions were set up using a flanking primer (forward primer *a*) and (reverse primer *d*) (Table 2.1). The PCR reactions were setup in a total volume of 50 µl as follows:

Pfu buffer (10 x)	5 µl
DNTP's (10 mM)	1.5 µl
Primers (100 uM)	2 x 0.5 µl
Template DNA	100 ng
MilliQ water	variable
Pfu DNA polymerase	1 µl

The flanking primers (*a* and *d*) hybridized at each end of the subunit A sequence, thereby incorporating *NdeI* and *SalI* restriction sites (underlined), and an internal primer (forward primer *b*) and (Reverse primer *c*), that hybridized at the internal site. The PCR reaction was set up on ice

and the lid of the PCR thermocycler (Biometra T personal) was preheated to 99 ºC before reaction tubes were placed inside the machine. The following PCR thermocycler program was used for the amplification:

Lid Temp	99 ºC		
Initial denaturation	99 ºC	2 min	
Denaturation	96 ºC	0.5 min	× 25
Annealing	65 ºC	1 min	
Extension	72 ºC	2 min	
Final extension	72 ºC	10 min	
Hold	4 ºC		

In separate PCRs two fragments of the subunit A gene were amplified by using primers *a* and *b* and primers *c* and *d*, respectively. The amplified fragments coding the N-terminal and C-terminal exteins were fused together via a second PCR using the primers *a* and *d*. The overlap allowed one strand from each fragment to act as a primer on the other, and extension of this overlap by flanking primers (*a* and *d*) in second PCR reaction resulted in the product. To check the amplification and purity of the desired product, 5 µl of PCR amplified product was applied onto the analytic agarose gel (1%). If the product was found sufficiently pure, remaining reaction mixture was applied onto preparative agarose gel and purified by gel extraction kit (QIAGEN) as per the manufacturer's protocol. The purified PCR product was finally eluted in 50 µl volume of elution buffer (Qiagen). The purity of gel extracted PCR product was ascertained by running 1 µl sample on 1% analytical agarose gel. Following the same strategy as described above, five different mutant constructs (F236A, S238A, G239A, K240A and T241A) of subunit A were made using overlap extension polymerase chain reaction (PCR) method (HO *et al.*, 1989) using subunit A insert in pET-22b(+) as template. Same flanking primers (*a* and *d*) were used for all the mutant constructs. The sequences of flanking primers (*a* and *d*) internal primers (*b* and *c*) used for the mutants are enlisted in table 2.1. The primers (*b* and *c*) contain the mutation. A flow chart summarizing the procedures involved in site directed mutagenesis is given in Figure 2.1.

Flanking primers		**Primer sequence (5'-3')**
Primer *a*	Forward	GAGGTGAGTACATATGGTGGCGAAGGGGAG
Primer *d*	Reverse	CTTGCTCAGTCGACTCACGCCCCATACTTC
Mutant constructs		**Primer sequence (5'-3')**
F236A	Forward	GCAATTCCTGGGCCTGCGGGCAGCGGTAAGACGG
F236A	Reverse	CGTCTTACCGCTGCCCGCAGGCCCAGGAATTGCAG

Mutant constructs		Primer sequence (5'-3')
S238A	Forward	CAATTCCTGGGCCTTTCGGCGCGGGTAAGACGGTGAC
S238A	Reverse	GTCACCGTCTTACCCGCGCCGAAAGGCCCAGGAATTG
G239A	Forward	CCTGGGCCTTTCGGCAGCGCGAAGACGGTGACTC
G239A	Reverse	GAGTCACCGTCTTCGCGCTGCCGAAAGGCCCAGG
K240A	Forward	GGCCTTTCGGCAGCGGTGCGACGGTGACTCAGCTAG
K240A	Reverse	CTAGCTGAGTCACCGTCGCACCGCTGCCGAAAGGCC
T241A	Forward	CCTTTCGGCAGCGGTAAGGCGGTGACTCAGCATCAGCTAGC
T241A	Reverse	GCTAGCTGATGCTGAGTCACCGCCTTACCGCTGCCGAAAGG

Table 2.1.Sequences of flanking primers (*a* and *d)* and internal primers (*b* and *c)* used for subunit A and its mutant constructs. The primers were synthesized either at *1st Base Pte Ltd* Singapore or at *Research Biolabs Pte Ltd* Singapore.

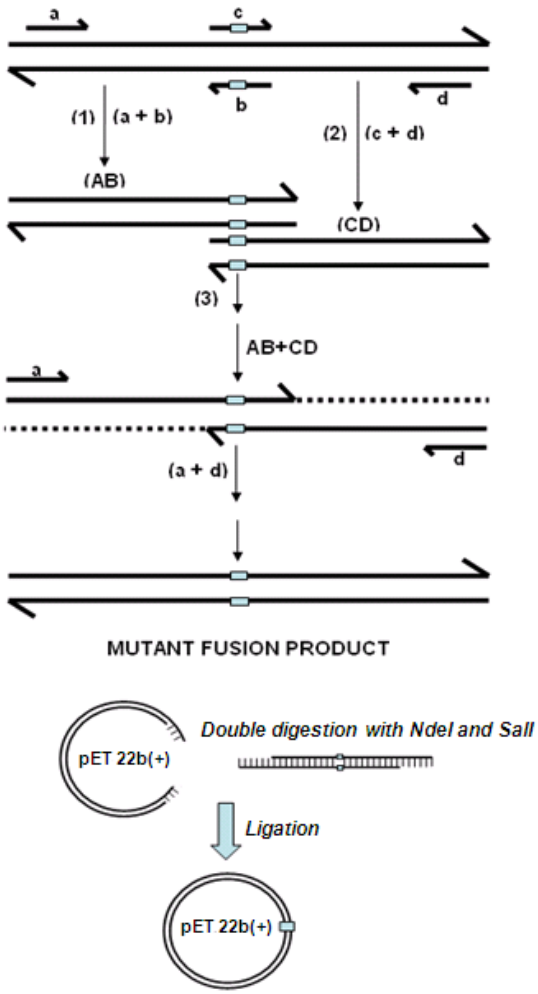

Figure 2.1. A flow chart showing the procedures involved in site directed mutagenesis using overlap extension polymerase chain reaction method (HO *et al.*, 1989). The same strategy was used to generate the mutant constructs of subunit A.

2.2.2 Restriction digestion and ligation

The purified PCR product (insert) and the pET-22b(+) vector, were double digested with restriction enzymes *NdeI* and *SalI* for 12 h at 37 °C. The digested vector was additionally treated with Calf Intestinal Alkaline Phosphate (CIAP) for 30 min. The digested vector and inserts were applied onto preparative agarose gel and purified by gel extraction kit (QIAGEN) as per the manufacturer's protocol. Analytical agarose gel (1%) was run to ensure complete digestion. The double digested PCR product and the pET-22b(+) vector were then ligated. The ligation reaction mixture of the vector and amplified product was setup as follows:

Ligase buffer (10x)	1.0 µl
Vector (V)	50-100 ng
Insert (I)	variable (1:1-1:3; V: I molar ratio)
T4 DNA Ligase	1 µl
MilliQ water	variable
Total	10 µl

The ligation mixture was incubated at 18 °C for 1 h. After the incubation is over, the reaction was stopped by the addition of 1 ml of n-Butanol, which precipitates the DNA out of solution. After thoroughly mixing the contents, it was centrifuged at 13,000 rpm (*miniSpin*, Eppendorf) for 10 min. The supernatant was removed gently and the DNA pellet was resuspended in 100 µl of 70% ethanol and again centrifuged at 13,000 rpm for 5 min. Supernatant was removed gently and the pellet was dried thoroughly for 5 min. The dried pellet was then resuspended in 10 µl of elution buffer (Qiagen). 2.5 µl of this purified ligation mixture was then transformed into electrocompetent DH5α cells by electroporation method as described in section 2.3. Followed by overnight incubation at 37 ºC, 5-10 larger colonies were picked up from the selection plate for plasmid preparation. Plasmids were purified using QIAGEN miniprep kit as per manufacturer's protocol. In order to ascertain if the subunit A inserts has ligated into the vector, the purified plasmids were double digested with restriction enzymes *NdeI* and *SalI*. The sizes of vector and insert were then confirmed with appropriate markers and positive controls. The mutations were verified by DNA sequencing. The verified plasmids were finally transformed into *Escherichia coli* (BL21–CodonPlus (DE3)–RIL) cells (Stratagene) for protein expression.

2.2.3 Electroporation transformation

For the transformation of wild type subunit A and mutant constructs, electroporation transformation method was used. Electro-competent cells were prepared as per the protocol from Current Protocols in Molecular Biology manual (Wiley InterScience). The wild type subunit A and mutant plasmids were transformed into electrocompetent DH5α and BL21–CodonPlus

(DE3)–RIL cells as follows: 100 µl of the electrocompetent cells were thawed on ice and the 50 ng of plasmid to be transformed was added and incubated for 5 min. The mixture was then transferred to electroporation cuvettes (Gene pulser^{R}, 0.2 cm, Bio-Rad) and electroporation was performed at a constant voltage of 2.5 KV (Micropulser Electroporator, Bio-Rad). The cuvettes were then transferred back on ice for 1 min and subsequently 1 ml of LB media was added and incubated on a shaker incubator (Infors HT Minitron shaker) set at 37 °C, 220 rpm for 45 min. After the incubation was over, the cultured cells were gently pelleted down at a slow speed of 1000 rpm (centrifuge name) for 5 min and 800 µl of the supernatant was discarded. The cells were then resuspended into remaining 200 µl of the media and the whole volume was plated on selection plates containing ampicillin and chloremphenicol, followed by overnight incubation at 37 ºC.

2.2.4 Induction Test

Reagents: *4X Lysis buffer:* *250 mM Tris/HCl, pH 6.8*
9.2 % SDS
40 % Glycerol
0.2 % Bromophenol Blue
1 mM DTT

Induction test was performed to verify the production of the wild type and mutant proteins in *E. coli*. (BL21–CodonPlus (DE3)–RIL) cells. A total of five large sized colonies were picked up from the ampicillin and chloremphenicol selection plate and cultures of the wild type and mutant of subunit A were grown in LB medium containing ampicillin (100 µg/ml) and chloremphenicol (34 µg/ml) for about 15 h at 37 °C until an optical density OD_{600} of 0.6–0.7 (Ultraspec 2100 *Pro*, Amersham Biosciences) was reached. To induce production of His_6-mutant protein, the cultures were supplemented with isopropyl-β-D-thiogalactoside (IPTG) to a final concentration of 1 mM. Following incubation for another 2 h at 30 °C, the cells were centrifuged at 8,000 x g for 20 min, at 4 °C. Supernatant was discarded and the cells were lysed using lysis buffer (1 x) and 1 mM DTT. The lysed cell mixture was heated at 95 °C on a heating block (Vortemp 56, Labnet) for 5 min and then 20 µl of the sample was applied on 17 % sodium dodecyl sulfate–polyacrylamide gel electrophoresis (SDS-PAGE) gel (LAEMMLI *et al.*, 1970). Un-induced cultures were treated in the same way and applied on SDS gel as negative controls.

2.2.5 Protein purification

To produce subunit A, liquid cultures were shaken in LB medium containing 100 µg/ml ampicillin and 34 µg/ml chloramphenicol. At an OD_{600} of 0.6, the cells were induced by the

addition of 1 mM IPTG and growth continued at 30 °C for 4 h. The cultured cells were pelleted down by centrifugation at 8000 x g (Biofuge *Primo* R, Heraeus) for 10 min. The cell pellet was then resuspended in Tris-HCl buffer A (50 mM Tris-HCl, pH 8.5, 50 mM NaCl, 1 mM DTT and 1 mM phenylmethylsulfonyl fluoride (PMSF) and disrupted using sonication method. The cell lysate was incubated at 70 ºC for 30 min, kept on ice and then centrifuged at 40,000 x g for 30 min. Ammonium sulfate was added to the supernatant to 60% saturation. The solution was mixed thoroughly till ammonium sulphate dissolved completely, followed by centrifugation at 20,000 x g for 20 min. The protein pellet thus obtained was resuspended in buffer 50 mM Tris-HCl, pH 8.5, 50 mM NaCl, 1 mM DTT. The resuspended protein solution was applied on PD-10 (GE Healthcare) desalting column (equilibrated with 50 mM Tris-HCl, pH 8.5, 1 mM DTT) to get rid of excess salt. The protein was eluted in 50 mM Tris-HCl, pH 8.5, 1 mM DTT. The eluted protein was then loaded onto a Resource Q column (GE Healthcare) equilibrated with the buffer (50 mM Tris-HCl pH 8.5, 1 mM DTT). The bound protein was eluted from a linear NaCl gradient (0.05 - 1.0 M). Subunit A eluted at a concentration of 0.14 M NaCl. The peak fractions were pooled together and concentrated using 50 kDa concentrators (Amicon) to a volume of 500 ul. The fractions containing subunit A was applied onto a column of 26/60 Superdex200 (GE Healthcare) equilibrated with the buffer B (50 mM Tris-HCl, pH 8.5, 1 mM DTT, 50 mM NaCl). The subunit A protein eluted at 13.75 ml volume. Buffer exchange was performed for the eluted protein during concentration process using 50 kDa concentrators (Amicon) in a stepwise manner such that the pH of the buffer (50 mM Tris-HCl, pH 8.5) was reduced gradually from 8.2 to 7.8 and finally the protein was obtained in the buffer (50 mM Tris-HCl, pH 7.5). The purity of the protein sample was analyzed by SDS–PAGE (Laemmli, 1970). The SDS-gels were stained with Coomassie Brilliant Blue G250. Peak fractions were pooled and concentrated on Centricon 50 kDa concentrators (Amicon). Protein concentrations were determined by the bicinchonic acid assay (BCA; Pierce, Rockford, IL. USA). I have modified and optimized the protocols for the purification of subunit A and all its mutant proteins and have performed all the protein purification work mentioned in the present study. The protein concentration estimation was done by bicinchoninic acid assay (BCA; Pierce, Rockford, IL, USA) as per the manufacturer's instructions. BSA (0 – 250 µg/ml) was used as standard. At least two dilutions of the protein were made and each dilution of protein was measured in triplicate. Optical density of the samples was measured at 562 nm against blank.

2.2.6 ATP hydrolysis assay

The ATP hydrolysis assay was performed using Malachite Green Assay Kit (Cayman) to

determine hydrolytic ability of the subunit A. The principle of the assay is based on the complex formation between malachite green molybdate and free orthophosphate under acidic conditions. The formation of the green colored molybdophosphoric acid complex has an absorption maximum at 620 nm and OD_{620} is directly related to the free organic phosphate concentration in the solution. The experiments were performed following manufacturer's instructions using increasing concentrations of subunit A protein (1 – 4 mg/ml) and 2 mM of MgATP, incubated at different temperature points (25 ºC and 37 ºC) for 20 min. Phosphate (0 – 1.25 nM/50 µl) was used as standard. Each dilution of the protein was prepared in triplicate and the optical densities of the samples were measured on microplate reader at 620 nm against the phosphate standard.

2.2.7 Crystallization of the subunit A

Crystallization setup for subunit A-WT and its mutant proteins were done according to the modified protocol of MAEGAWA *et al.*, 2004. Larger subunit A crystals suitable for X-ray diffraction measurements were obtained by the hanging-drop vapor diffusion method at 18 °C from a solution containing 50% (v/v) MPD and 0.1 M acetate pH 4.5. According to the improved condition 2 µl protein solution was mixed with an equal volume of reservoir solution and equilibrated against 500 µl reservoir solution. Paraffin oil and silicone oil (v/v 1:1) were overlaid onto the mother liquor in the reservoir to a final volume of 200 µl. This overlaying of oils prolonged the nucleation time and hence large sized crystals could be obtained.

2.2.8 Co-crystallization of subunit A (WT) and its mutants with nucleotides

For co-crystallization with nucleotides, the purified subunit A and its mutants were divided into three batches and incubated separately with 2 mM MgATP, 2 mM MgADP and 2 mM MgAMPPNP at 4 °C for 30 min on a sample rotator and this mixture was then concentrated to 10 - 12 mg/ml using 50 kDa centricon concentrators (Amicon). Buffer exchange was performed for the eluted protein during concentration process using 50 kDa concentrators (Amicon) in a stepwise manner to finally obtain the protein in the crystallization buffer (50 mMTris-HCl, pH 7.5). The protein-ligand complexes were then set up for crystallization in the same optimized conditions in hanging drop plates and incubated at 18 °C. The presence of 50% (v/v) MPD in the crystallization buffer acted as a good cryo-protactant. Therefore, the crystals thus obtained were directly flash-cooled in liquid nitrogen.

2.2.9 Data collection

Datasets for the nucleotide free empty form and ADP-bound crystals of wild type subunit A were collected at 140 K on beamline 13B1 at the National Synchrotron Radiation Research Center

(NSRRC, Hsinchu, Taiwan) using the ADSC Quantum 315 CCD detector. For the AMP-PNP (5'-adenylyl-β,γ-imidodiphosphate) bound form and the S238A mutant of subunit A the data were collected at 100 K in SPring-8 Taiwan Beamline 12B2 (SPring-8, Japan) using Mar CCD 225 detector. Technical assistance was kindly provided by staff at beamline 13B1 and 13C1 (NSRRC) and at beamlines 12B2 (SPring-8 Taiwan Beamline) and BL26B2 (SPring-8 RIKEN Beamline). All the diffraction data were indexed, integrated and scaled using the HKL2000 suite program (OTWINOWSKI and MINOR, 1997). All the crystals belong to tetragonal space group $P4_32_12$ and have similar unit cell parameters.

2.2.10 Structure determination

The wild type subunit A structure (PDB 1VDZ; MAEGAWA *et al.*, 2006) was used as a model for the structure determination by molecular replacement method using the programs PHASER (McCOY *et al.*, 2007) and MOLREP (VAGIN & TAPLYAKOV, 1997). Rigid body refinement was carried out followed by difference Fourier syntheses calculations. Inspection of the $F_O–F_C$ and $2F_O–F_C$ maps for the protein-ligand complexes, and the mutants clearly showed electron density corresponding to the bound ligand and the mutation. The ligand-bound forms of subunit A were confirmed by omit map calculations using the CNS program (BRUNGER *et al.*, 1998). An undefined mutation during cloning at position 79 from Gly to Arg has taken place, which is clearly visible in the electron density map for all the structures. Iterative cycles of model building and refinement were carried out using the programs COOT (EMSLEY and COWTAN, 2004) and REFMAC5 (MURSHUDOV *et al.*, 1997) of the CCP4 suite (1994). In all the structures the N-terminal region is disordered and there is no density for the first 60 amino acids. The N-terminal region is highly flexible as evident by the high B-factors (residues 60-69 and 90-110). High solvent content may have caused flexibility and since this region is predominantly loops and beta sheet. The geometry of the final models was checked with PROCHECK (LASKOWSKI *et al.*, 1993) and the figures are drawn using the program PyMOL (DeLANO, 2002). Structural comparison analysis are carried out using the SUPERPOSE program (KRISSINEL and HENRICK, 2004) as included in the CCP4 suite.

2.2.11 Protein Data Bank accession code

Atomic coordinates and structure factors for the nucleotide free, AMP-PNP- and ADP-bound forms of subunit A and the S238A-mutant have been deposited in the RCSB Protein Data Bank under accession codes 3I72, 3I4L, 3I73 and 3IKJ, respectively. Atomic coordinates and structure factors for the K240A mutant structure will be submitted to the PDB database.

2.2.12 Isothermal titration calorimetry

Isothermal titration calorimetry (ITC) is used to study macromolecular interactions in solution. It permits determination of binding affinities of small molecule interacting with large protein molecules. Thermodynamic parameters such as entropic and enthalpic components of such binding reactions can be resolved using ITC. The nucleotide binding affinities of subunit A-WT and the mutants: F236A, S238A, G239A, K240A and T241A were determined by isothermal titration calorimetry. Both, the protein and the nucleotide were equilibrated in the same buffer (50 mM Tris-HCl, pH 7.5), filtered and degassed before titration. The nucleotides (0.5 mM ATP or ADP) were loaded in the syringe and were titrated in 1.5 µl injections against 10 µM of the protein placed in the sample cell in a MicroCal iTC_{200} microcalorimeter (Microcal, Northampton, UK). Unless otherwise stated, all the experiments were performed in 50 mM Tris-HCl, pH 7.5, under identical conditions at 25 ºC. The control experiments were performed by titrating the nucleotides in the buffer. The nucleotides were maintained in the same buffer at 25 ºC and titrated in 1.5 µl injections into the buffer. The heat of dilution, determined by titrating nucleotide into the buffer, was subtracted from the raw data before curve fitting and refinement. The dissociation constants of subunit A-WT and the mutants to the nucleotides were determined by least squares method and the binding isotherm was fitted using Origin v7.0 (Microcal) assuming a single-site binding model.

2.2.13 Cloning and mutagenesis of subunit B constructs

2.2.13.1 Vector purification:

Reagents, Chemicals and Kit:

Luria-Bertani (LB) media: 10 g/l Tryptone
5 g/l Yeast Extract
5 g/l NaCl
Vector Isolation: Nucleobond AX Kit

In order to generate mutant constructs of subunit B of the A_1A_O ATP synthase from *Methanosarcina mazei* Gö1, the modified vector pET-9d1 containing subunit B insert (GRÜBER *et al.*, 2002) was used. The vector was amplified in DH5α cells and was purified from an overnight culture in LB medium (200 ml) using Nucleobond AX or Qiagen midi-prep kit as per the manufacturer's protocol. The purity of the vector was ascertained on 1% analytical agarose gel.

2.2.13.2 Generation and purification of subunit B mutant proteins

Mutant constructs of subunit B were produced and amplified by overlap extension polymerase

chain reaction (PCR) method (HO *et al*., 1989). Ten different point mutants (F149W, L154C, L154S, P155G, H156K, I185E, Y338R, Y338W, A373W, and R416W) and one double mutant (H156K/R416W) of subunit B were made using overlap extension polymerase chain reaction (PCR) method (HO *et al.*, 1989) using subunit B insert in pET-9d as template. The same strategy was used as described in section 2.2.1 for the construction of subunit A mutants. The sequences of flanking primers (*a* and *d*) internal primers (*b* and *c)* used for the mutants are enlisted in table 2.2. Same flanking primers (*a* and *d*) were used for all the mutant constructs (Table 2.2). Following digestion with *Nco*I and *Sac*I, the PCR product was ligated into the pET-9d vector following the procedure as described in section 2.2.2. The mutations were verified by DNA sequencing. The plasmids were then transformed into *Escherichia coli* BL21 DE3 cells (Novagene, Darmstadt, Germany) using electroporation method followed by an induction test to verify the production of the mutant proteins as described in section 2.2.3 and 2.2.4, repsectively. Purification of subunit B was done according to SCHÄFER *et al*., 2006b and the protein concentrations were determined by BCA assay as described in section 2.2.6.

Flanking primers		**Primer sequence (5'-3')**
Primer *a*	Forward	TTTCTCCATGGTCAAAGAGTACAAGACGATCACTCAGATTGCAGGGCC
Primer *d*	Reverse	TTTGAGCTCTCACTTAGCCTTTCTGTGTGCCGGGTGATATTTCTGG

Mutant constructs		**Primer sequence (5'-3')**
F149W	Forward	GTGGGCAGAAACTGCCTATTTGGTCAGCATCAGGTCTCCCAC
F149W	Reverse	GTGGGAGACCTGATGCTGACCAAATAGGCAGTTTCTGCCCAC
L154C	Forward	CTATTTTCTCAGCATCAGGTTGCCCACACAATGAAATCGCCCTGC
L154C	Reverse	GCAGGGCGATTTCATTGTGTGGGCAACCTGATGCTGAGAAAATAG
L154S	Forward	CTATTTTCTCAGCATCAGGTAGCCCACACAATGAAATCGCCCTGC
L154S	Reverse	GCAGGGCGATTTCATTGTGTGGGCTACCTGATGCTGAGAAAATAG
P155G	Forward	CTATTTTCTCAGCATCAGGTCTCGGCCACAATGAAATCG
P155G	Reverse	CGATTTCATTGTGGCCGAGACCTGATGCTGAGAAAATAG
H156K	Forward	CAGCATCAGGTCTCCCAAAAAATGAAATCGCCCTGC
H156K	Reverse	GCAGGGCGATTTCATTTTTTGGGAGACCTGATGCTG
I185E	Forward	CAGTAGTTTTCGCAGCAATGGGTGAAACCAATGAAGAAGCC
I185E	Reverse	GGCTTCTTCATTGGTTTCACCCATTGCTGCGAAAACTACTG
Y338R	Forward	CACAGGAAGGGTATTCGCCCGCCAATTAATGTGCTG
Y338R	Reverse	CACATTAATTGGCGGGCGAATACCCTTCCTGTGC
Y338W	Forward	GCACAGGAAGGGTATTTGGCCGCCAATTAATGTGC
Y338W	Reverse	GCACATTAATTGGCGGCCAAATACCCTTCCTGTGC
R416W	Forward	GTTTGTCCGTCAGGGCTGGAACGAAAACAGGACAATC
R416W	Reverse	TGTCCTGTTTTCGTTCCAGCCCTGACGGACAAAC
A373W	Forward	CGGTTTCTGACCAGATGTATTGGGGTTATGCAGAAGGGCGTGAC

Mutant constructs		**Primer sequence (5'-3')**
A373W	Reverse	GTCACGCCCTTCTGCATAACCCCAATACATCTGGTCAGAAACCG
H156K/R416W	Forward	GTTTGTCCGTCAGGGCTGGAACGAAAACAGGACAATC
H156K/R416W	Reverse	TGTCCTGTTTTCGTTCCAGCCCTGACGGACAAAC

Table 2.2. Sequences of flanking primers (*a* and *d)* and internal primers (*b* and *c)* used for the mutant constructs of subunit B. The primers were synthesized either at *1st Base Pte Ltd* Singapore or at *Research Biolabs Pte Ltd* Singapore.

2.2.13.3 Intrinsic tryptophan fluorescence spectroscopy

Aromatic amino acids (tryptophan, tyrosine and phenylalanine) in proteins upon excitation with light give fluorescence signal which can be used to monitor the localized structural changes in proteins, induced either by protein-protein interaction or protein-ligand interactions. In the

present study, nucleotide binding to the protein was monitored using intrinsic tryptophan fluorescence spectroscopy. A *Varian Cary Eclipse* spectrofluorimeter was used, and all experiments were carried out at 20 °C. The sample volume of the fluorescence cuvette was 120 µl and 8-10 µg of protein sample was used for each reading. The samples were excited at 295 nm, and the emission was recorded from 310 to 380 nm with excitation and emission band passes set to 5 nm. For nucleotide titration of the tryptophan fluorescence of mutant R416W the emission wavelength was 340 nm (KUMAR *et al*., 2008). Before titration, the mutant protein and increasing amounts of MgADP and MgATP, respectively, were incubated in a buffer of 50 mM Tris/HCl (pH 8.5) and 100 mM NaCl for 5 min on ice.

2.2.13.4 Fluorescence correlation spectroscopy (FCS)

Fluorescence correlation spectroscopy (FCS) was performed at room temperature on a ConfoCor 3 (Zeiss, Jena, Germany) using the ATP- and ADP-analogues EDA-ATP ATTO-647N and EDA-ADP ATTO-647N (*ATTO-TEC*, Siegen, Germany). The 488 nm laser line of an HeNe633 laser were attenuated to 5 mW and focused into the aqueous solution by a water immersion objective (40 x / 1,2 W Korr UL-VIS-IR, Zeiss). FCS was measured in 50 µl droplets of the diluted fluorescent derivatives of ATP and ADP, which were placed on Nunc 8 well chambered cover glass. Before usage, the cover glasses were treated with 3 % of gelatin, in order to prevent unspecific binding of the fluorophors and removed by H_2O (HUNKE *et al*., 2007). The following filter sets were used: MBS: HFT UV/488/543/633, EF1: LP 655, EF: None, DBS: Plate, DBS1: Plate, DBS3: Mirror. Out-of-focus fluorescence was rejected by a 90 µm pinhole in the detection pathway, resulting in a confocal detection volume approximately 0.25 fl. Fluorescence autocorrelation functions were measured for 30 sec each with 10 repetitions. Solutions of Cy5 in pure water (*Fluka*) were used as references for the calibration of the confocal microscope. To analyze the autocorrelation functions of fluorescent nucleotides bound, in part, both the subunit *B* and its mutant R416W, respectively, models with the diffusion time and the triplet state were used for fitting (FCS-LSM software, ConfoCor 3, Zeiss). The diffusion times of fluorescent nucleotides and fluorescently labeled subunits were measured independently, and kept fixed during the fitting of the FCS data (KUMAR *et al*., 2008). Therefore, the determination of the binding constants required only the calculation of the relative amounts of free nucleotides with the short diffusion time and of the bound nucleotides with the diffusion time of subunit B. The calculations of the bound fractions and the dissociation constants were done by the ConfoCor 3-software 4.2, Origin 7.5 and Prism 5.01.

2.2.13.5 Crystallization of mutant R416W of subunit B

Crystallization of subunit B and its mutants were attempted using vapour diffusion method. Sitting drops were set up by mixing 2 µl of the subunit B mutant R416W (8-10 mg/ml) in buffer B (50 mM Tris/HCl, pH 8.5 and 100 mM NaCl) with 2 µl of the precipitant solution (20 % (v/v) polyethylene glycol (PEG) 400, 0.1 M NaCl, 0.1 M sodium citrate (pH 5.0) and 2 mM Tris (2-carboxyethyl) phosphine (TCEP)), incubated at 18 °C (SCHÄFER *et al*., 2006). Initial crystallization attempts led to quick nucleation, which yielded very small and poorly diffracting crystallites. The best diffraction obtained with these small crystallites were not better than 4.5 Å at in-house X-ray sources (RAXIS and MAR345). Therefore, the initial crystallization condition was further optimized by using glycerol in the grid screening to slow down the nucleation rates. The final crystallization condions where large diffracting crystals could be obtained comprised of 20 % (v/v) glycerol, 20 % (v/v) polyethylene glycol (PEG) 400, 0.1 M NaCl and 0.1 M sodium citrate (pH 5.0). The crystals were serially transfered using a nylon loop (Hampton Research) from the crystallization drop into a cryoprotectant solution comprising of 25 % (v/v) glycerol, 20 % (v/v) polyethylene glycol (PEG) 400, 0.1 M NaCl and 0.1 M sodium citrate (pH 5.0) and 30 % (v/v) glycerol, 20 % (v/v) polyethylene glycol (PEG) 400, 0.1 M NaCl and 0.1 M sodium citrate (pH 5.0), respectively. After soaking for 10 min in each cryoprotectant solution, the crystals were flash-frozen in liquid nitrogen at 100 K.

2.2.13.6 Co-crystallization of the wild type and R416W mutant with nucleotides

One of the common methods of obtaining crystals of a protein-ligand complex is co-crystallization, where the ligand is added to the protein to form a complex that is subsequently used in crystallization trials. The R416W mutant protein was incubated with 2 mM MgATP at 4 °C for 30 min on a sample rotator. The protein-ligand complex formed was then concentrated to 8 – 10 mg/ml using 30 kDa Centricon concentrators (Millipore) (KUMAR *et al*., 2008). The protein-ligand complex was set up for crystallization in the same optimized conditions in sitting drop plates and incubated at 18 °C. The same procedure, as explained above for the co-crystallization of R416W mutant with MgATP was followed for the co-crystallization of the subunit B (WT) with MgATP and MgADP to obtain diffraction quality crystals.

2.2.13.7 Data collection

Single-wavelength datasets of subunit B (WT) co-crystallized with MgADP was collected at 140K on beamline 13B1, while data for empty R416W mutant crystals and the crystals co-crystallized with MgATP were collected at beamline 13C1, at the National Synchrotron

Radiation Research Center (NSRRC, Hsinchu, Taiwan) using the ADSC Quantum 315 CCD (13B1) and 210 CCD (13C1) area detectors. The empty R416W mutant crystals diffracted to 2.8 Å, whereas R416W mutant co-crystallized with MgATP diffracted to 2.1 Å. The subunit B (WT) co-crystallized with MgADP diffracted to 2.7 Å (KUMAR *et al*., 2008). All data sets were indexed, integrated and scaled using the HKL2000 suite of programs (OTWINOWSKI and MINOR, 1997). In-house data collection was done on RAXIS and MAR345 machines under cryo conditions (140 K). All data were indexed, integrated and scaled using d*TREK and MOSFLM programs (PFLUGRATH *et al*., 1999; MURSHUDOV *et al*., 1997).

2.2.13.8 Structure determination

As the subunit B (WT) co-crystallized with ADP, and its R416W mutant empty and co-crystallized with ATP, crystallized in the same space group with similar unit-cell dimensions, the coordinates of the wild type subunit B (SCHÄFER *et al*., 2006b) was used as a model for structure solution by molecular replacement using the program MOLREP (VAGIN and TAPLYAKOV, 1997). Difference Fourier syntheses were calculated after rigid-body refinement for the structures. Inspection of the F_O–F_C and $2F_O$–F_C map of protein-ligand complex clearly showed electron density corresponding to the bound ligand. To ensure that the structure of the ATP and ADP bound complexes was correct, a series of simulated-annealing refinement was undertaken, followed by omit map calculations using the CNS program (omitting the nucleotide molecule from map calculation) (BRUNGER *et al*., 1998). Iterative cycles of model building and refinement were carried out using the programs COOT (EMSLEY and COWTAN, 2004), Refmac5 of the CCP4 suite (MURSHUDOV *et al*., 1997) and CNS (BRUNGER *et al*., 1998). The geometry of the final model was checked with PROCHECK (LASKOWSKI *et al*., 1993) and the figures are drawn using the program PyMOL (DELANO, 2002). I have solved the ADP bound form of wild type subunit B and the nucleotide free empty form of the R416W mutant of subunit B.

2.2.13.9 Atomic coordinates and structure factors

Atomic coordinates and structure factors for subunit B (WT) with ADP, its mutant R416W and its ATP-bound forms have been deposited in the Protein Data Bank under accession codes 3DSR, 2RKW, 3B2Q, respectively (KUMAR *et al*., 2008).

3. Results

3.1 Insight into nucleotide-binding of the catalytic subunit A of the A_1A_o ATP synthase by X-ray crystallography and Isothermal Titration Calorimetry

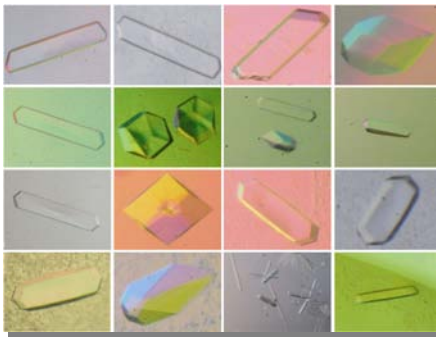

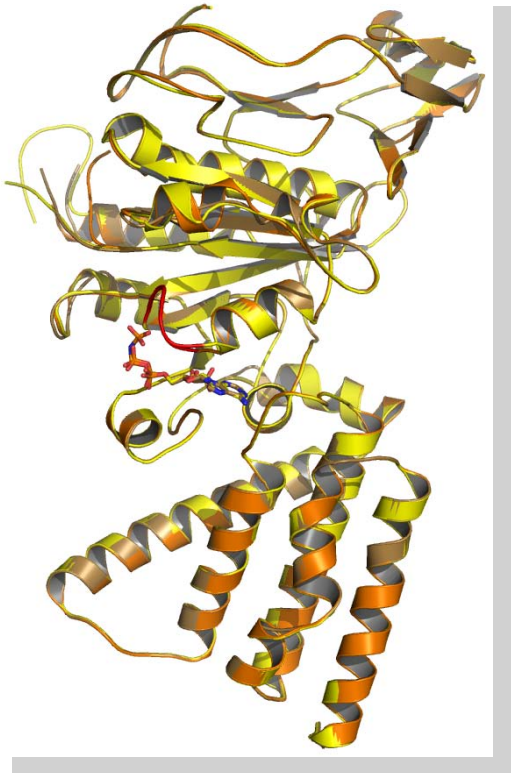

3.1.1 Cloning, production and purification of subunit A

The subunit A gene of the A_1A_O ATP synthase from *Pyrococcus horikoshii* OT3 was successfully cloned in pET-22b(+) expression vector (Novagen) as described in section 2.2.1. The subunit A gene exists as a split gene with coding regions called "Exteins" and a non-coding region "Intein". The DNA fragments encoding the N-terminal extein (720 nucleotides) and C-terminal extein (1044 nucleotides) were amplified by PCR from the genomic DNA of *P. horikoshii* OT3 with the primers *a*-*b* and *c*-*d*, respectively as described in section 2.2.1 (Figure 3.1.1A). The amplified fragments coding the N-terminal and C-terminal exteins were fused together via a second PCR using the primers *a* and *d* (Figure 3.1.1B). The fused DNA fragment was digested with *Nde*I and *Sal*I restriction enzymes and ligated into *Nde*I/*Sal*I-digested pET-22b(+) vector (Novagen).

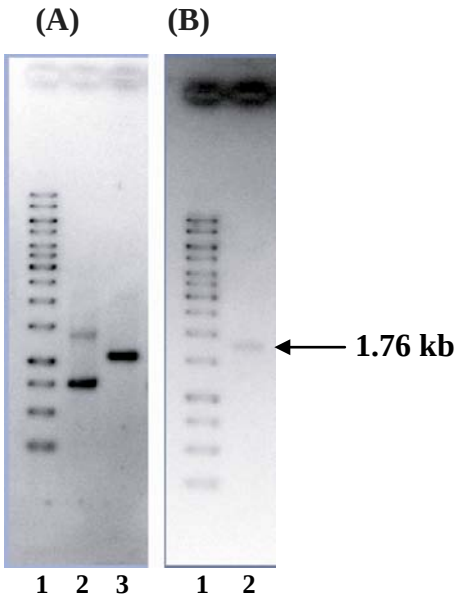

Figure 3.1.1. **PCR amplification of subunit A (WT).** (A) PCR I products; Marker DNA (1kb, Fementas) (*lane 1*); A (WT) (*lane 2* and *3*). (B) PCR II product; Marker DNA (1 kb, Fermentas) (*lane 1*); A (WT) (*lane 2*).

The full length subunit A protein was purified successfully by modification of an earlier method (MAEGAWA *et al*., 2004). In order to get rid of contaminating proteins, the subunit A protein was loaded onto a Resource Q column (GE Healthcare) equilibrated with buffer (50 mM Tris-HCl, pH 8.5, 1 mM DTT). The bound protein was eluted at 140 mM NaCl concentration, using a linear NaCl gradient (0.05 - 1.0 M) (Figure 3.1.2A). The peak fractions were pooled together and concentrated using 50 kDa concentrators (Amicon) to a volume of 500 µl. The protein was then applied onto a column of 26/60 Superdex200 (GE Healthcare) equilibrated with buffer (50 mM Tris-HCl, pH 8.5, 1 mM DTT, 50 mM NaCl). Subunit A protein eluted at 13.75 ml volume (Figure 3.1.2B). Buffer exchange was performed for the eluted protein during concentration

process using 50 kDa concentrators (Amicon) in a stepwise manner such that the pH of the elution buffer (50 mMTris-HCl, pH 8.5) was reduced gradually to 8.2 to 7.8 and finally the protein was obtained in the crystallization buffer (50 mMTris-HCl, pH 7.5). The purity of the protein was ascertained by SDS gel (inset Figure 3.1.2B).

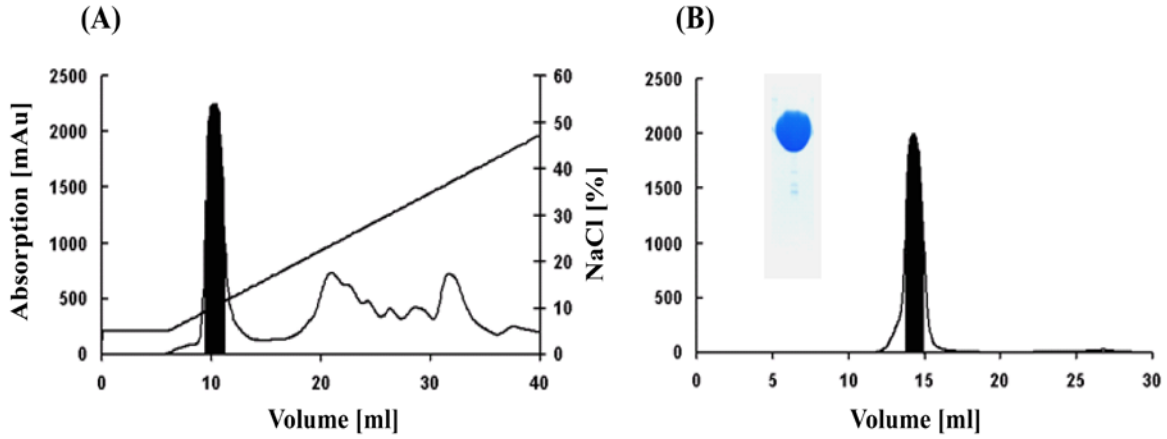

Figure 3.1.2. **Purification of subunit A.** (A) Purification of subunit A by a linear gradient of NaCl (0.05 - 1.0 M) on an anion exchange column Resource Q (6 ml). (B) The fractions containing subunit A was applied onto a column of 26/60 Superdex200 (GE Healthcare) equilibrated with buffer (50 mM Tris-HCl, pH 8.5, 1 mM DTT, 50 mM NaCl). The subunit A protein eluted at 13.75 ml volume. Inset picture shows 1 µl of purified protein on an SDS-PAGE (KUMAR *et al*., 2009b).

3.1.2 Determination of ATP hydrolysis and nucleotide binding traits of subunit A

The ability of subunit A to hydrolyze ATP was determined using Malachite Green Assay Kit (Cayman). The principle of the assay is based on the complex formation between malachite green molybdate and free orthophosphate under acidic conditions. The formation of the green colored molybdophosphoric acid complex (absorption maximum at 620 nm) is directly related to the free organic phosphate concentration in the solution. The results showed that there was no release of free phosphate and hence no hydrolysis of MgATP could be observed. Similar results were also obtained in the lab of Prof. Renate Genswein (Germany). The nucleotide-binding traits of the wild-type subunit A was determined using isothermal titration calorimetry (ITC) (Figure 3.1.3). For all the reactions, each injection gave a negative heat of reaction indicating that the overall reactions were exothermic in nature. The binding isotherms fit to a single set of binding site model, suggesting an equimolar binding between nucleotides and the protein. Negative ΔG values for each reaction show that the interaction between nucleotides and the protein is thermodynamically allowed. The calculated K_d values for wild-type subunit A were 2.38 µM and 1.50 µM for Mg-ATP and Mg-ADP, respectively (Table 3.1.1). The measured K_d values showed the preferential binding of MgADP to subunit A protein.

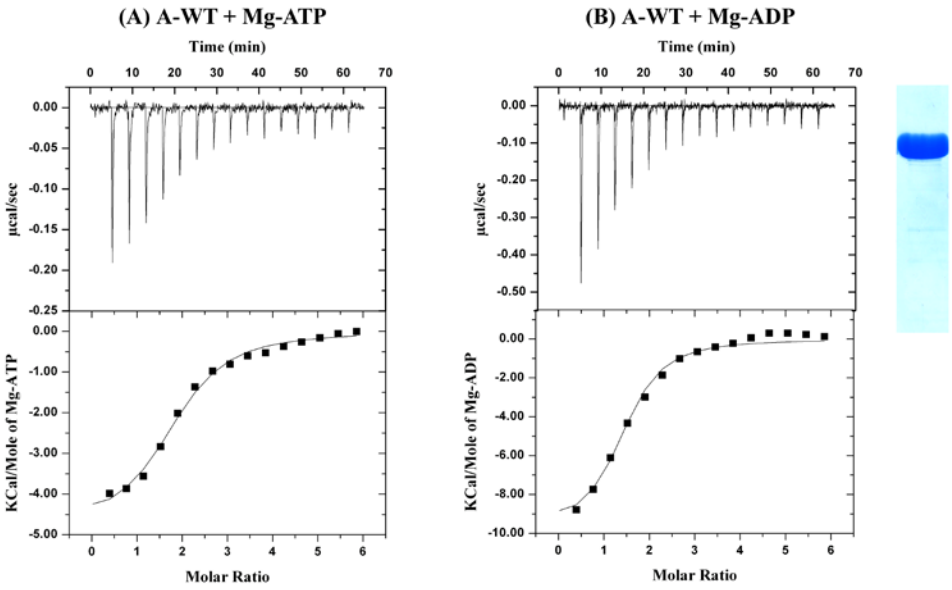

***Figure 3.1.3*. Nucleotide binding affinity measurements for subunit A (WT) using isothermal titration calorimetry**. Representative ITC profiles are shown for A-WT with Mg-ATP (*A*) and Mg-ADP (*B*), respectively. The nucleotides (0.5 mM ATP or ADP) were titrated in 1.5 µl injections against 10.0 µM of the protein, placed in the sample cell in a MicroCal iTC200 microcalorimeter (Microcal, Northampton, UK). All the experiments were performed in 50 mM Tris-HCl, pH 7.5, under identical conditions at 25 °C. The top panel in the figures show the injection profile after baseline correction and the bottom panels show the integration (heat release) for each injection (except the first one). The solid lines in the bottom panel reveal the fit of the data to a function based on a one-site binding model. Inset picture shows 1 µl of the protein on an SDS-PAGE (KUMAR *et al*., 2009b).

	K_a (x10^6 M^{-1})	K_d (µM)	ΔH (kcal/mol)	ΔG (kcal/mol)
A-WT + Mg-ATP	0.42 ± 0.07	2.38	- 4.80 ± 0.19	- 7.66
A-WT+ Mg-ADP	0.66 ± 0.17	1.50	- 9.8 ± 0.56	- 7.95

Table 3.1.1. Nucleotide binding affinity measurements for subunit A (WT).

3.1.3 Crystallization and co-crystallization of subunit A (WT) with nucleotides

Crystallization setup for subunit A (WT) and its mutant proteins were done according to a modified protocol of MAEGAWA *et al.* (2004) using hanging-drop vapor diffusion method. Subunit A crystals were obtained by the hanging-drop vapor diffusion method at 18 °C from a solution containing 50% (v/v) 2-Methyl-1,3Propanediol (MPD) and 0.1 M sodium acetate, pH 4.5 (Figure 3.1.4A). Accordingly, in the modified condition, 2 µl protein solution was mixed with an equal volume of reservoir solution and equilibrated against 500 µl reservoir solution. Paraffin oil and silicone oil (v/v 1:1) were gently overlaid onto the mother liquor to a final volume of 200 µl. In general, for subunit A (WT), the nucleation process begins in 6 to 8 hours leading to several small crystallites. The overlaying of paraffin oil and silicone oil thus assisted to prolong the nucleation time and hence large sized diffraction quality crystals could be

obtained. Figure 3.1.4A shows the crystal image of the subunit A (WT) which could be successfully crystallized. For co-crystallization with nucleotides, the purified subunit A was divided into three batches and incubated separately with 2 mM MgATP, –MgADP and –MgAMPPNP, respectively at 4 °C for 30 minutes on a sample rotator and this mixture was then concentrated to 10 - 12 mg/ml and the protein-ligand complexes were then set up for crystallization in the same optimized conditions in hanging drop plates and incubated at 18 °C.

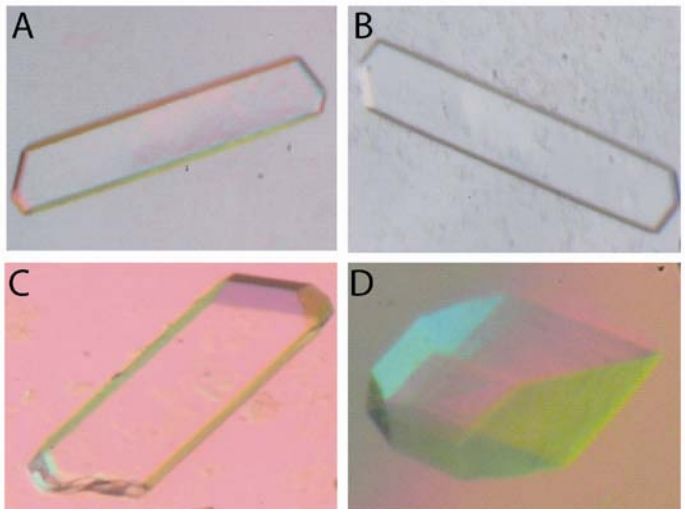

***Figure 3.1.4*. Crystals of subunit A (WT).** The subunit A (WT) was crystallized in the absence and presence of nucleotides (Mg-ATP, Mg-ADP or Mg-AMPPNP). (A) Crystal of subunit A (WT) empty form; crystal of A (WT) in the presence of Mg-ATP (B), Mg-ADP (C) and Mg-AMPPNP (D). Crystal dimensions were 0.5 × 0.2 × 0.1 mm for empty form and in the presence of Mg-ATP and Mg-ADP. The dimesions for Mg-AMPPNP bound form were 0.2 × 0.2 × 0.2 mm.

Compared to the empty form, the nucleation rate for the nucleotide bound form was slow. Initial nucleation appears after 2 to 3 days. It was noted that the nucleation rate was slowest in the MgAMPPNP bound proteins and the crystal morphology for the same varied significantly. The presence of 50% (v/v) MPD in the crystallization buffer acted as a good cryo-protactant. Therefore, the crystals thus obtained were screened on in-house X-ray machines (Rigaku R-AXIS IV and MAR345) under cryo conditions (140 K) for diffraction. Figure 3.1.4B-D shows the crystal images of the subunit A (WT), which were successfully co-crystallized with nucleotides.

3.1.4 Data collection and structure determination

The crystals of nucleotide free empty form diffracted to a resolution of 2.47 Å, while the ADP and AMPPNP-bound forms of the wild type subunit A diffracted to a maximum resolution of 2.4 Å (Figure 3.1.5). All the crystals belong to tetragonal space group $P4_32_12$ and have similar unit cell parameters. The diffraction dataset were indexed, integrated and scaled using the HKL2000

suite of programs (OTWINOWSKI and MINOR, 1997). The wild type subunit A structure (PDB 1VDZ; MAEGAWA *et al.*, 2006) was used as a model for the structure determination by molecular replacement method using the program PHASER (McCOY *et al.*, 2007) and MOLREP (VAGIN and TAPLYAKOV, 1997).

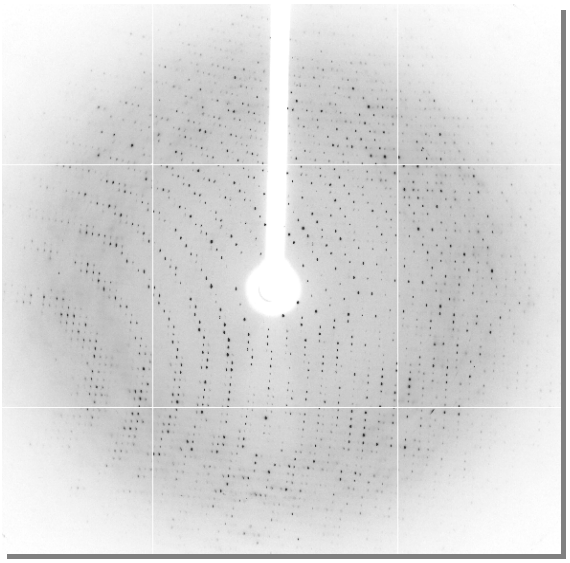

Figure 3.1.5. X-ray diffraction pattern of ADP bound subunit A (WT) crystal at a resolution of 2.4 Å.

Rigid body refinement was carried out followed by difference Fourier syntheses calculations. Inspection of the F_O–F_C and $2F_O$–F_C maps of protein-ligand complexes clearly showed electron density corresponding to the bound ligand. The ligand-bound form of subunit A was confirmed by omit map calculations using the CNS program (BRUNGER *et al.*, 1998). An undefined mutation during cloning at position 79 from Gly to Arg has taken place, which is clearly visible in the electron density map. Iterative cycles of model building and refinement were carried out using the programs COOT (EMSLEY and COWTAN, 2004) and REFMAC5 (MURSHUDOV *et al.*, 1997) of the CCP4 suite (1994). The geometry of the final models was checked with PROCHECK (LASKOWSKI *et al.*, 1993) and the figures are drawn using the program PyMOL (DeLANO, 2002). Structural comparison analysis were carried out using the SUPERPOSE program (KRISSINEL and HENRICK, 2004) as included in the CCP4 suite.

3.1.5 Structure of the ADP bound form of subunit A

Subunit A from *P. horikoshii* OT3 was successfully co-crystallized with Mg-ADP and I determined the structure of ADP bound form of subunit A (A_{DP}) to a resolution of 2.4 Å (Figure 3.1.6) (KUMAR *et al.*, 2009b). The structure was solved using molecular replacement method. The overall structure of the ADP bound form of subunit A (A_{DP}) has approximate

dimensions of 55 × 55 × 100 Å and can be divided into four major domains: an N-terminal domain (domain I (blue), residues 1-79, 110-116, 189-199), a knob-like β–sheet structure (domain II (red), residues 117-188), a nucleotide binding α–β domain (domain III (yellow), residues 80-99, 200-437) and a C-terminal α–helical domain (domain IV (green), residues 438-588) (Figure 3.1.6). The N-terminal domain (domain I) is primarily made up of loops and β sheets. Most of the residues in this domain could not be assigned due to lack of clear electron density as a result of high order of flexibility leading to high B factor values. The domain II (residues 117-188) is flanked by the N-terminal domain I and the nucleotide binding domain III, constitutes a part of the Non-Homologous Region (NHR), which in turn is made up of 90 amino acids (spanning residues P122 to P210 of the subunit A of the A_1A_O ATP synthase from *P. horikoshii* OT3) (Figure 3.1.6).

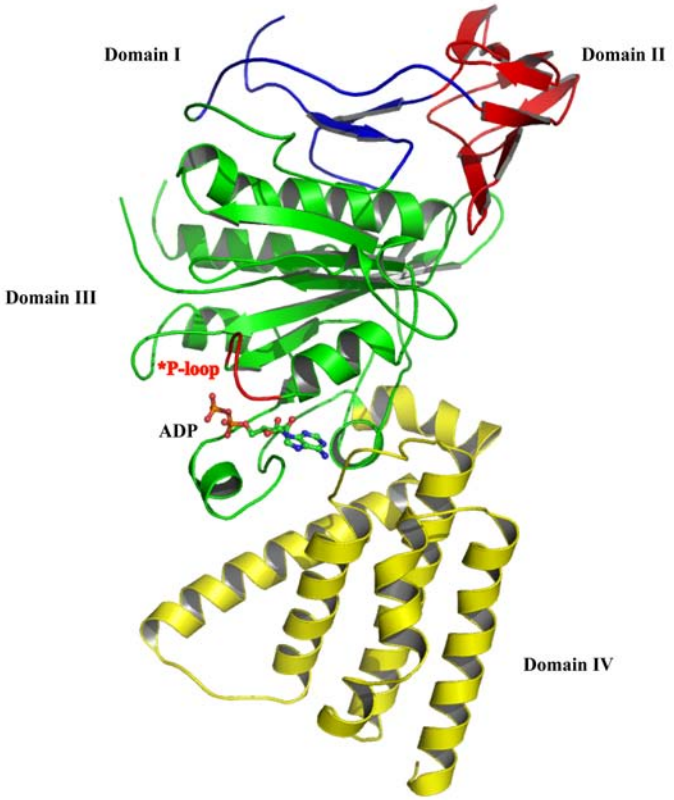

Figure 3.1.6. Crystal structure of the ADP bound form (A_{DP}) of subunit A from *Pyrococcus horikoshii* OT3 in cartoon representation (PDB: 3I73) (KUMAR *et al*., 2009b). The four domains of subunit A are labelled in different colour codes. The P-loop region ($_{234}$GPFGSGKT$_{241}$) is highlighted in red. The ADP molecule that is bound near the P-loop is shown in ball and stick representation.

The NHR domain is highly conserved in the nucleotide binding subunit A of A-ATP synthases and V-ATPases but the β subunits of F-type ATP synthases do not possess this domain. Domain II is made up of eight β-strands, which are folded into a β-sandwich structure with two fold symmetry and according to the subunit topology model proposed for A_1A_O ATP synthase

(COSKUN *et al*., 2004a; COSKUN *et al*., 2004b) it corresponds a the knob-like structure in the electron microscopy projection in the entire complex it is located such that it protrudes towards the opposite side of the central rotor, suggesting that the domain II might form a part of the peripheral stalk connecting A_1 and A_O domains in the entire A_1A_O complex. The nucleotide binding domain III in subunit A is an α–β domain comprised of residues 80-99 and 200-437 (Figure 3.1.6). Similar to the catalytic β subunit of F ATP synthases, two nucleotide binding motifs, the Walker A motif ($_{234}$GPFGSGKT$_{241}$), and the Walker B motif ($_{320}$RDMGYDDVALMAD$_{331}$), are conserved in subunit A. The C-terminal α–helical domain (domain IV) spans residues 438-588 (Figure 3.1.6). The final model of the ADP bound structure has good stereochemistry as can be inferred from the Ramachandran plot statistics (Table 3.1.2). The detailed statistics for data collection, phasing, and structure refinement are given in Table 3.1.2. In addition to the bound nucleotide (ADP), three 2-methyl-2,4 pentanediol (MPD), an acetate and a TRIS molecule were identified in the final model. A total of 310 water molecules could be assigned. The final electron density map for the structure has good density for almost all of residues except for the residues 1-62 and 340-353. These residues belong to the N-terminal domain and some regions of the nucleotide binding α–β domain (domain III). This high degree of disorder could be attributed to the fact that subunit A was not crystallized in complex with the other constituent subunits (like subunit B and D) which form the complete A_1 head piece of the entire A_1A_O ATP synthase. Other reason being the high solvent content (62.41 %) in the subunit A crystals. During the structure refinement procedure the ADP molecule could be identified very clearly from the positive peak in the difference Fourier maps (F_O–F_C and $2F_O$–F_C) (Figure 3.1.7). In the A_{DP} structure the nucleotide is found to have stabilizing interactions with the surrounding amino acids (Figure 3.1.7). All the three oxygen atoms of the β-phosphate make a tri-furcated hydrogen bond with a water molecule and one of the oxygen atoms also makes a hydrogen bond interaction with one another water molecule. The S238 of the phosphate binding P-loop makes hydrogen bonding with oxygen atoms of α- and β-phosphates of the ADP molecule via a water molecule. The oxygen atom of the α-phosphate also makes a polar interaction with the main chain carbonyl atom of the P-loop residue, K240. Similarly, the adenine moiety of the ADP molecule is nicely stabilized inside the adenine-ribose binding pocket, which shares a π–π interaction with the aromatic residues F427 and F508. The main chain carbonyl atom of Q505 makes a bifurcated hydrogen bonding with the nitrogen atoms (N1 and N6) of the adenine ring. The N6 atom of the adenine ring interacts via a hydrogen with one of the water molecule. The oxygen atom of the ribose ring shares polar interactions with the backbone amino groups of V242 and T243.

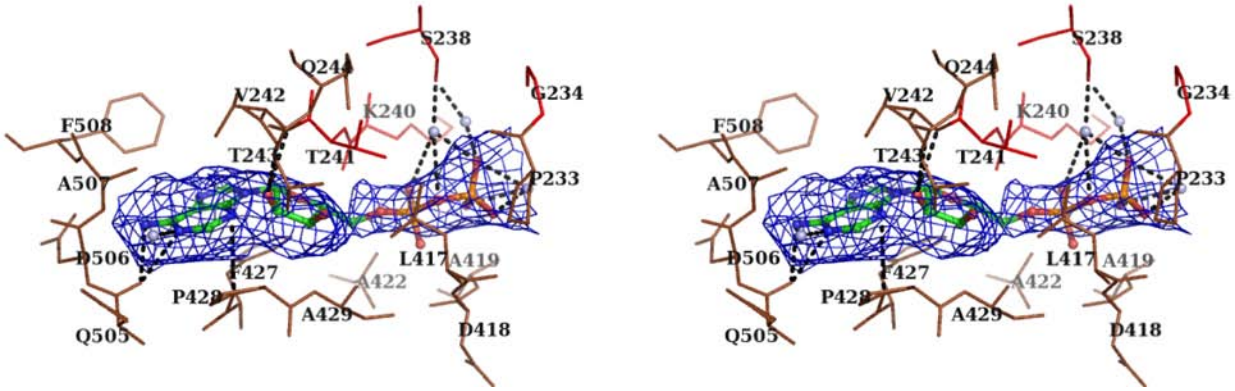

Figure 3.1.7. ADP binding region of A_{DP} with omit map (F_O-F_C) contoured at 2.5 σ-level (blue). The surrounding amino acids within 5 Å radius are represented by stick with water molecules shown as spheres. The hydrogen bonds are shown by black dotted lines (KUMAR *et al*., 2009b).

	A_{DP}
Data collection statistics	
Wavelength (Å)	0.97
Space group	$P4_32_12$
Unit cell parameters (Å)	
a = b =	128.47
c =	104.99
α = β = γ (°)	90
Resolution range (Å)	30.0 - 2.40
Solvent content (%)	62.46
Number of unique reflections	32954
I/σ^a	53.2 (5.1)
Completeness (%)	99.8 (100.0)
R merge[b] (%)	5.1 (45.7)
Multiplicity	8.6 (8.9)
Refinement statistics	
R factor[c] (%)	22.5
R free[d] (%)	25.8
Number of amino acid residues	512
Number of water molecules	295
Number of MPD molecules	3
Number of Acetate molecules	1
Number of TRIS molecules	1
Ramachandran statistics	
Most favored (%)	88.1
Additionally allowed (%)	9.4
Generously (%)	2.5
Disallowed (%)	0.0
R.M.S. deviations	
Bond lengths (Å)	0.013
Bond angles (°)	1.62

	A_{DP}
Mean atomic B values	
Protein atoms	57.50
Nucelotide	54.88
Overall	57.50
Wilson plot	56.30

[a] Values in parentheses refer to the corresponding values of the highest resolution shell (2.49 –2.40).

[b] $R_{merge} = \Sigma\Sigma_i|I_h - I_{hi}|/\Sigma\Sigma_i I_h$, where I_h is the mean intensity for reflection h.

[c] R-factor = $\Sigma||F_O| - |F_C||/\Sigma|F_O|$, where F_O and F_C are measured and calculated structure factors, respectively.

[d] R-free = $\Sigma||F_O| - |F_C||/\Sigma|F_O|$, calculated from 5% of the reflections selected randomly and omitted during refinement.

Table 3.1.2. Statistics of crystallographic data collection and refinement for the A_{DP} structure of subunit A.

3.1.6 Structure of the nucleotide-free form of subunit A

The structure of subunit A (WT) empty form (A_E) was determined together with Dr. Malathy Sony Subramanian Manimekalai to a resolution of 2.47 Å. The structure was solved using molecular replacement method (Figure 3.1.8A). The final model of the subunit A empty form contains one sulphate ion, three MPDs, an acetate and a TRIS molecule in addition to 310 water molecules (Figure 3.1.8A). The B factor for the bound sulphate ion is 88.10. The presence of sulphate ion is plausible since the protein purification involved a step of ammonium sulphate precipitation. The final electron density map for the structure has good density for almost all of the residues except for the residues 1-60 and 341-354 which belong to the N-terminal domain and some regions of the nucleotide binding α–β domain (domain III). In the structure, the side chains for the N-terminal P61-V66 residues could be assigned and density for three of the amino acid residues G355, Y356 and P357 in the central domain were identified, which were missing in the recently determined 2.55 Å structure (MAEGAWA *et al*., 2006). Interestingly, the sulphate ion (SO_4^{2-}) binds to the P-loop region ($_{234}$GPFGSGKT$_{241}$) by interacting via a water molecule with S238 (Figure 3.1.8B). This water bridge interaction is very strong as the water molecule makes bifurcated hydrogen bond with two of the oxygen atoms in the sulphate molecule. Two more oxygen atoms of the sulphate molecule interact with three water molecules through one bifurcated and two hydrogen bonds such that it is well stabilized in the structure. The sulphate interaction with various residues within 5 Å is shown in figure 3.1.8B. In addition to the non-polar interactions from G234, P233, F399, L417 and A419, the polar non-bonded interactions from T241, K240 and D418 help position the sulphate molecule in this orientation. The statistics for data collection, phasing, and structure refinement is given in appendix section.

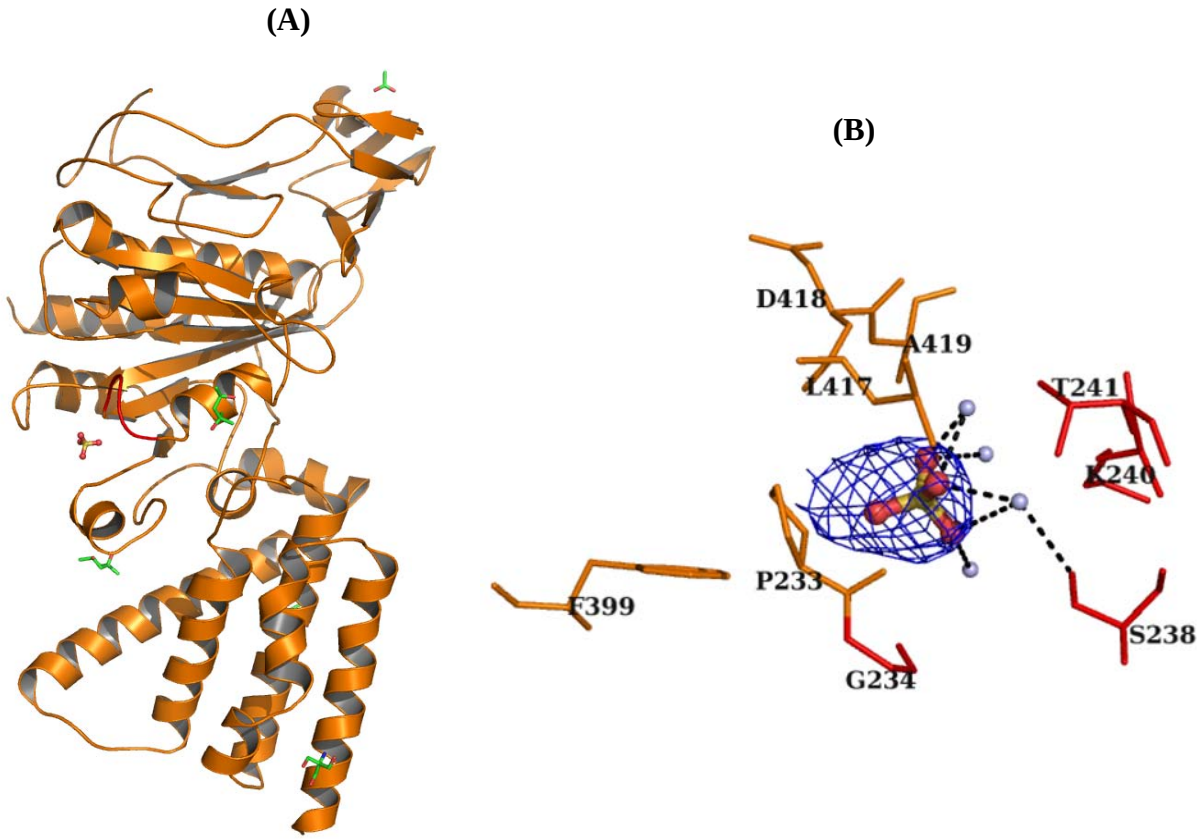

Figure 3.1.8. (A) Crystal structure of the empty form of subunit A from *Pyrococcus horikoshii* OT3 in cartoon representation (PDB 3I72). The P-loop region ($_{234}$GPFGSGKT$_{241}$) is highlighted in red. The sulphate molecule that is bound near the P-loop is shown in ball and stick representation. The other solvent molecules MPD, TRIS and acetate molecules are shown in stick representation. (B) Binding region of the sulphate molecule within 5 Å radius in the empty structure. The sulphate (ball and stick representation) omit electron density map (F_O-F_C) contoured at 3.0 σ-level is shown in blue while the amino acid residues surrounding it are shown in sticks. The P-loop residues are coloured red. The water molecules that interact with sulphate are given in light blue sphere and the hydrogen bonding interactions are shown in dotted lines (KUMAR *et al*., 2009b).

3.1.7 Structure of the AMPPNP bound form of subunit A

I successfully co-crystallized subunit A from *P. horikoshii* OT3 with the non-hydrolyzable ATP-analogue, Mg-AMP-PNP (5'-adenylyl-β,γ-imidodiphosphate) and the structure (A_{MP}) was determined to 2.4 Å resolution by Dr. Malathy Sony (Figure 3.1.9). The detailed statistics for data collection, phasing, and structure refinement are given in the appendix section. Similar to the A_E structure, the electron density map for the structures show good density for almost all of the residues, except for the residues 1-60 and 342-345. It is worth mentioning here that when compared to all the other structures the region 340-355 (which belong to the nucleotide binding domain III) is clearly well defined in the A_{MP} form with as many as ten residues were identified. The residues 340-355 of the domain III occupy a place just above the nucleotide binding P-loop region. The final structure has good stereochemistry as can be inferred from the Ramachandran plot statistics given in the appendix section. In addition to the bound nucleotides, three MPD, an acetate and a TRIS molecule were also identified in the structure.

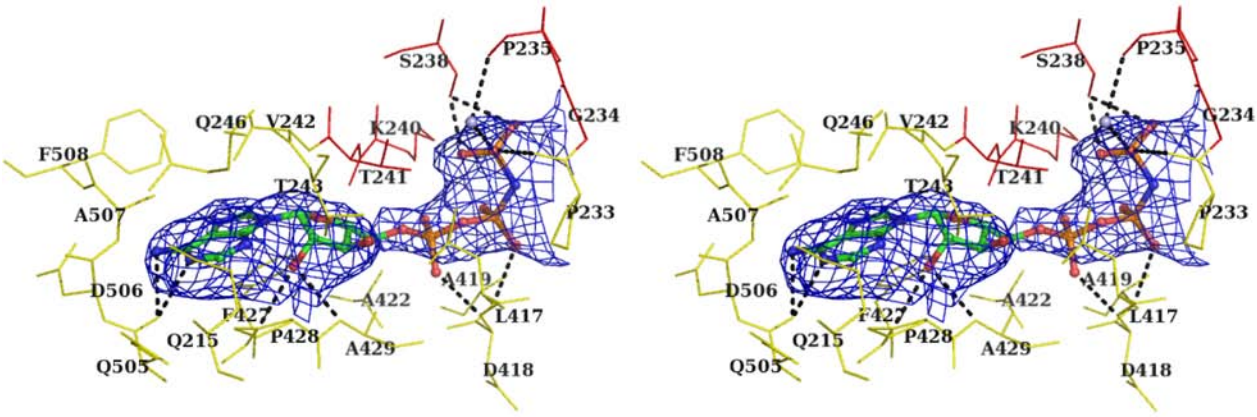

Figure 3.1.9. AMPPNP binding region in A_{MP} with omit map (F_O-F_C) contoured at 2.5 σ-level (blue). The surrounding amino acids (5 Å region) are represented by stick with water molecules in sphere. The hydrogen bonds are given by black dotted lines (KUMAR *et al*., 2009b).

Overall the structure is similar to the empty form (A_E) and the ADP bound form (A_{DP}) and consist of the four domains (Figure 3.1.6A and 3.1.7A). During the structure refinement procedure the AMP-PNP molecule could be identified very clearly from the positive peaks in the difference Fourier maps (F_O–F_C and $2F_O$–F_C) in the structure (Figure 3.1.9). The AMP-PNP molecule in the A_{MP} structure is well stabilized by both hydrophilic and hydrophobic interactions. The residues within 5 Å region of the AMP-PNP molecule are shown in figure 3.1.9. Two of the oxygen atoms of the γ–phosphate form a bifurcated hydrogen bond with the side chain oxygen atom of the P-loop residue S238 and the other oxygen atom interacts with P233 main chain carbonyl oxygen atom and a water molecule, which again interacts with P235 main chain carbonyl oxygen atom. One of the β–phosphate oxygen atoms interact with the main chain nitrogen atom of the A419 residue and the α–phosphate is held in place through hydrogen bonding interaction with the main chain nitrogen atom of the D418 to its oxygen atom. The P-loop residues T241, K240, P235 and G234 surround the phosphate groups and interact through van der Waals forces. The sugar ring oxygen atom makes bifurcated hydrogen bond with the main chain nitrogen atom of P428 and A429. Furthermore, the five-membered ring in the adenine moiety forms offset π–π interaction with F427 and the N1 and N6 nitrogen atoms of the adenine ring form bifurcated hydrogen bond with the main chain carbonyl oxygen atom of Q505. In addition, the adenine ring is also stabilized by van der Waals interaction from the D506, A507, F508, Q246, Q215, T243 and V242 residues.

3.1.8 Structural comparison of the nucleotide bound structures with the empty form

3.1.8.1 Structural comparison of A_E and A_{DP}

Structural overlap of the A_{DP} and A_E structures yielded an r.m.s.d. of 0.666 Å for the backbone

Cα atoms (Figure 3.1.10A). Larger than average deviation were concentrated on the following regions E93 – P110 (T99 – 1.93 Å), C261 – E273 (G262 – 3.56 Å), S334 – Y356 (W336 – 6.68 Å) and G397 – V403 (P402 – 2.73 Å). The short helix in the nucleotide binding domain III in the region C261 – E273 is disordered, probably indicative of ligand binding disturbances. P-loop residues G234, P235, K240 and T241 show notable side chain deviations, wherein T241 and S238 are showing maximum and minimum alterations, respectively (Figure 3.1.10B). In addition, analysis of side chain deviations for the residues that have interaction with the adenine molecule showed that along with the P-loop disturbances, T243 and P428 has significant differences (Figure 3.1.10B).

3.1.8.2 Structural comparison of A_E and A_{MP}

The empty form (A_E), when compared with the AMPPNP bound structure shows an overall r.m.s. deviation of 0.849 Å indicating more similarity of A_{DP} relative to the A_{MP} bound form (Figure 3.1.10A) for the backbone Cα atoms. Similar structural deviation profile as that of the A_{DP} structure was also observed for the regions; N-terminal, P91-P110 (maximum deviation occurring for V94 with 3.66 Å), G262 – G265 (G262 – 1.81 Å) and R335 – A358 (L340 – 9.90Å).

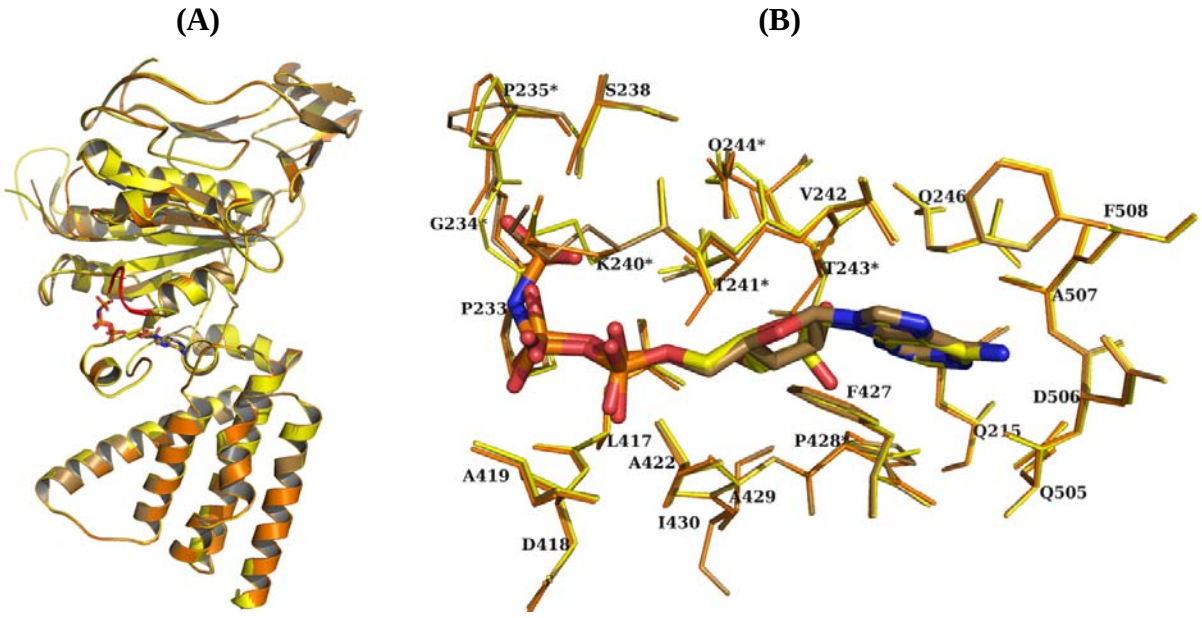

Figure 3.1.10. (A) Structure comparison between the A_E (orange, PDB 3I72), and A_{MP} (yellow, PDB 3I4L) and A_{DP} forms (sand, PDB 3I73) of subunit A. (B) Side chain variations for the nucleotide (stick) binding region indicating the conformational change (starred) in T243, Q244 and P428 residues in addition the P-loop region (KUMAR *et al*., 2009b).

Few of the individual residues, G234 and D270, also show significant differences in the backbone Cα atom. G234 belongs to the P-loop region while D270, that is present in the short

helix which connects the loop region G262-G265 above the P-loop, disrupts the orderliness in the A_{MP} structure when compared with the A_E form. Significant side chain deviations in the P-loop region are noted for the residues G234, P235, K240, and T241 (Figure 3.1.10B). Furthermore, if the side chain deviations for the residues in the adenine-pocket are analyzed, significant deviations are noted for the residues T243, Q244 and P428 (Figure 3.1.10B).

3.1.8.3 Structural comparison of A_{MP} and A_{DP}

AMP-PNP and ADP bound structures reveal a r.m.s. deviation of 0.582 Å, when they both are superimposed with respect to the Cα atoms. The segments of P91 – V107 (V94 – 3.36 Å), C261 – E273 (G262 – 3.5 Å), S334 – P358 (W336 – 3.52 Å) and G397 – V403 (G397 – 2.42 Å) show considerable deviations. The short helical region C261-E273 belonging to domain III, above the P-loop is predicted to be disturbed due to nucleotide binding and it shows orderliness in the N-terminal when AMP-PNP is bound, whereas it is ordered in the C-terminal when ADP is bound. G234 in the P-loop also reveals significant backbone deviation, while for the residues P235 and K240 side chain differences are noted (Figure 3.1.10B). These differences indicate that T241 makes a conformational change when nucleotide binds to the P-loop region and other residues such as G234, P235 and K240 flexibly interacts with the nucleotide. When the residues surrounding the nucleotides are compared, Q244 and P428 show deviations in their side chain atoms (Figure 3.1.10B). Q244 will presumably differentiate the two nucleotides and changes conformation according to the ligand bound to it, whereby P428 flexibly interacts with the adenine ring.

3.1.9 P-loop mutants of subunit A

The availability of nucleotide bound structures (A_{DP} and A_{MP}) of subunit A has enabled us to identify the amino acids interacting with the nucleotides and thereby allowing us to select the ideal candidates for mutations in order to get an insight into the role of individual amino acids in nucleotide binding and catalysis events. F236, S238 and G239 are the amino acid residues, in the P-loop which appear to have a structural role in maintaining the characteristic strained conformation of this loop region in subunit A, while K240 and T241 are presumed to be the residues, which take part in catalytic events. Therefore, five different mutant constructs F236A, S238A, G239A, K240A and T241A of subunit A were planned in the P-loop region ($_{234}$GPFGSGKT$_{241}$) of subunit A. All the mutant constructs of subunit A were successfully produced by overlap extension polymerase chain reaction (PCR) method (Ho *et al*., 1989) as described in section 2.15 (Figure 3.1.11A-B).

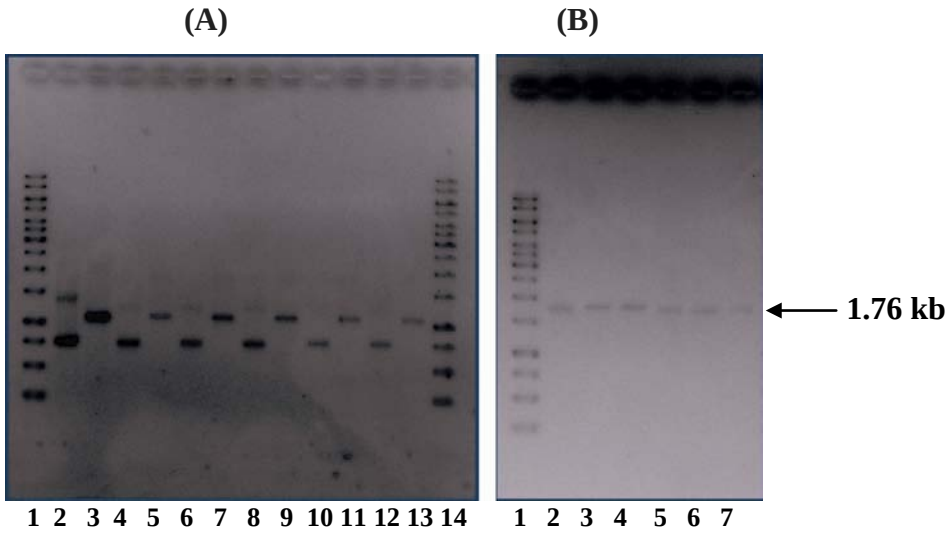

***Figure 3.1.11*. PCR amplification of subunit A (WT) and its mutants.** (A) PCR I products; Marker DNA (1Kb, Fementas) (*lane 1* and *14*); A (WT) (*lane 2* and *3*); F236A (*lane 4* and *5*); S238A (*lane 6* and *7*); G239A (*lane 8* and *9*); K240A (*lane 10* and *11*); T241A (*lane 12* and *13*). (B) PCR II products; Marker DNA 1 (Kb, Fermentas) (*lane 1*); A (WT) (*lane 2*); F236A (*lane 3*); S238A (*lane 4*); G239A (*lane 5*); K240A (*lane 6*); T241A (*lane 7*).

3.1.10 Determination of nucleotide binding traits and ATP hydrolysis for S238A mutant

The mutant protein was isolated according to modified protocol for the purification of wild type subunit A (KUMAR *et al*., 2009b). The nucleotide-binding traits of the S238A mutant of subunit A was determined using isothermal titration calorimetry (ITC) (Figure 3.1.12).

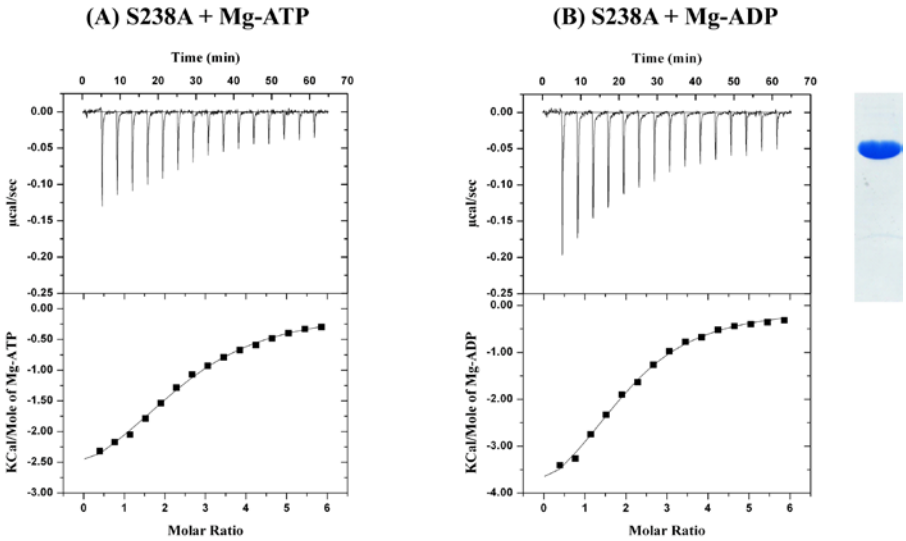

***Figure 3.1.12*.** Determination of nucleotide binding affinity for S238A mutant using ITC (KUMAR *et al*., 2009b). Representative ITC profiles are shown for the mutant S238A with Mg-ATP (*A*) and Mg-ADP (*B*), respectively. The nucleotides (0.5 mM ATP or ADP) were titrated in 1.5 µl injections against 10 µM of the protein, using MicroCal iTC200 microcalorimeter. All the experiments were performed in 50 mM Tris-HCl, pH 7.5, under identical conditions at 25 °C. The top panel in the figures show the injection profile after baseline correction and the bottom panels show the integration (heat release) for each injection (except the first one). The solid lines in the bottom panel reveal the fit of the data to a function based on a one-site binding model. Inset picture shows 1 µl of the mutant protein on an SDS-PAGE.

For all the reactions, each injection gave a negative heat of reaction indicating that the overall reactions were exothermic in nature. The binding isotherms fit to a single set of binding site model, suggesting an equimolar binding between nucleotides and the protein. Negative ΔG values for each reaction show that the interaction between nucleotides and the protein is thermodynamically allowed. The calculated K_d values for the mutant S238A was 8.47 µM for Mg-ATP, and 6.50 µM for Mg-ADP, respectively (Table 3.1.3). The measured K_d values showed the preferential binding of MgADP to S238A mutant of subunit A protein. The ability of the S238A mutant to hydrolyze Mg-ATP was checked using phosphate release assay as described in section 3.1.2. No hydrolysis of Mg-ATP could be observed.

	K_a (x10^6 M^{-1})	K_d (µM)	ΔH (kcal/mol)	ΔG (kcal/mol)
S238A+ Mg-ATP	0.118 ± 0.01	8.47	- 3.30 ± 0.12	- 6.91
S238A+ Mg-ADP	0.152 ± 0.014	6.50	- 4.88 ± 0.19	- 7.06

Table 3.1.3. Nucleotide binding affinity measurements for S238A mutant of subunit A.

3.1.11 Crystallization and structure determination of the S238A mutant of subunit A in the presence and absence of AMPPNP

3.1.11.1 Crystallization of S238A mutant of subunit A

The S238A mutant protein has been successfully crystallized using the same procedure as discussed in section 3.1.3. The crystals for the empty form and AMPPNP co-crystallized form of the mutant were obtained.

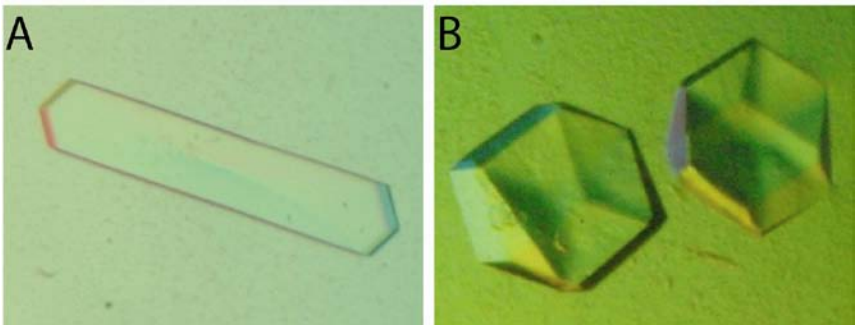

***Figure 3.1.13*. Crystals of S238A mutant of subunit A.** (A) Crystal of S238A empty form (dimensions: 0.5 × 0.2 × 0.1 mm); (B) crystal of S238A in the presence of Mg-AMPPNP (dimensions: 0.2 × 0.2 × 0.1 mm).

3.1.11.2 Structure determination of S238A mutant of subunit A

The structure of S238A was determined to 2.4 Å using molecular replacement method (Figure 3.1.13A). The structure was solved by Dr. Manikkoth Balakrishna Asha. Similar to the wild type structure, no interpretable densities were identified for the N-terminal 1-59 residues and for the

341-356 residues with all other amino acids showing good density. The final model has good stereochemistry and includes 512 amino acids, 3 MPD molecules, 1 Tris molecule and 267 water molecules (appendix). The X-ray diffraction datasets for the S238A protein crystals co-crystallized with MgAMPPNP were obtained at a resolution of 2.35 Å and were analyzed. These datasets upon refinement, does not show any density for the bound ligand (AMPPNP).

3.1.11.3 Structural comparison of the mutant S238A with A_E

Structural comparison of the mutant with the A_E form superposed with an r.m.s.d of 1.313 Å (Figure 3.1.14A). Larger than average deviation were concentrated on six regions that included the P-loop region in addition to the previously mentioned five regions; namely, N-terminal, L92 - T108 (R96 – 2.741 Å), P233 – T241 (G237 – 9.439 Å), C261 - Asn266 (E263 – 3.745 Å), S332 - A361 (L340 – 8.917 Å) and S393 - V403 (P398-5.03 Å). Because of the S238A mutation, the P-loop flips down into a relaxed form (Figure 3.1.14A). The r.m.s. deviation between the two structures in the P-loop region is 1.95 Å with maximum deviation occurring for the residue F236 and G237.

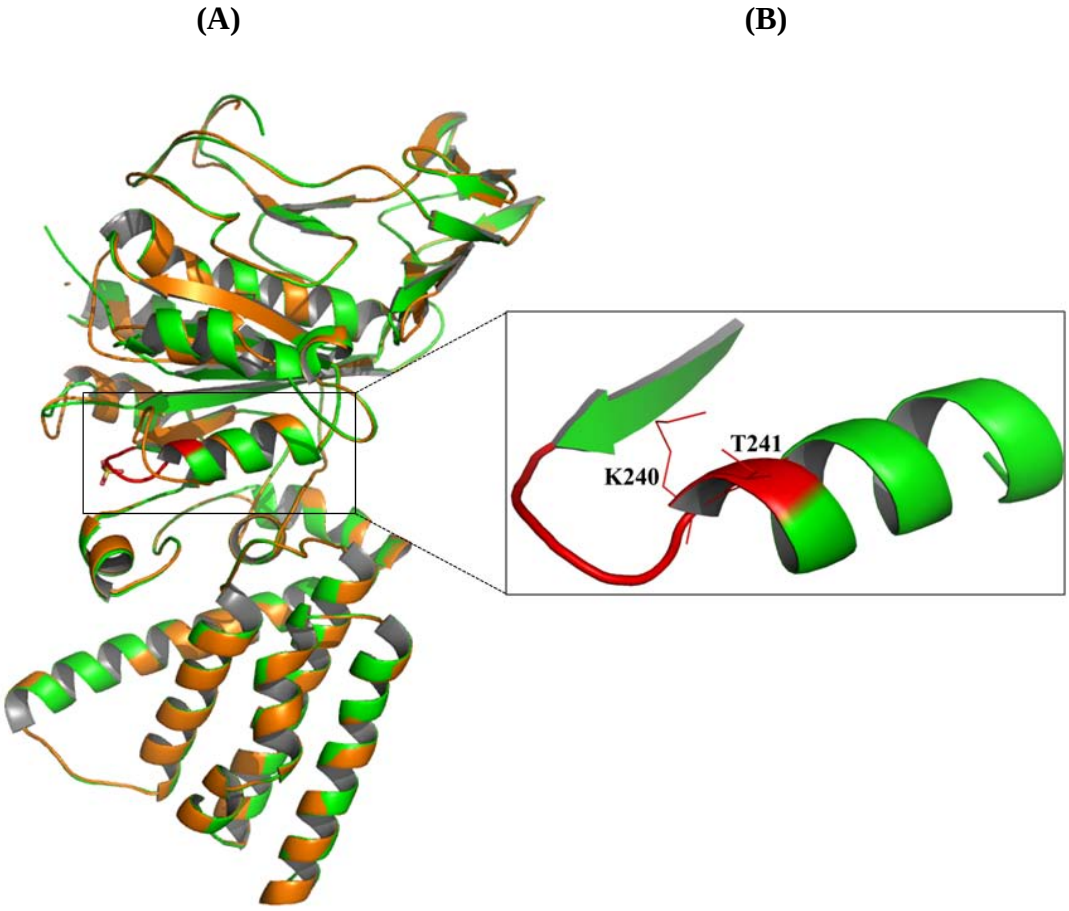

Figure 3.1.14. (A) Structural comparison of empty (orange, PDB 3I72) and S238A mutant (green, PDB 3IKJ) structures of subunit A (KUMAR *et al*., 2009b). The P-loop highlighted in red shows a momentous deviation. (B) The strand-loop-helix motif of the P-loop region of S238A structure.

In addition, when the side chains of the P-loop region are compared with the corresponding residues in the wild type, significant deviation could be noted for G234 (6.4 Å), P235 (8.03 Å), F236 (7.516 Å), G237 (9.43Å), A238 (7.05 Å), G239 (5.84), K240 (5.96 Å) and T241 (4.99 Å). During the structure refinement procedure P-loop region residues could be assigned very clearly from the positive peaks in the difference Fourier maps (F_O–F_C and $2F_O$–F_C) (Figure 3.1.14B). Moreover, the helical region in the strand-loop-helix motif is well formed, with the helix starting from K240, whereas in the empty structure it starts from T243 (Figure 3.1.14C). The other region of interest is the short helical region, C267 – E273 which is well structured in the mutant. Furthermore, the loop preceding the helix deviate significantly when compared with the wild type A subunit, with maximum deviation observed for E263 (3.705 Å).

3.1.12 Determination of nucleotide binding traits and ATP hydrolysis for K240A and T241A mutants of subunit A

Nucleotide binding to the mutants K240A and T241A of subunit A was determined using isothermal titration calorimetry (ITC) (Figure 3.1.15). The resultant injection profiles indicate that the overall reactions were exothermic in nature. The binding isotherms fit to a single set of binding site model, suggesting an equimolar binding between nucleotides and the protein. Negative ΔG values for each reaction show that the interaction between nucleotides and the protein is thermodynamically allowed. The calculated K_d values for the mutant T241A were 6.13 µM for Mg-ATP, and 4.04 µM for Mg-ADP, respectively (Table 3.1.4), and showed the preferential binding of Mg-ADP to the mutant protein. The result shows that K240A mutant of subunit A does not bind to either nucleotide. The ability of the mutants (K240A and T241A) to hydrolyze Mg-ATP was checked using phosphate release assay as described in section 3.1.2. No hydrolysis of Mg-ATP could be observed.

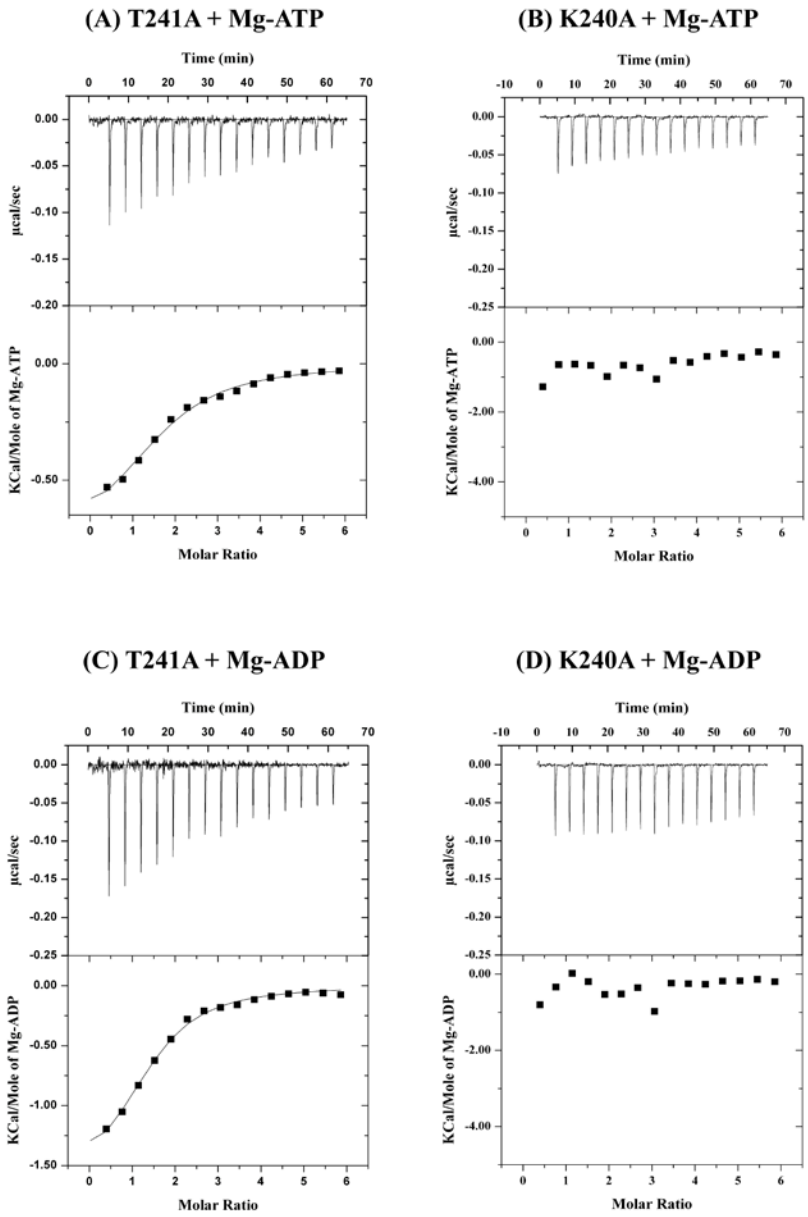

Figure 3.1.15. Determination of nucleotide binding affinity for K240A and T241A mutants using ITC. Representative ITC profiles are shown for the mutants T241A and K240A with Mg-ATP (*A*, *B*) and Mg-ADP (C, *D*), respectively. All the experiments were performed in 50 mM Tris-HCl, pH 7.5, under identical conditions at 25 °C.

	K_a (x10^6 M^{-1})	K_d (µM)	ΔH (Kcal/mol)	ΔG(Kcal/mol)
T241A+ Mg-ATP	0.163 ± 0.02	6.13	- 0.79 ± 0.06	- 7.11
K240A+ Mg-ATP	0	0	0	0
T241A+ Mg-ADP	0.25 ± 0.03	4.04	- 1.68 ± 0.08	- 7.34
K240A+ Mg-ADP	0	0	0	0

Table 3.1.4. Nucleotide binding affinity measurements for T241A and K240A mutant of subunit A.

3.1.13 Crystallization and structure determination of the K240A mutant of subunit A

3.1.13.1 Crystallization and data collection for K240A mutant of subunit A

The mutant K240A has been successfully crystallized using the same procedure as discussed in section 3.1.3. For K240A, crystals could be obtained for the empty form as well as ATP, ADP and AMPPNP co-crystallized conditions (Figure 3.1.16). The crystals of empty forms of K240A diffracted to a resolution of 2.4 Å. X-ray diffraction datasets were collected at 2.4 Å, 2.55 Å and 2.35 Å resolutions for Mg-ATP, Mg-ADP and Mg-AMPPNP bound forms, respectively.

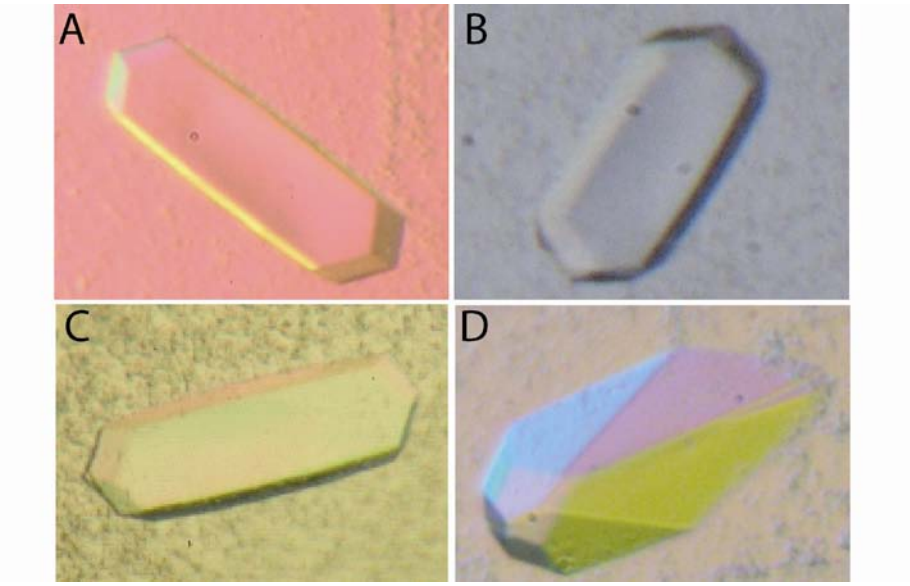

***Figure 3.1.16*. Crystals of K240A mutant of subunit A.** The mutants K240A and T241A were crystallized in the absence and presence of nucleotides (Mg-ATP, Mg-ADP and Mg-AMPPNP). (A) Crystal of K240A empty form; crystal of K240A in the presence of Mg-ATP (*B*), Mg-ADP (*C*) and Mg-AMPPNP (*D*). The crystal dimensions were 0.35 × 0.2 × 0.1 mm for empty form and in the presence of Mg-ATP and Mg-ADP. The dimesions for Mg-AMPPNP bound form were 0.3 × 0.2 × 0.2 mm.

3.1.13.2 Structure determination of K240A mutant of subunit A

I solved the nucleotide free structure of K240A mutant of subunit A from *Pyrococcus horikoshii* OT3 to a resolution of 2.40 Å using molecular replacement method (Figure 3.1.17A). The final model contains one sulphate ion, six MPDs and 310 water molecules. The detailed statistics for data collection, phasing, and structure refinement is given in Table 3.1.5. The overall structure is similar to the wild type and other nucleotide bound structures and consists of four domains. The final electron density map for the structure show good density for almost all of the residues except for the residues 1-62 and 341-356 and the stereochemistry of the model was checked using the Ramachandran plot statistics (Table 3.1.5). The $2F_O$-F_C map contoured at 1σ shows nice density for all the P-loop residues including A240. Similar to the wild type structure, a sulphate ion from the precipitant buffer binds to the P-loop region ($_{234}$GPFGSGKT$_{241}$) by interacting via a water molecule with S238 and A240 (Figure 3.1.17C). This water bridge

interaction is strong as the water molecule makes a hydrogen bond with one of the oxygen atoms in the sulphate molecule. Three more oxygen atoms of the sulphate molecule interact with one water molecule through hydrogen bonds such that it is well stabilized in the structure. The sulphate interaction with various residues within 5 Å is shown in Figure 3.1.17C. In addition to the non-polar interactions from L417, A419 and A422, the polar non-bonded interactions from T241, K240 and D418 help positioning the sulphate molecule in this orientation.

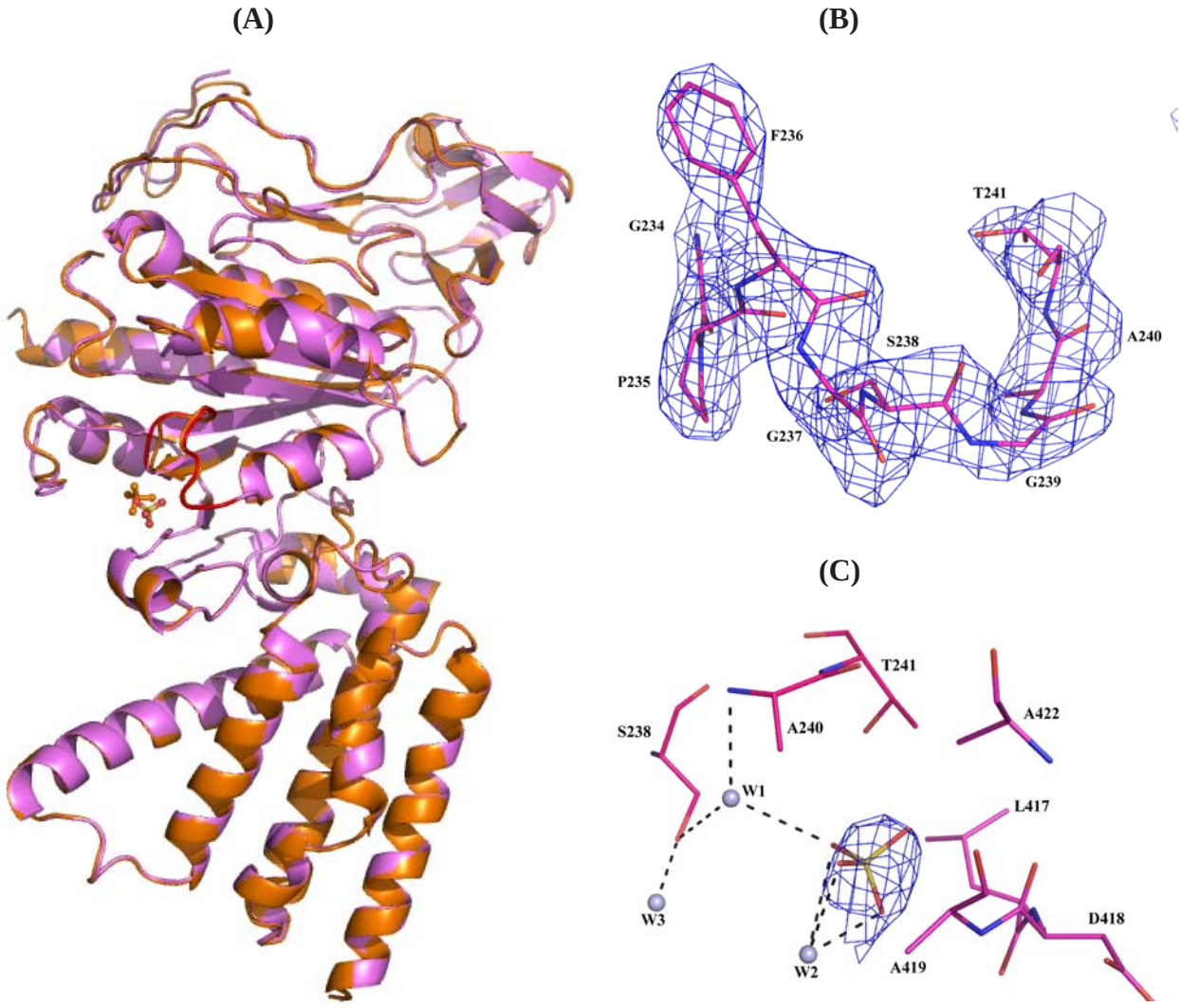

***Figure 3.1.17*. (A) Structural comparison of empty (orange, PDB 3I72) and K240A mutant structures of subunit A**. The P-loop region ($_{234}$GPFGSGKT$_{241}$) is highlighted in red. The sulphate molecule, that is bound near the P-loop in A-WT and K240A, is shown in ball and stick representation. (B) The $2F_O$-F_C electron density map contoured at 1.0 σlevel for the P -loop region in the K240A mutant. (C) Binding region of the sulphate molecule within 5 Å radius in the empty structure. The sulphate (ball and stick representation) omit electron density map contoured at 1.0 σ-level is shown in blue, while the amino acid residues surrounding it, are shown in sticks. The P-loop residues are coloured in red. The water molecules that interact with sulphate are given in light blue sphere and the hydrogen bonding interactions are shown in dotted lines.

3.1.13.3 Structural comparison of K240A with A_E, A_{DP} and A_{MP}

The structural comparison of K240A with A_E, A_{DP} and A_{MP}, yielded r.m.s deviations of 0.42 Å,

0.78 Å and 0.85 Å, respectively, indicating that the structures K240A and A_E are very much similar except for the region from G262 – E273, which form a small helical structure, located just above the P-loop region (Figure 3.1.17A). The relatively high r.m.s.d. values upon structural comparison of K240A with A_{DP}, A_{MP} might be attributed to the larger than average deviations in the regions (E93 – G100, C261 – E273, G397 – V403) and (L92 – D101, C262 – D270) for A_{DP} and A_{MP} structures, respectively. The K240A structure showed maximum structural differences when compared with S238A structure especially in the regions (G106 – T108, P140 – E141 and S393 – T407). The superposition of the P-loop residues from the K240A and A_E structures shows that the bound sulphate ions are not present at the same location in both the structures though the interaction profile is the same (Figure 3.1.18). Surprisingly, the orientation of the interacting hydroxyl group from S238 is directed in the opposite direction compared to that of the A_E form (Figure 3.1.17A). The structural overlap of P-loop regions from A_E, A_{DP}, A_{MP} and K240A of subunit A, showing side chain deviations for the P-loop residues have maximum deviation for G234, P235, S238 and T241 residues (Figure 18).

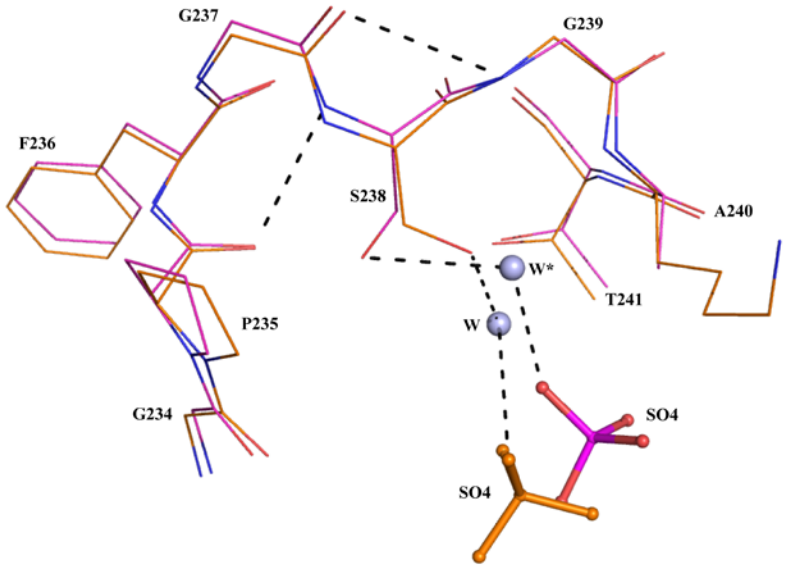

***Figure 3.1.18*. Superposition of the P-loop region from A_E (orange) and K240A (violet) of subunit A**. Bound sulphates are shown in sticks and the water molecules that interact with sulphate are given in light blue sphere and the hydrogen bonding interactions are shown in dotted lines.

3.1.13.4 Structure determination of K240A attempted to co-crystallized with nucleotides

The X-ray diffraction datasets for the K240A protein crystals co-crystallized with nucleotides were analyzed. In these datasets upon refinement, the initial electron density map does not show any density for any of the bound ligands (ATP, ADP or AMPPNP). Most strikingly, when compared to the K240A empty structure, in these structures, the density for the sulphate ion was also not observed.

	K240A
Data collection statistics	
Wavelength (Å)	1.0
Space group	$P4_32_12$
Unit cell parameters (Å)	
a = b =	127.81
c =	104.09
α = β = γ (°)	90
Resolution range (Å)	22.08 - 2.40
Solvent content (%)	62.39
Number of unique reflections	32281
I/σ^a	24.25 (3.77)
Completeness (%)	99.5 (99.9)
R merge[b] (%)	5.3 (47.7)
Multiplicity	6.8 (6.4)
Refinement statistics	
R factor[c] (%)	22.37
R free[d] (%)	27.24
Number of amino acid residues	508
Number of water molecules	278
Number of MPD molecules	6
Number of Acetate molecules	1
Number of TRIS molecules	-
Ramachandran statistics	
Most favored (%)	88.1
Additionally allowed (%)	11.4
Generously (%)	0.5
Disallowed (%)	0.0
R.M.S. deviations	
Bond lengths (Å)	0.017
Bond angles (°)	1.70
Mean atomic B values	
Protein atoms	55.58
Nucelotide	55.01
Overall	54.83
Wilson plot	

[a] Values in parentheses refer to the corresponding values of the highest resolution shell (2.49 – 2.40).

[b] $R_{merge} = \Sigma\Sigma_i|I_h - I_{hi}|/\Sigma\Sigma_i I_h$, where I_h is the mean intensity for reflection h.

[c] R-factor $= \Sigma||F_O| - |F_C||/\Sigma|F_O|$, where F_O and F_C are measured and calculated structure factors, respectively.

[d] R-free $= \Sigma||F_O| - |F_C||/\Sigma|F_O|$, calculated from 5% of the reflections selected randomly and omitted from the refinement.

Table 3.1.5. Statistics of crystallographic data collection and refinement for K240A mutant structure of subunit A.

3.1.14 Crystallization and structure determination of the T241A mutant of subunit A

The T241A mutant of subunit A has been successfully crystallized using the same procedure as discussed in section 3.1.3. Crystals could be obtained for the empty and ADP co-crystallized forms (Figure 3.1.19). The crystals of empty and ADP co-crystallized form diffracted to a resolution of 3.25 Å and 3.1 Å, respectively. The structure determination is under progress.

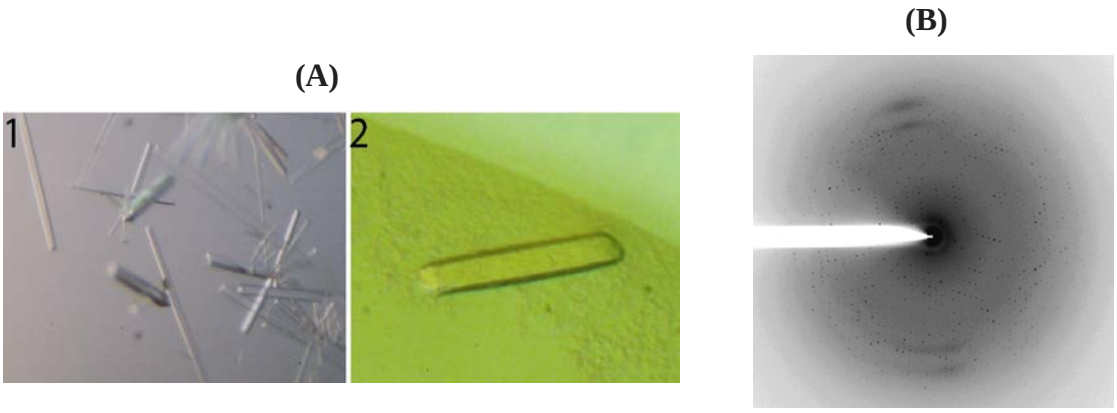

Figure 3.1.19. (A) Crystals of T241A mutants of subunit A in the absence (1) and in the presence of Mg-ADP (2). The crystal dimensions were 0.2 × 0.1 × 0.1 mm and 0.3 × 0.2 × 0.2 mm in the absence and presence of Mg-ADP. (B) Diffraction image of T241A mutant co-crystallized with 2 mM MgADP at 3.1 Å resolution.

3.1.15 Crystallization of the F236A and G239A mutants of subunit A

The mutants F236A and G239A have been successfully crystallized using the same procedure as discussed in section 3.1.3. The mutant proteins were crystallized in the absence and presence of nucleotides (2 mM MgATP, –MgADP or –MgAMPPNP). For both mutants, crystals could be obtained for the empty form and AMPPNP co-crystallized conditions (Figure 3.1.20). X-ray diffraction datasets were collected at 2.3 Å, and 2.4 Å resolutions for the empty form and MgAMPPNP bound form of F236A. Datasets were obtained for the empty form and MgAMPPNP bound form of G239A at 2.7 Å and 3.0 Å, respectively.

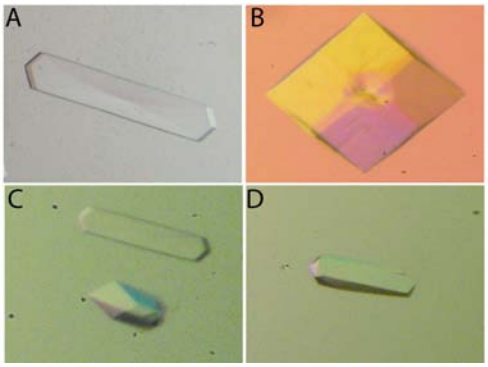

***Figure 3.1.20*. Crystals of F236A and G239A mutants of subunit A.** The mutants F236A and G239A were crystallized in the absence and presence of nucleotides. (A) Crystal of F236A empty form (0.4 × 0.15 × 0.1 mm); crystal of F236A in the presence of Mg-AMPPNP (B) (0.35 × 0.35 × 0.35 mm), crystal of G239A empty form (C) (0.3 × 0.1 × 0.1 mm); crystal of G239A in the presence of Mg-AMPPNP (D) (0.2 × 0.1 × 0.1 mm).

3.1.16 Determination of nucleotide binding constants for F236A and G239A mutants of subunit A

The nucleotide-binding constants of the mutants F236A and G239A of subunit A was determined using isothermal titration calorimetry (ITC) (Figure 3.1.21). The calculated K_d values for the mutant F236A were 6.13 µM for Mg-ATP, and 4.04 µM for Mg-ADP, respectively (Table 3.1.6) revealed the preferential binding of MgADP to the mutant protein. The G239A mutant of subunit A does not bind to either nucleotide.

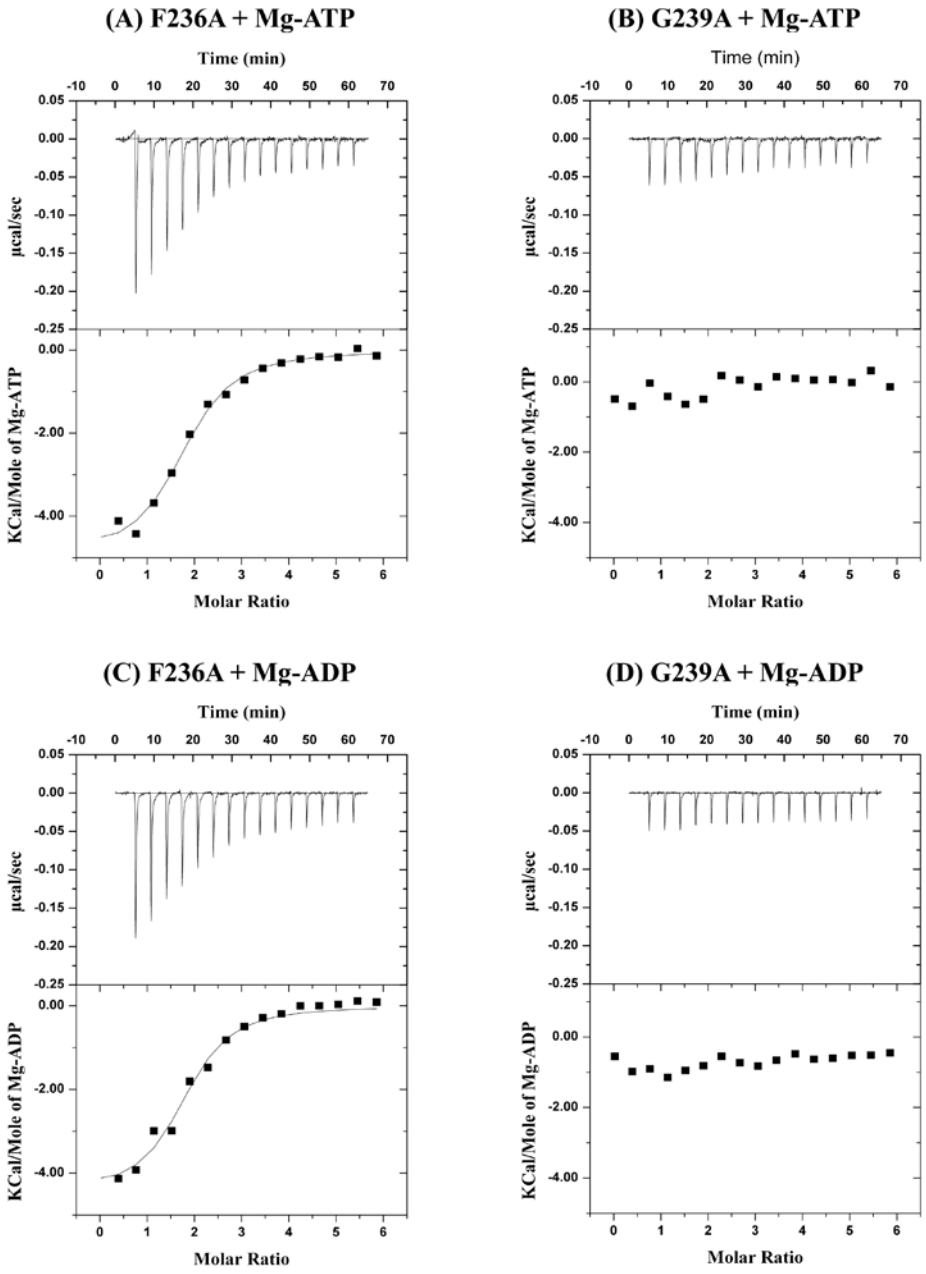

Figure 3.1.21. Determination of the nucleotide binding affinity for F236A and G239A mutants using ITC. Representative ITC profiles are shown for the mutants F236A and G239A with Mg-ATP (*A*, *B*) and Mg-ADP (*C*, *D*), respectively. All the experiments were performed in 50 mM Tris-HCl, pH 7.5, under identical conditions at 25 °C.

	K_a (x10^6 M^{-1})	K_d (μM)	ΔH (kcal/mol)	ΔG (kcal/mol)
F236A+ Mg-ATP	0.56 ± 0.011	1.78	- 4.96 ± 0.22	- 7.83
G239A+ Mg-ATP	0	0	0	0
F236A+ Mg-ADP	0.66 ± 0.019	1.5	- 4.47 ± 0.26	- 7.93
G239A+ Mg-ADP	0	0	0	0

Table 3.1.6. Nucleotide binding affinity measurements for F236A and G239A mutants of subunit A.

3.2 Nucleotide transition positions in subunit B of the A_1A_O ATP synthase: A crystallographic and spectroscopical approach

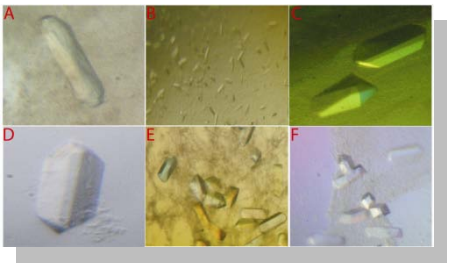

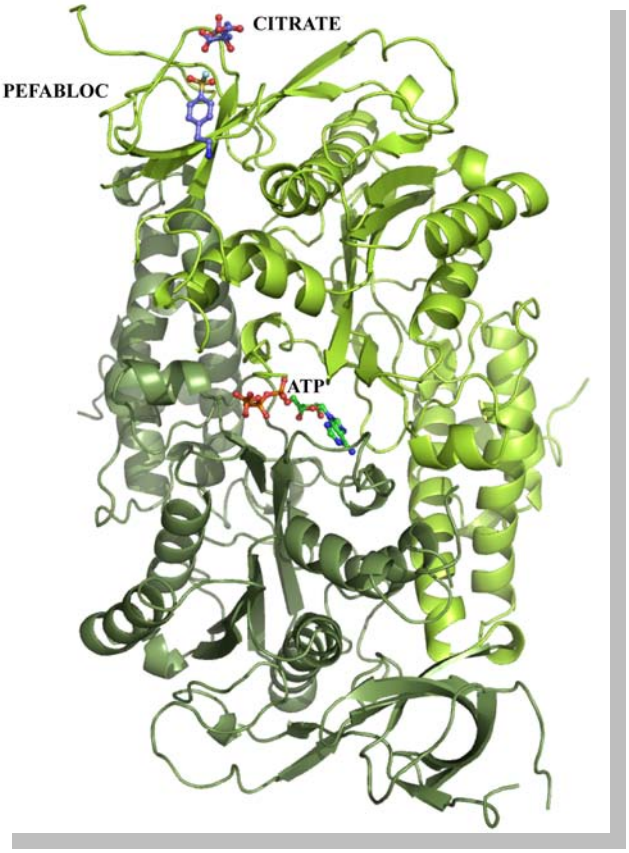

3.2.1 Cloning, production and purification of subunit B mutants

Amino acids from the P-loop region and adenine binding site were successfully mutated in a systematic way to generate mutants of subunit B from the A_1A_O ATP synthase of *Methanosarcina mazei* Gö1. Ten different point mutants (F149W, L154C, L154S, P155G, H156K, I185E, Y338R, Y338W, A373W and R416W) and one double mutant (H156K/R416W) of subunit B were successfully generated. The mutants were created by overlap extension PCR method using the subunit B insert in pET-9d1 vector (SCHÄFER *et al*, 2006b) with the primers *a-b* and *c-d*, respectively as described in section 2.2.2 (Figure 3.2.1A and B).

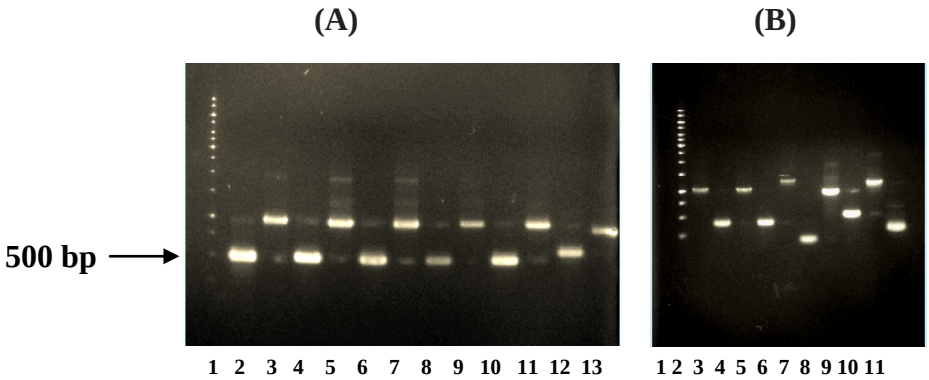

***Figure 3.2.1*. PCR amplification of subunit B mutants. (A)** PCR I products; Marker DNA (1Kb, Fermentas) (*lane 1*); F149W (*lane 2* and *3*); L154C (*lane 4* and *5*); L154S (*lane 6* and *7*); P155G (*lane 8* and *9*); H156K (*lane 10* and *11*); I185E (*lane 12* and *13*). **(B)** PCR I products; Marker DNA 1 (Kb, Fermentas) (*lane 1*); Y338R (*lane 2* and *3*); Y338W (*lane 4* and *5*); R416W (*lane 6* and *7*); H156K/R416W (*lane 8* and *9*); A373W (*lane 10* and *11*).

The amplified half fragments thus produced were then fused together via a second PCR using the flanking primers *a* and *d* (Figure 3.2.2). The fused DNA fragments were digested with *Nco*I and *Sac*I restriction enzymes and successfully ligated into pET-9d1 vector (GRÜBER *et al*, 2002).

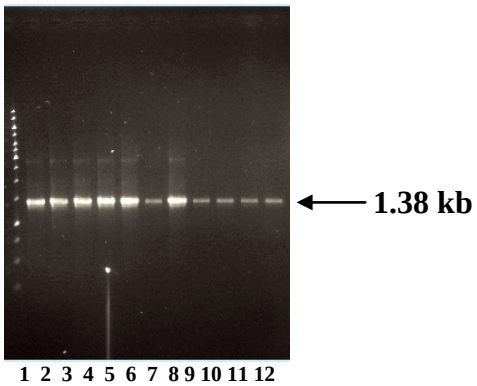

***Figure 3.2.2*. PCR amplification of subunit B mutants.** PCR II products; Marker DNA (1Kb, Fermentas) (*lane 1*); F149W (*lane 2*); L154C (*lane 3*); L154S (*lane 4*); P155G (*lane 5*); H156K (*lane 6*); I185E (*lane 7*); Y338R (*lane8*); Y338W (*lane 9*); R416W (*lane 10*); H156K/R416W (*lane 11*); A373W (*lane 12*).

3.2.2 Determination of nucleotide binding behavior of subunit B mutant R416W

In order to determine the nucleotide binding behavior, intrinsic tryptophan fluorescence quenching experiments were performed with subunit B-WT and its mutant R416W. The wild type subunit B (B-WT) of the A_1A_O ATP synthase from *M. mazei* Gö1 contains one native tryptophan residue (W430) and is located at the C-terminal region of the structure (SCHÄFER *et al*, 2006b). There was no observable quenching of fluorescence signal for the B-WT protein upon addition of 2 mM MgATP (Figure 3.2.3A, curve ×). While the tryptophan fluorescence spectrum of the nucleotide-free mutant R416W of subunit B increases the total tryptophan content compared to B-WT, indicating the increased fluorescence signal due to the engineered tryptophan residue (curve Δ). There was a red shift observed in the λmax values from 333nm to 340 nm. Figure 3.2.3A shows the effect of MgATP binding on the fluorescence signals from subunit B (B-WT) and mutant R416W protein in the presence and absence of 2 mM Mg-ATP (KUMAR *et al*., 2009a). The addition of 2 mM of MgATP to R416W mutant led to quenching of the fluorescence signal, making the spectrum of the mutant similar to that of B-WT (curve o). Addition of MgADP (2 mM) caused the same quenching of fluorescence signal in the R416W mutant. Titration curves for the R416W mutant protein were generated by the addition of increasing amounts of Mg-ATP (curve □) and Mg-ADP (curve ×), respectively (Figure 3.2.3B). Saturation points were observed at around 120 µM of Mg-ATP and Mg-ADP concentrations. The calculated dissociation constants (K_d) for Mg-ATP and Mg-ADP were 28 ± 2 µM and 41 ± 2 µM, respectively (KUMAR *et al*., 2009a).

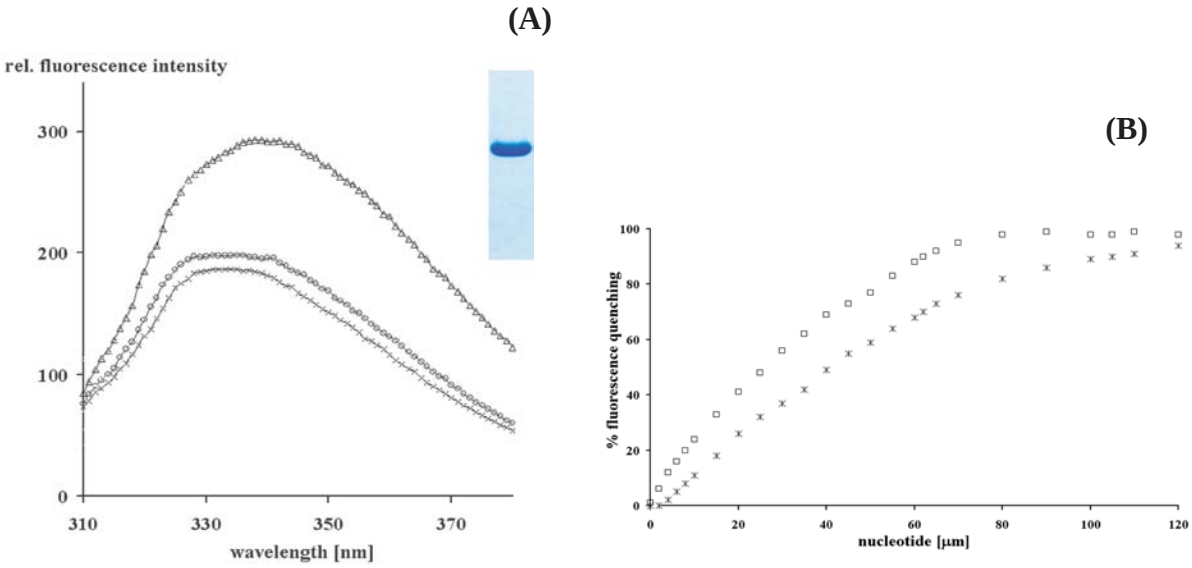

Figure 3.2.3. (A) Effect of Mg-ATP binding on the fluorescence of subunit B (B-WT) in the presence and absence of nucleotides is shown in curve (×). *Curve* (□) and (o), show the mutant R416W protein, in the absence or presence of 2 mM MgATP, respectively (KUMAR *et al*., 2009a). (B) Fluorescence titration of the mutant protein R416W with MgATP (□) and MgADP (×), respectively. Excitation and emission was measured at 295 nm and 340 nm, respectively (KUMAR *et al*., 2009a).

3.2.3 Determination of nucleotide binding constants for subunit B and its mutant R416W

using fluorescence correlation spectroscopy

Fluorescence correlation spectroscopy (FCS) is a technique which is used to study protein-ligand interactions in solution. In order to determine the nucleotide binding constants of the B-WT and its R416W mutant, FCS experiments were performed using the fluorescent ATP and ADP derivatives (Mg-ATP ATTO-647N and Mg-ADP ATTO-647N). The experiments and subsequent data analysis were done by Dr. Cornelia Hunke in our laboratory. Figure 3.2.4A shows the measured autocorrelation curves of Mg-ATP ATTO-647N in the absence and presence of wild type subunit B (B-WT) and the R416W mutant of subunit B (Figure 3.2.4B). It is observed that the addition of protein led to significant change of the mean diffusion time t_D, which increased up to 32.9 % and 30.5 % with increasing concentrations of B-WT and the mutant R416W, respectively (KUMAR *et al*., 2009a). The increase of the diffusion time was due to the increase in the mass of the diffusing particle, when Mg-ATP ATTO-647N was bound to either B-WT or the mutant protein. A binding constant of 22 ± 3 µM and 38 ± 2 µM of bound Mg-ATP ATTO-647N was calculated for the wild type and the mutant R416W protein of subunit B (Figure 3.2.5A and B) (KUMAR *et al*., 2009a).

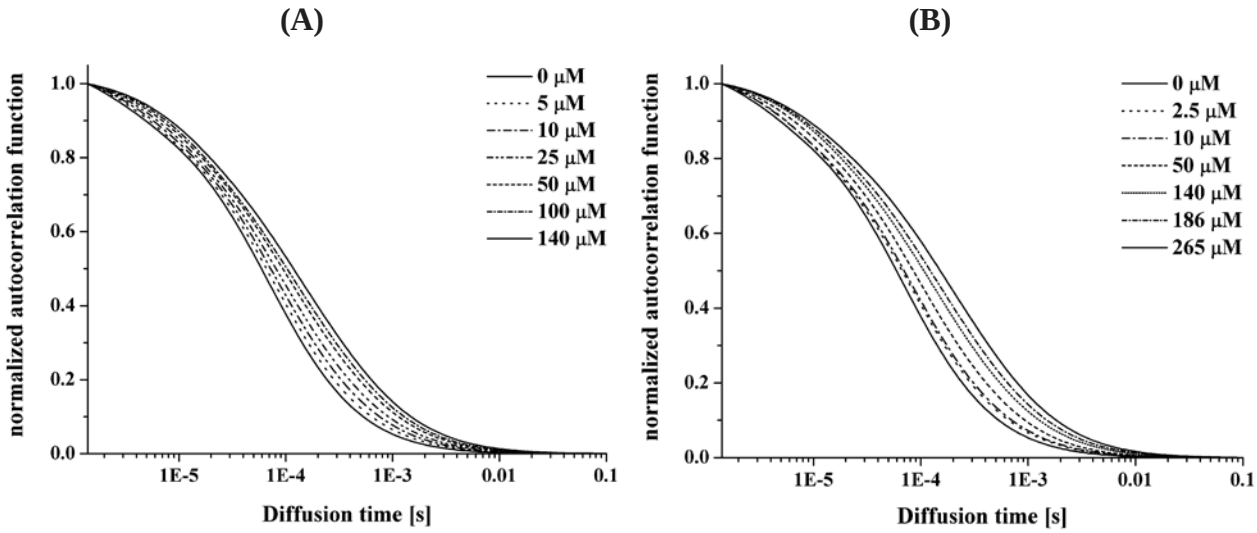

Figure 3.2.4. Nucleotide binding traits of subunit B and its mutant R416W by fluorescence correlation spectroscopy. Normalized autocorrelation functions of MgATP ATTO-647N by increasing the amount of wild type (A) and mutant of subunit B (B) (KUMAR *et al*., 2009a).

Measurements with Mg-ADP-ATTO-647N showed in general a distinct diminished binding when compared with the ATP-analogue. The addition of B-WT or mutant R416W resulted in an increase of the mean diffusion time t_D of about 33 % and 29 %, respectively. Binding constants of about 50 ± 3 µM bound Mg-ADP ATTO-647N to the wild type protein and about 100 ± 5 µM for the mutant were determined (Figure 3.2.5B) (KUMAR *et al*., 2009a).

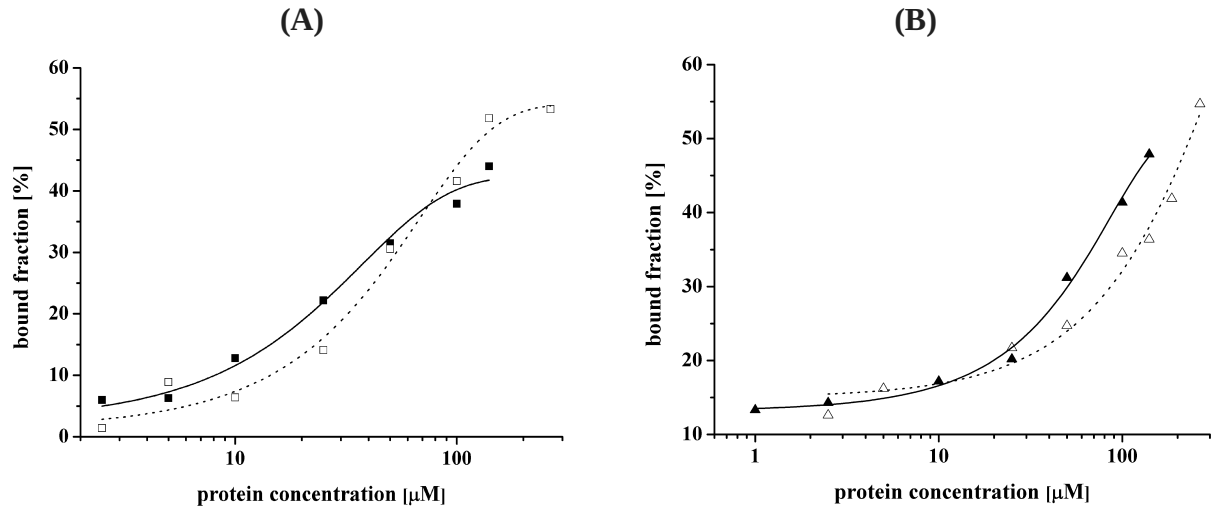

Figure 3.2.5. (A) Concentration-dependent binding of subunit B (■) and its mutated form R416W (□) to MgATP - ATTO-647N. The percentage of bound nucleotides was analyzed using a triplet model (ConfoCor3, Zeiss). Best fits yielding the binding constants are represented as fitted lines. (B) Comparison of wild type B(▲) and mutant R416W (Δ) to ADP-ATTO-647N (KUMAR *et al*., 2009a).

3.2.4 Crystallization of R416W mutant of subunit B

The structure of subunit B (wild type) has already been published in nucleotide free form (SCHÄFER *et al*., 2006b) and the crystallization conditions are known for obtaining the wild type crystals [20 % (v/v) polyethylene glycol (PEG) 400, 100 mM NaCl and 100 mM sodium citrate (pH 5.0)], therefore, same set of crystallization conditions were used initially to crystallize the R416W mutant of subunit B without nucleotides. Crystallization set ups were made in both hanging and sitting drops. In both cases the crystals did appeared but there was quick nucleation and the number of crystallites thus formed was large in number (Figure 3.2.6B). These crystallites were not of significant sizes and could not be used for X-ray diffraction. Therefore, a series of screening attempts were made by varying the PEG concentrations. Diffraction-quality crystals were obtained (without nucleotide) using 15 % (v/v) glycerol, 20 % (v/v) polyethylene glycol (PEG) 400, 100 mM NaCl and 100 mM sodium citrate (pH 5.0) as the precipitant solution in sitting drops. Addition of 15 % glycerol has helped in slowing down the rate of nucleation and hence had assisted in improving the size of the crystals thus produced (Figure 3.2.6C). One of the common methods of obtaining crystals of a protein-ligand complex is co-crystallization, where the ligand is added to the protein to form a complex that is subsequently used in crystallization trials. The subunit B R416W mutant protein was incubated with 2 mM MgATP, –MgADP and –MgAMPPNP (in separate crystallization setups) at 25 °C for 30 minutes and was setup for crystallization in both hanging and sitting drop plates. Protein crystals were obtained under these conditions but the size of the crystals was very small and hence needed further optimization for diffractable quality crystals. In order to improve the size and quality of the liagand bound protein crystals, seeding experiments were also attempted where these tiny

crystals were transferred to fresh protein drops equilibrated overnight (where concentration of the protein was 3 – 4 mg/ml in protein drop). The idea behind this strategy was that these small crystals will act as pre-nucleated seeds for subsequent growth. But success could not be achieved.

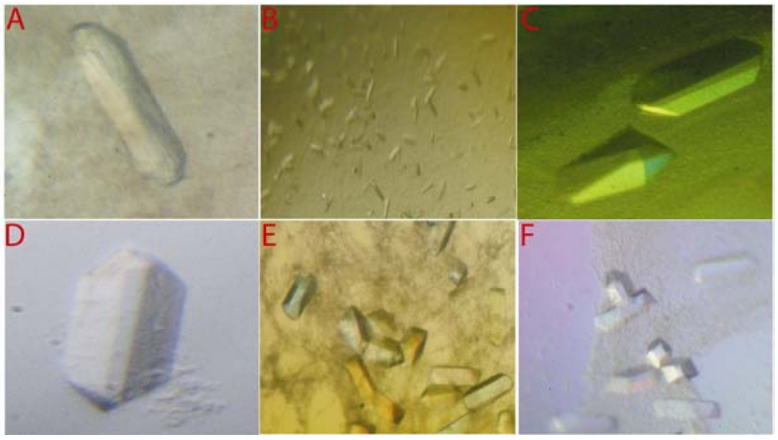

Figure 3.2.6. (A) Crystals of wild type subunit B-WT (0.2 × 0.1 × 0.1 mm). (B) crystallites of R416W mutant as a result of rapid nucleation (0.02 × 0.01 × 0.01 mm). (C) Crystals of R416W mutant protein without nucleotide (0.25 × 0.2 × 0.15 mm). (D) Crystals of R416W mutant protein co-crystallized with 3 mM MgATP (0.3 × 0.2 × 0.2 mm). (E) Crystals of R416W mutant protein co-crystallized with 3 mM MgADP (0.15 × 0.1 × 0.1 mm). (F) Crystals of R416W mutant protein co-crystallized with 3 mM MgAMPPNP (0.15 × 0.1 × 0.1 mm).

It was then planned to add nucleotides in the protein during concentration procedure (when the protein is dilute), hence, the subunit B mutant R416W protein was incubated with 2 mM MgATP and 2 mM MgADP (in separate crystallization setups) at 4 °C for 30 minutes and mixed on a sample rotator and concentrated to 8-10 mg/ml and was setup for crystallization in sitting drops. Protein crystals of significantly larger sizes were obtained (co-crystallized with MgATP) under these conditions (Figure 3.2.6D). Little improvement could be achieved for the protein crystals co-crystallized with Mg-ADP and Mg-AMPPNP (Figure 3.2.6E and F). The protein crystals co-crystallized with Mg-ATP were tested on in-house X-ray machines (Rigaku and Mar345; under cryo conditions (140 K)) for diffraction and the best resolution obtained was 3.0 Å. The protein crystals co-crystallized with Mg-ADP and Mg-AMPPNP upon testing did diffract but the best resolution obtained was not better than 4.5 Å. The best diffracting crystals were taken to National Synchrotron Radiation Research Center (NSRRC) at Taiwan for data collection at a stronger X-ray beamline.

3.2.5 Data collection and structure determination

The crystals of nucleotide free empty form diffracted to a resolution of 2.8 Å while the ATP bound form of the R416W mutant of subunit B diffracted to a maximum resolution of 2.1 Å (Figure 3.2.7). All the diffraction data were indexed, integrated and scaled using the HKL2000 suite of programs (OTWINOWSKI and MINOR, 1997). The details of the data collection

statistics are given in table 3.2.1. All the crystals belong to orthorhombic space group $P2_12_12_1$ and have similar unit cell parameters. The wild type subunit B structure (PDB 2C61; SCHÄFER *et al*, 2006b) was used as a model for the structure determination by molecular replacement method using the program PHASER (McCOY *et al.*, 2007) and MOLREP (VAGIN & TAPLYAKOV, 1997). Rigid body refinement was carried out followed by difference Fourier syntheses calculations. Inspection of the $F_O–F_C$ and $2F_O–F_C$ maps of protein-ligand complexes clearly showed electron density corresponding to the bound ligand. The ligand-bound forms of subunit B were confirmed by omit map calculations using the CNS program (BRUNGER *et al.*, 1998). Iterative cycles of model building and refinement were carried out using the programs COOT (EMSLEY and COWTAN, 2004) and REFMAC5 (MURSHUDOV *et al.*, 1997) of the CCP4 suite (1994). The geometry of the final models was checked with PROCHECK (LASKOWSKI *et al.*, 1993) and the figures are drawn using the program PyMOL (DeLANO, 2002). Structural comparison analysis were carried out using the SUPERPOSE program (KRISSINEL and HENRICK, 2004) as included in the CCP4 suite.

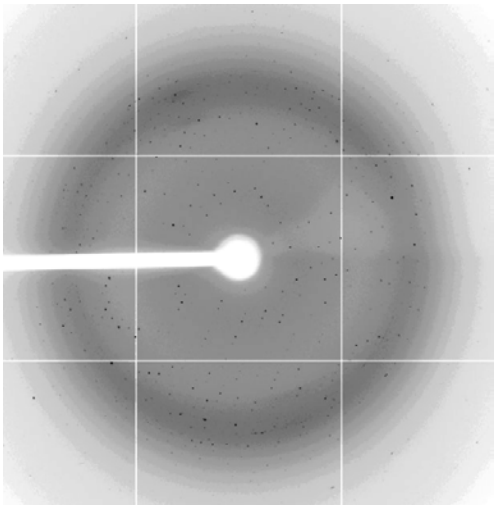

Figure 3.2.7. X-ray diffraction pattern of ATP bound subunit B (R416W) crystal at a resolution of 2.1 Å.

3.2.6 Structure determination of nucleotide free R416W mutant of B-subunit

I have determined the structure of nucleotide free R416W mutant of subunit B from *Methanosarcina mazei* Gö1 to a resolution of 2.8 Å. During structure refinement, assistance was kindly provided by Dr. Malathy Sony Subramanian Manimekalai and Dr. Manikkoth Balakrishna Asha. The empty form of the mutant structure is similar to the wild type subunit B structure with two molecules in the asymmetric unit (SCHÄFER *et al*, 2006b) (Figure 3.2.8A and B). Both the subunits (chain A and chain B) superimpose with a root mean square deviation (r.m.s.d) value of 0.7. The overall structure of the empty form of the mutant has approximate dimensions of 50 × 50 × 80 Å and is composed of three major domains. These are an N-terminal six stranded β barrel (formed by the residues G13–L76), an intermediate α/β domain (residues K77–G358) and a C-terminal four α–helical bundle (residues K359–460). The middle α/β domain (the nucleotide binding domain) consists of a nine-stranded β sheet surrounded by seven helices. The nucleotide free mutant structure consists of 914 amino acid residues for both the

molecules (chain A and chain B) in the asymmetric unit (water molecules were not assigned in the structure due to limiting resolution), and the numbering of the amino acids in the final model corresponds to the sequence of the protein. Due to poor electron densities for the amino acids, 1-10, 56-69, 261-271 and 458-460 in chain A and for residues, 1-9, 59-70, 262-275 and 458-460 in chain B of the nucleotide-free R416W mutant no amino acid could be assigned (KUMAR *et al*., 2009a). Although the mutant structure is similar to the wild type protein, the r. m. s deviation being 0.70 Å, appreciable deviations were observed in the regions Q257-Y277 and P306-Y320. The maximum deviation occur for Y277 (3.26 Å) in the Q258-Y277 region and P315 (4.43 Å) for the P306-E323 region. These two regions are part of a loop region, above the P-loop, that would face the central stalk region in the intact A_1A_O ATP synthase. The R416 in the B-WT structure is found to make a salt bridge with E158 and due to its substitution by tryptophan in the R416W mutant structure the salt bridge is abolished and the side chain of E158 orients in opposite direction with respect to the B-WT structure. The detailed statistics for data collection, phasing, and structure refinement are given in Table 3.2.1.

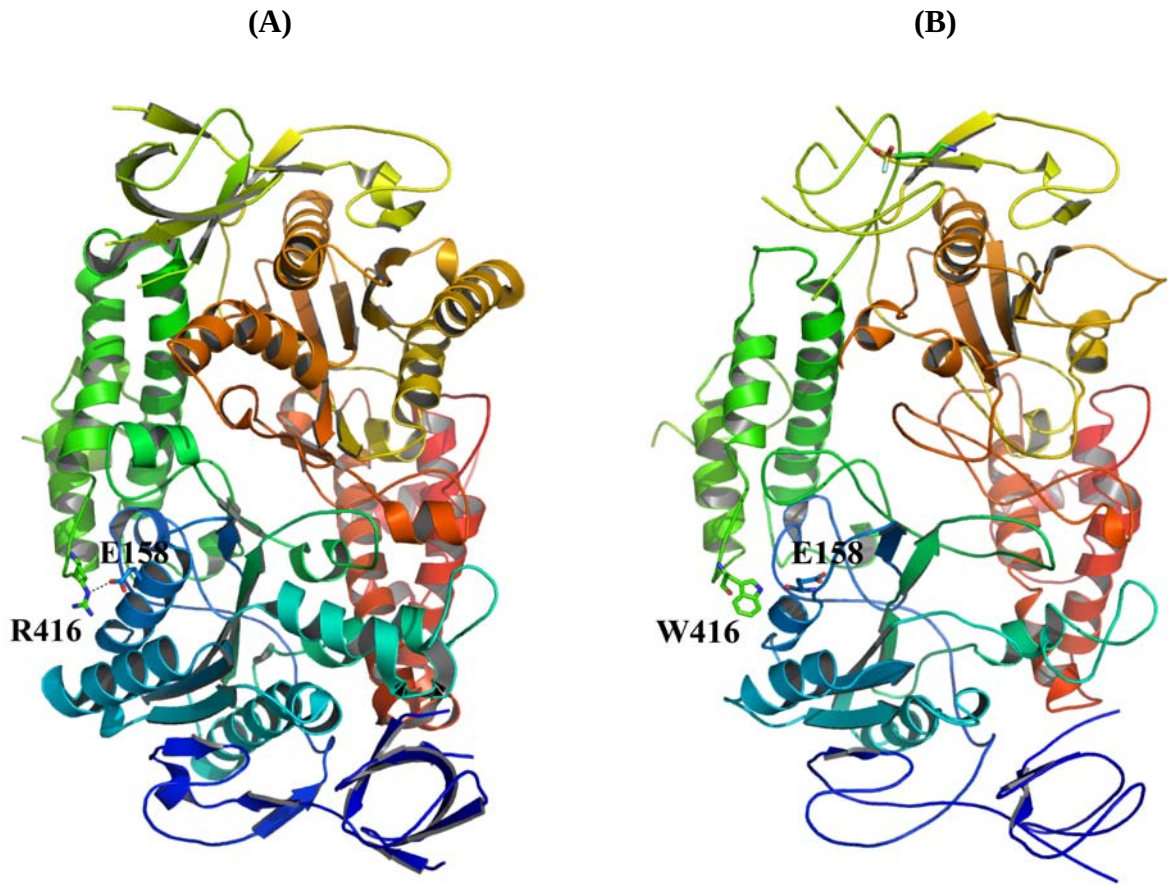

Figure 3.2.8. (A) Structure of the wild type subunit B at 1.5 Å resolution (SCHÄFER *et al*., 2006b) (PDB 2C61). Label mark the salt bridge forming residues R416 and E158. (B) Structure of the nucleotide free R416W mutant of subunit B (resolution 2.8 Å) (KUMAR *et al*., 2009a) (PDB 2RKW). Label mark the abolished salt bridge between residues W416 and E158.

3.2.7 Structure of ATP-bound transient-I of R416W mutant of subunit B

The R416W mutant of the Subunit B from *Methanosarcina mazei* Gö1 was successfully co-crystallized with ATP (Adenosine tri-phosphate) and its structure (B_{TP}) was determined to a resolution of 3.4 Å (Figure 3.2.9A and B). The structure was solved by Dr. Malathy Sony Subramanian Manimekalai, using molecular replacement method. In this structure the ATP molecule is bound near the helix-turn-helix motif of the C-terminal domain of chain A. Since, the bound nucleotide is not located inside the predicted binding site, we term this structure as transient-I structure. Similar to the nucleotide free R416W mutant, the transient ATP bound form of the R416W mutant of subunit B also crystallized in orthorhombic ($P2_12_12_1$) space group with two molecules in the asymmetric unit (chain A and chain B). The overall structure is similar to the nucleotide free R416W mutant structure of the subunit B (SCHÄFER *et al*., 2006b). The final model has good stereochemistry as can be seen from the Ramachandran plot statistics given in appendix section.

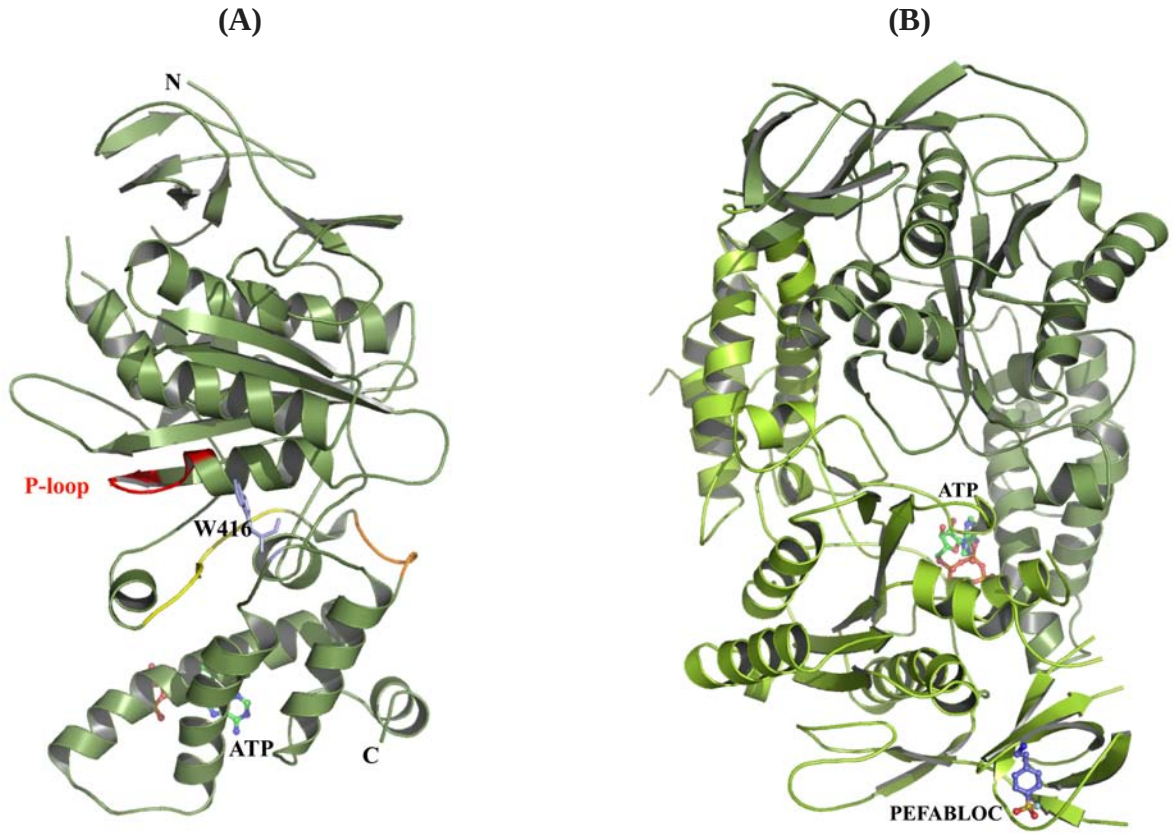

Figure 3.2.9. (A) Structure of nucleotide-bound transient-I R416W mutant of subunit B from *M. mazei* Gö1 shown in ribbon representation (PDB 3DSR) (MANIMEKALAI *et al*., 2009). The mutated residue W416 is labeled. The ATP molecule that is bound to the transition site is shown in orange color ball and stick representation, while the actual site of binding is shown by cyan dotted surface with nucleotide (cyan line representation) docked inside. The P-loop region (S150-E158) is highlighted in red and the peptide G336 to R349 that is reported to covalently bind 8-N3-3'-biotinyl-ATP (SCHÄFER *et al*., 2006b) is shown in magenta color. (B) Crystal structure of nucleotide-bound transient-I R416W mutant of B-subunit from *M. mazei* Gö1 shown in ribbon representation (dark green—chain A; lemon—chain B). The ATP molecule is shown as CPK model and the Pefabloc^{SC} is shown in stick representation.

In the structure, the ATP molecule is located asymmetrically in between the two chains of the dimer, wherein it interacts at the helix-turn-helix motif of the C-terminal domain of chain A and associates more through stronger hydrophilic interactions with chain A rather than with the B chain (Figure 3.2.9B). During structure refinement the ATP molecule could be identified very clearly from the positive peaks in the difference Fourier maps (F_O–F_C and $2F_O$–F_C).

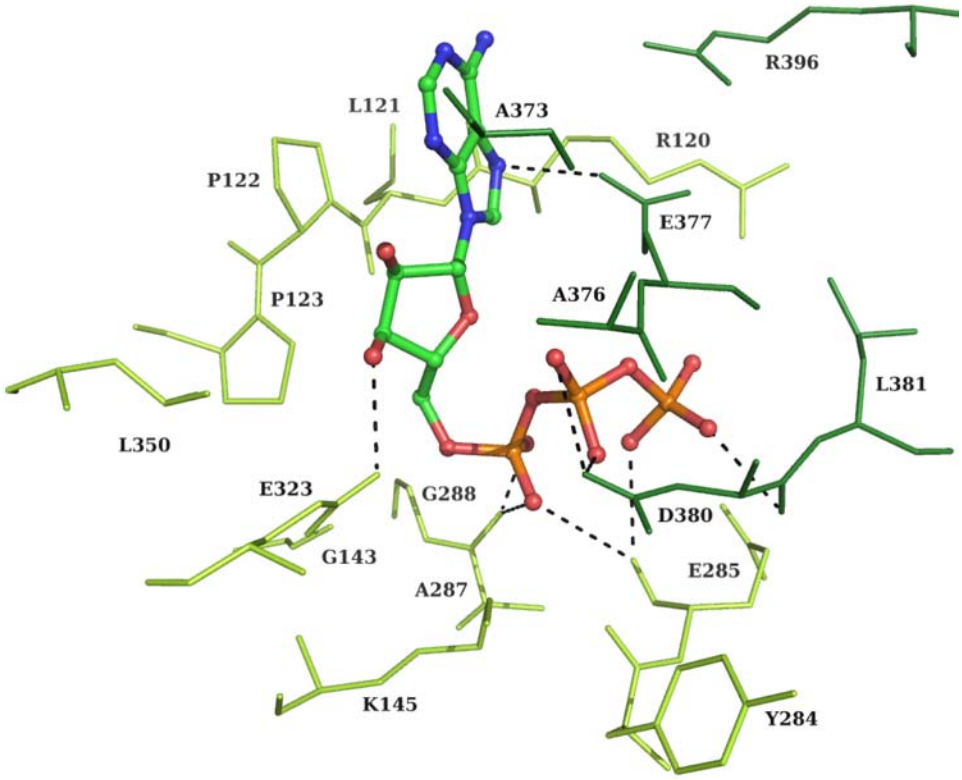

Figure 3.2.10. Amino acid residues that surround the ATP molecule within 5 Å radius in the transient-I subunit B R416W mutant structure (PDB 3DSR) (MANIMEKALAI *et al*., 2009). The ATP molecule is shown in ball and stick representation and the amino acid residues are represented by sticks. Chain A residues are shown in green and chain B in lemon color. The hydrogen bonding interactions between the ATP molecule and the amino acid residues are shown in dotted lines.

The ATP molecule is found to be stabilized through several interactions in the protein molecule. The phosphate groups are well stabilized by hydrogen bonding interactions with surrounding polar groups. The γ-phosphate has hydrogen bonding interaction with main chain carbonyl oxygen atoms of D380(A) and E285(B) through its oxygen atom (Figure 3.2.10). In turn the β-phosphate interacts with side chain oxygen atom of D380(A) which forms a bifurcated hydrogen bond with two of its oxygen atoms. The α-phosphate is held in place through hydrogen bonding interaction by its oxygen atom to main chain carbonyl oxygen atom of A287(B) via a bifurcated hydrogen bond. One of the oxygen atom of the α-phosphate interacts with E285(B) by main chain carbonyl oxygen atom. The side chain oxygen atom of E323(B) makes hydrogen bond with the oxygen atom in sugar ring and E377(A) interacts with the nitrogen atom of the adenine

ring through its side chain oxygen atom. Hydrophobic interaction by non-polar residues such as L121(B), P122(B) and P123(B) stabilizes the adenine ring moiety of the ATP molecule. In addition to the ATP molecule, one prominent peak near the N-terminus of chain B was observed in the Fo-Fc difference map at 3σ level in the asymmetric unit. It was assigned as Pefabloc^{SC} (4-(2-Aminoethyl) benzenesulfonyl fluoride) (Figure 3.2.9B), which makes hydrogen bonding interaction with the side chain OH group of the Y26(B) through its amino group.

3.2.8 Detection of ATP-binding to subunit B mutant A373W by Trp-fluorescence quenching

Intrinsic tryptophan fluorescence quenching experiments were performed with subunit B-WT and its newly created mutant A373W, generated and purified according to section 2.2.13.2 (SCHÄFER *et al*., 2006b), to ascertain ATP binding to these proteins. The residue A373 is in a 4.7 Å distance to the adenine ring of ATP (Figure 3.2.10). Therefore, a substitution was made by a tryptophan and the subunit B mutant A373W was generated, to enable the detection of any ATP-binding with this residue by intrinsic fluorescence and confirming that the trapped transition nucleotide-binding site is crucial for ATP-binding. Figure 3.2.11 shows the absorbance spectrum of the A373W mutant protein with a maximum at about 336 nm (*curve* Δ). Addition of ADP (*curve* *) dropped the fluorescence intensity by up to 20 % indicating that the trytophan fluorescence spectrum of mutant A373W is sensitive to ATP binding (MANIMEKALAI *et al*., 2009).

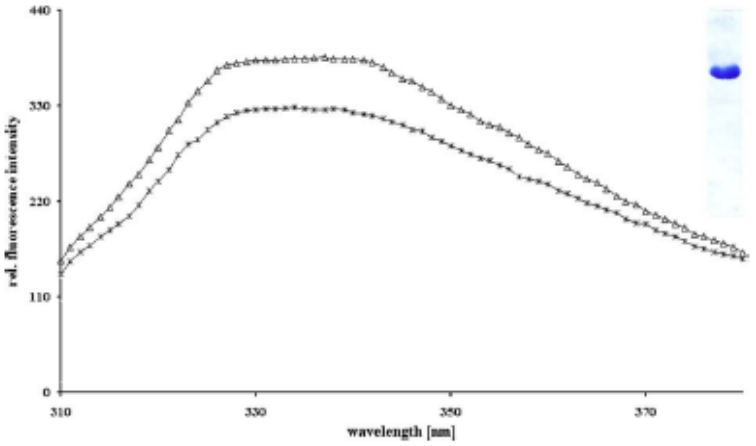

Figure 3.2.11. Fluorescence emission spectra of subunit B mutant A373W in the presence and absence of ATP (MANIMEKALAI *et al*., 2009). The fluorescence emission spectra (excitation wavelength (λ_{ex}) of 295 nm with excitation and emission bandpasses of 5 nm) of mutant A373W were measured at 20 ˚C. A373W mutant protein in the absence (Δ) and presence (x) of 2 mM MgATP. The purified mutant protein A373W is revealed by the SDS gel in the inset.

3.2.9 Structure of ATP-bound transient-II of R416W mutant of subunit B

Following the same strategy of co-crystallization, I have also successfully co-crystallized R416W mutant with ATP molecule bound at another transient site. The ATP bound structure was solved together with Dr. Malathy Sony and Dr. Manikkoth Balakrishna Asha. Similar to the nucleotide free R416W mutant the ATP bound form of the R416W mutant of subunit B also

crystallized in orthorhombic ($P2_12_12_1$) space group with two molecules in the asymmetric unit (chain A and chain B). Due to lack of significant electron densities in the following regions, 1-10, 59-69 and 457-460 in chain A and for regions 1-11, 59-67 and 261-269 in chain B no amino acid residues could be assigned. 846 water molecules could be identified and assigned. In ATP bound structure of the R416W mutant, the ATP molecule is in a sandwiched state between chain A and chain B (Figure 3.2.12A). It has been observed that the ATP molecule makes maximum interactions with chain A residues rather than chain B residues. The oxygen atoms of the γ-phosphate were found to make close contact with the P-loop residues, A151(A) and L154(A) with distances of 3.21 Å and 3.57 Å, respectively.

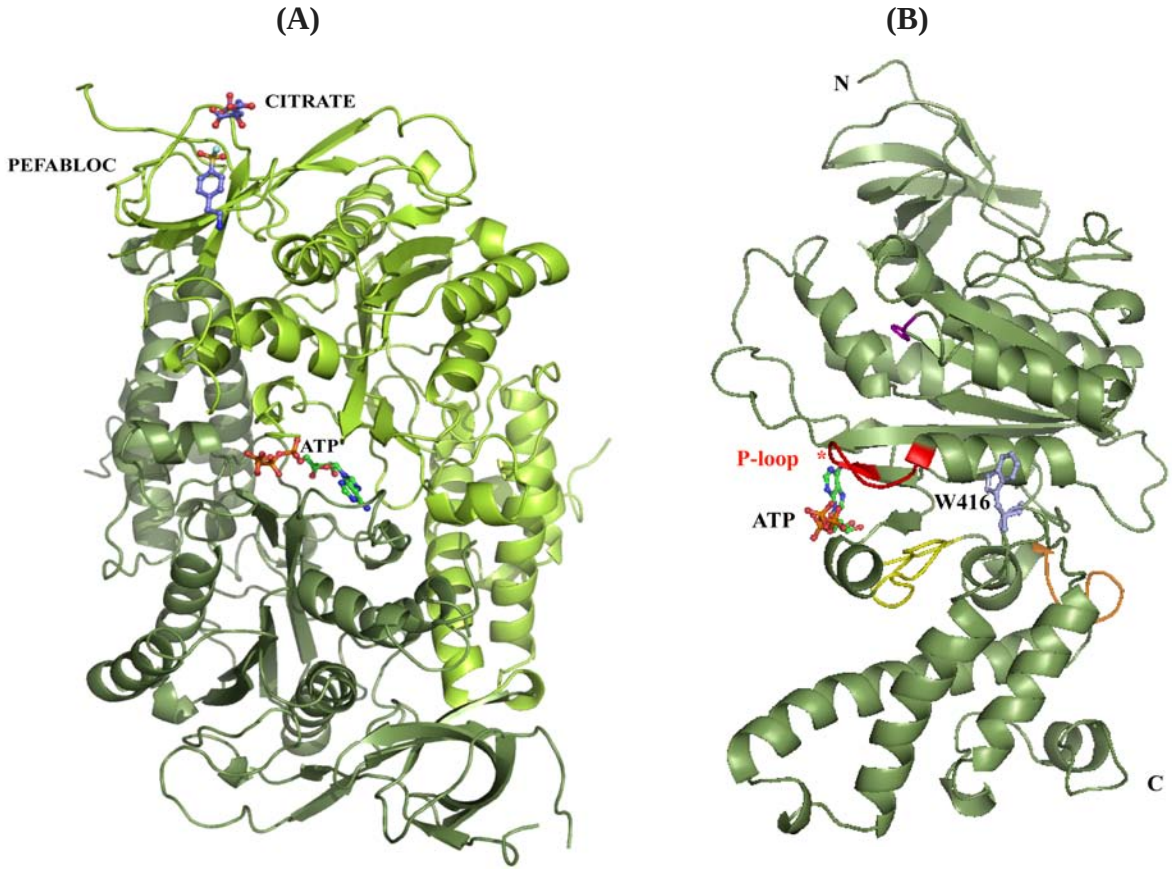

Figure 3.2.12. (A). Structure of the ATP bound form of R416W mutant of subunit B at 2.1 Å resolution (KUMAR *et al*., 2009a) (PDB 3B2Q). The ATP molecule is shown as spheres (marked by arrow head) and is sandwiched between two molecules. (B) A cartoon diagram of chain A of ATP bound R416W mutant structure with ATP molecule (ball and stick representation) shown. The P-loop sequence $_{150}$SASGLPHN$_{157}$ is highlighted in red color (KUMAR *et al*., 2009a). The substituted W416 is shown as in stick representation (blue). The glycine rich P-loop like sequence is shown in orange color.

Other than the ATP molecule two more prominent electron density peaks were observed in the Fo-Fc difference map contoured at 3σ level in the asymmetric unit. These electron density peaks were assigned as the protease inhibitor Pefabloc^{SC} (4-(2-Aminoethyl)benzenesulfonylfluoride) and as a citrate molecule. Pefabloc^{SC} molecule interacts with K20, V24, Y26 and D46 of chain B

via a hydrogen bond while the citrate molecule interacts with K20 of chain B through a water molecule (Figure 3.2.12A). Hydrogen bonding interactions are observed between the main chain nitrogen of R330(A) and one of the oxygens of γ-phosphate and between the main chain oxygen atom of V328(A) with one of the oxygen atoms of the β-phosphate of the ATP molecule. The residues: S150(A), M305(A), S318(B), D316(B) helps in maintaining a polar environment and hence helps in further stabilization of the ATP molecule. Q325(A) interacts with the oxygens atoms from the sugar ring of the ATP molecule as well as with the main chain nitrogen of S318(A) (KUMAR *et al*., 2009a) (Figure 3.2.13). The adenine ring of the ATP molecule is stabilized by two main factors: (1) F149(A) confers π - π interaction and hence stabilizes the adenine ring. (2) The non-polar environment created by the residues L317(A), I321(A), V327(B), P345(B) and V327(B) also stabilize the adenine ring of the ATP molecule.

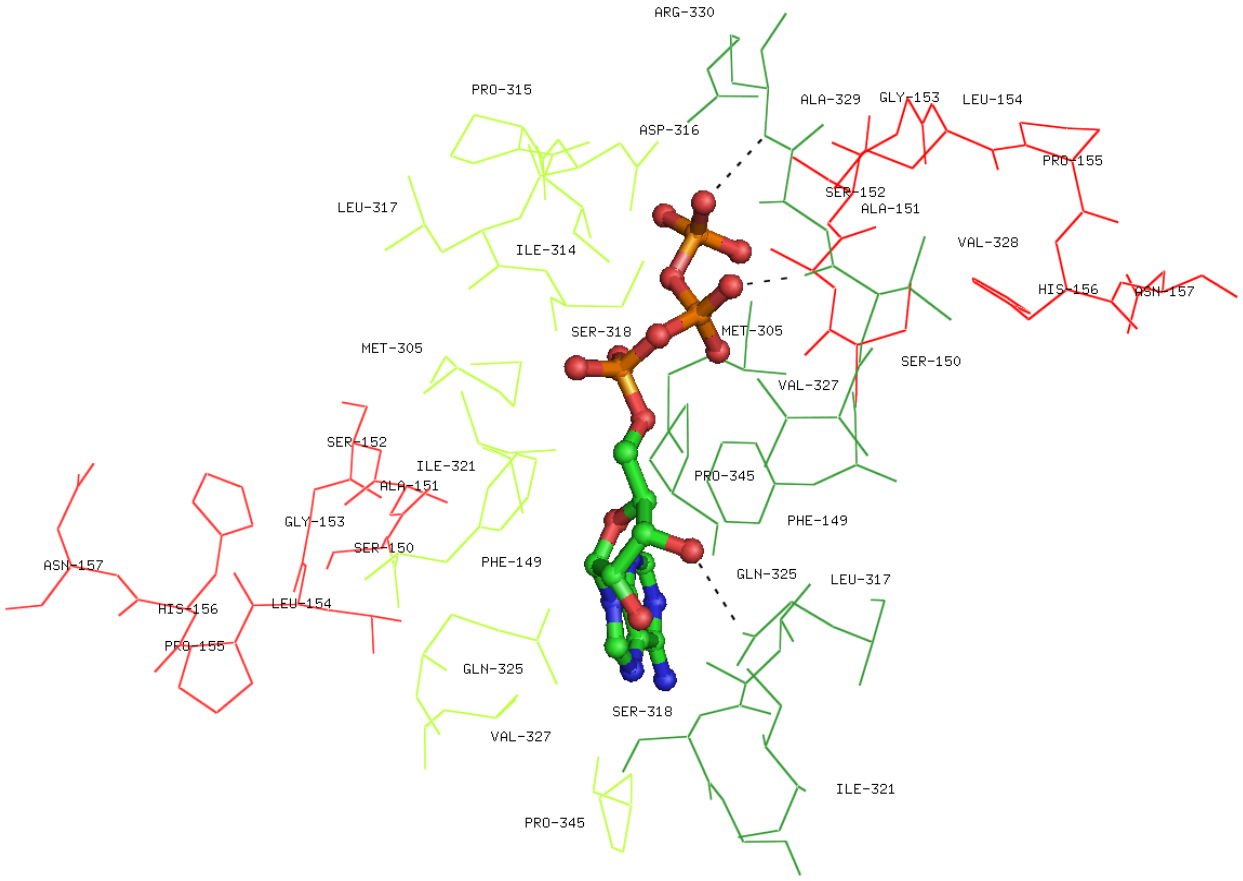

Figure 3.2.13. The amino acid residues surrounding the ATP molecule within 5 Å radius for the nucleotide bound R416W mutant structure (PDB 3B2Q). Chain A residues are shown in green and chain B in olive color as line representation. Residues from the P-loop are shown in red as line representation. The hydrogen bonding interactions between the ATP molecule and the amino acid residues are shown in dotted lines. The π - π interaction between Phe149 and the adenine ring is also highlighted in dotted lines (KUMAR *et al*., 2009a).

Since in this mutant structure the ATP is not bound to the actual binding site, we term this site as a transient binding site (KUMAR *et al*., 2009a) and the structure as transient-II. One water

molecule could be identified at 4.86 Å away from the γ phosphate of the ATP which makes hydrogen bond interaction with the side chain nitrogens of R330(A) and main chain oxygen of I314(B). Furthermore, since this R330(A) also has hydrogen bonding interaction with the ATP molecule, in a way this residue act as a bridge between the water molecule and the ATP. The overall structure of the ATP bound form is similar to the nucleotide free mutant protein, the r. m. s. deviation being 0.64 Å. Larger than average deviation occur in regions Q258-Y277 and P306-Y320 wherein the maximum deviation occur for N264 (2.7 Å) for the Q258-Y277 region and P315 (4.5 Å) for the P306-Y320 region (KUMAR *et al*., 2009a). These two regions are part of the loop region that would face the central stalk region in the intact complex. Even though there is not much difference for the back bone atoms of W416 residue between the nucleotide free and bound structure, the r. m. s deviation being 0.64 Å, the side chain atoms show observable differences. The indole ring of the Tryptophan residue is oriented in such a way that they are slightly tilted from each other, the angle between the two planes of the indole ring is found to be 19° (KUMAR *et al*., 2009a). The detailed statistics for data collection, phasing, and structure refinement are given in Table 3.2.1.

	B_E	B_{TP} (Transient-II)
Data collection statistics		
Wavelength (Å)	1.0	0.97
Space group	$P2_12_12_1$	$P2_12_12_1$
Unit cell parameters (Å)		
a =	73.05	73.47
b =	96.09	96.09
c =	129.94	130.28
α = β = γ (°)	90	90
Resolution range (Å)	50.0 - 2.8	50.0 - 2.10
Number of unique reflections	20054	51314
I/σ^a	14.29 (2.78)	15.39 (3.35)
Completeness (%)	87 (60)	99.5 (99.8)
R merge[b] (%)	13 (39.5)	7.7 (41.7)
Multiplicity	5.9 (4.8)	3.3 (3.3)
Refinement statistics		
R factor[c] (%)	27.1	18.9
R free[d] (%)	33.0	23.7
Number of amino acid residues	844	866
Number of water molecules	-	846
Number of AES molecules	-	1
Number of CIT molecules	-	1
Ramachandran statistics		
Most favored (%)	76.6	88.9
Additionally allowed (%)	18.9	11.1
Generously (%)	3.1	0.0
Disallowed (%)	1.4	0.0

R.M.S. deviations		
Bond lengths (Å)	0.01	0.01
Bond angles (°)	1.36	1.8
Mean atomic B values		
Overall	79.45	31.0

[a] Values in parentheses are corresponding value of the highest resolution shell (B_E = 2.89 – 2.80; B_{TP} = 2.19 – 2.10).

[b] $R_{merge} = \Sigma\Sigma_i|I_h - I_{hi}|/\Sigma\Sigma_i I_h$, where I_h is the mean intensity for reflection h.

[c] R-factor = $\Sigma||F_O| - |F_C||/\Sigma|F_O|$, where F_O and F_C are measured and calculated structure factors, respectively.

[d] R-free = $\Sigma||F_O| - |F_C||/\Sigma|F_O|$, calculated from 5% of the reflections selected randomly and omitted during refinement.

Table 3.2.1. Statistics of crystallographic data collection and refinement for the B_E and B_{TP} structures of R416W mutant of subunit B.

3.2.10 Detection of ATP-binding to subunit B mutant F149W by Trp-fluorescence quenching

In the nucleotide bound transient structure, the adenine ring of the ATP molecule is found to make a π - π interaction with the F149 residue (Figure 3.2.13). The residue F149 precedes the P-loop sequence ($_{150}$SASGLPHN$_{158}$). Therefore, intrinsic tryptophan fluorescence quenching experiments were performed with subunit B-WT and its newly created mutant F149W; generated and purified according to section 2.2.13.2 (SCHÄFER *et al*., 2006b), to ascertain comparative ATP binding to these proteins. Since the residue F149 confers π - π interactions with the adenine ring of ATP, a substitution was made by a tryptophan and the subunit B mutant F149W was generated, to enable the detection of any ATP-binding with this residue by intrinsic fluorescence and confirming that the trapped transition nucleotide-binding site is crucial for ATP-binding. As shown in Figure 3.2.14 the absorbance spectrum of the F149W mutant protein shows a maximum at 336 nm and a higher quantum yield (19%) compared to WT subunit

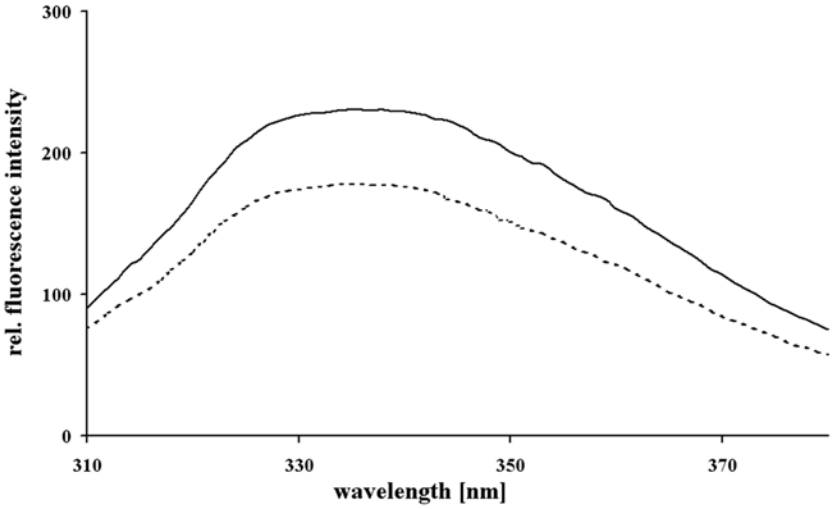

Figure 3.2.14. Fluorescence emission spectra of subunit B mutant F149W in the presence and absence of ATP. The fluorescence emission spectra (excitation wavelength (λ_{ex}) of 295 nm with excitation and emission bandpasses of 5 nm) of mutant F149W were measure at 20 °C. F149W mutant protein in the absence (—) and presence (- -) of 2 mM MgATP (KUMAR *et al*., 2009a).

B. Addition of ATP (*curve* --) dropped the fluorescence intensity up to 18 %. Therefore, the data showed that the trytophan fluorescence spectrum of mutant F149W is sensitive to ATP binding.

3.2.11 Structure comparison of the different ATP transient structures and the empty form of subunit B

The difference between the ATP bound transient-I structure (Figure 3.2.9) and transient-II structure is that the ATP molecule is bound at different positions in both the structures (Figure 3.2.12). In the transient II structure, the ATP is bound near the P-loop region, whereas in transient-I structure, it is bound near the helix-turn-helix motif in the C-terminal domain of the protein (Figure 3.2.9). Structural comparison of both transient structures gave an r.m.s. deviation of 0.788 Å for the overall backbone Cα atoms. Larger than average deviation is found near the N-terminal region and for the loop region G307-D316 (maximum deviation of 3.506 Å occurs for the residue G 307). It could be noted that the loop region G307-D316 is close to the ATP binding region of the transient-I structure and therefore the structural variation could also be attributed to the binding of the ATP molecule. There is no major structural difference for the W416 residue between the two transient structures except, that the indole ring of the Trp residue is slightly tilted by an angle of 3°. Among the three domains of the B-subunit, the N-terminal β-barrel (13-76) shows least deviation with an r.m.s.d of 0.558 Å, whereas the central nucleotide binding α-β domain (77-358) show maximum deviation of 0.763 Å and the C-terminal α-helical bundle (359-460) has 0.568 Å deviation. When the N-terminal domains of both the transient structures are superimposed, their C-terminal domains are related by a rotation of 6°. Furthermore, the helical region N187 to R205 shows significant helical movement. This helical region is found above the loop region G307-D316, which revealed marked deviations in the overall structure comparison and therefore it could be reinstated that the disturbance created by the nucleotide in the loop region is also carried forward to this helical region. In addition, slight movement is also noted for the P-loop region and distinct deviation is observed in the adenine binding pocket. Similar to transient-II structure, the empty form of the wild type subunit B (2C61) structure has an r.m.s. deviation of 0.828 Å with the transient-I structure, where notable differences occur in region M305-D316 with maximum deviation of 4.480 Å observed for the residue G307. The N-terminal, nucleotide binding and the C-terminal domains show r.m.s. deviation of 0.643, 0.872 and 0.663 Å, respectively and when the N-terminal domain is superimposed, their C-terminal domains are rotated by 5.8°. Therefore, it could be concluded that the binding of ATP molecule in transient-I structure has imposed a conformation change on the C-terminal domain by way of rotating it by around 6°.

3.2.12 Crystallization and Structure determination of subunit B (WT) in the presence of nucleotides

3.2.12.1 Crystallization of subunit B (WT) in complex with ATP and ADP

In order to get an insight into the binding mode of the nucleotides (ATP/ADP) in the nucleotide-binding subunit B (B-WT) of the A-ATP synthase from *M. mazei* Gö1 attempts were made to get a nucleotide bound structure of the protein. To achieve this, soaking experiments were tried initially with the native crystals (SCHÄFER *et al.*, 2006b) by varying the incubation time and the concentration of either the ATP or ADP molecule, which did not yield any successful results. Therefore, co-crystallization was attempted, wherein the ligand is added to the protein to form a complex that is subsequently used in crystallization trials. Several X-ray intensity datasets were collected for the protein in complex with ADP at reasonable resolutions for all of the crystals obtained under different conditions In none of the datasets positive electron density for ADP molecule could be observed at reasonable σ cut-off. The third protocol, using the ligand before crystallization setups was successfully attempted. Here, subunit B was incubated with ADP before concentration to 10 mg while it is in the dilute and monodisperse form. The size of crystals including the protein-ADP complex was improved by adjusting the glycerol concentration. Such crystals grow to a size of 0.07 x 0.04 x 0.03 mm^3 over a period of three weeks and diffracted to 2.7 Å resolution. The protein crystals co-crystallized with ATP did not diffract better than 3.5 Å.

3.2.12.2 Structure determination of subunit B (WT) in complex with ADP

I have determined the structure of subunit B (WT) in complex with ADP at 2.7 Å resolution. The structure was solved using molecular replacement method. Similar to the nucleotide free R416W mutant and the transient ATP bound forms of the R416W mutant of subunit B also crystallized in orthorhombic ($P2_12_12_1$) space group with two molecules in the asymmetric unit (chain A and chain B). The overall structure is similar to the nucleotide free R416W mutant and the transient ATP bound forms of the R416W mutant structures of the subunit B (SCHÄFER *et al.*, 2006b; KUMAR *et al.*, 2008). The final model has good stereochemistry as can be seen from the Ramachandran plot statistics given in table 3.2.2. The ADP molecule is bound in between the two monomer, which have maximum interaction with chain A residues rather than

Figure 3.2.15. Crystal of subunit B-WT co-crystallized with 2 mM Mg-ADP. The crystal dimensions were approximately 0.07 x 0.04 x 0.03 mm.

chain B. Similar to that of the nucleotide-empty subunit B (2C61) structure, the ADP bound protein also consists of three domains, an N-terminal β barrel (residues 13–76), an intermediate α-β domain (residues 77–358) and a C-terminal α–helical bundle (residues 359–460) (Figure 3.2.16A and B). The model of the ADP-bound B subunit comprises of 920 residues for both the molecules in the asymmetric unit. No noticeable density was observed for residues 1-11, 60-69, 262-272, 307-312 and 458-460 in chain A and 1-10, 59-67, 263-268, 306-311 and 457-460 in chain B. A total of 402 water molecules could be identified in the nucleotide bound structure.

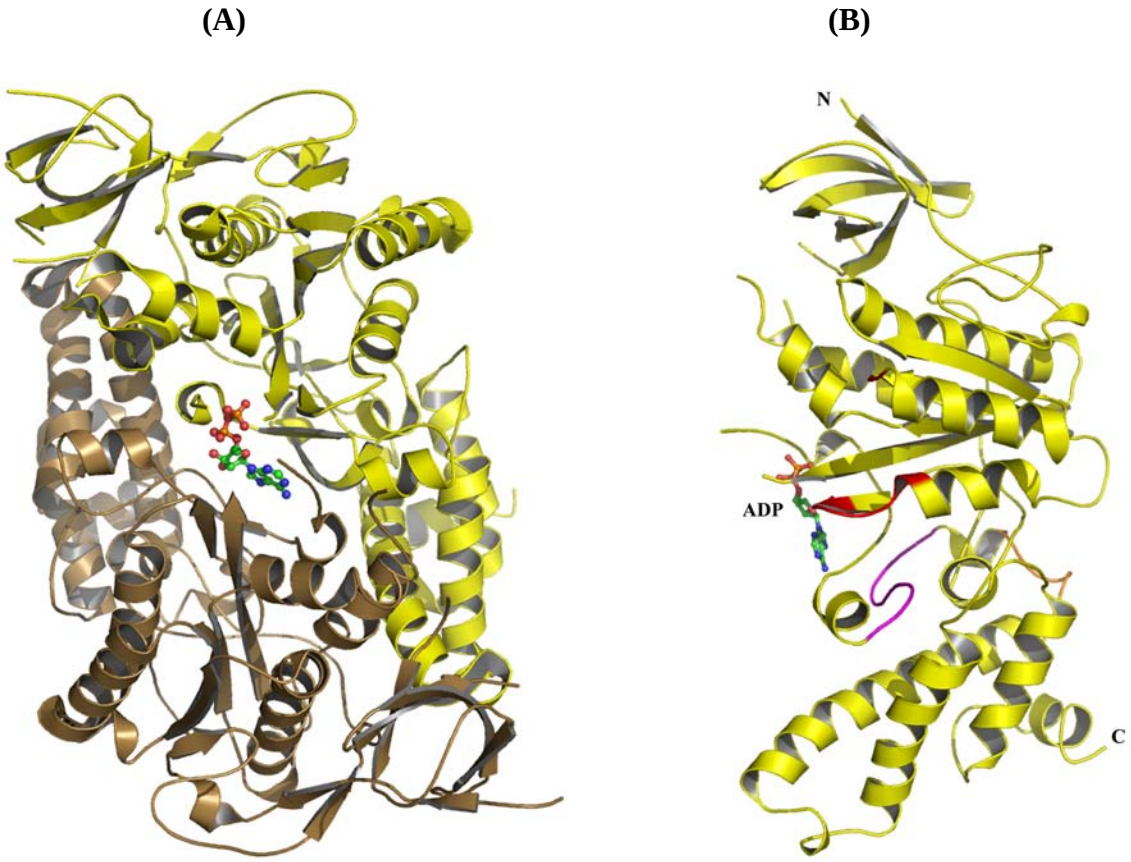

Figure 3.2.16. (A). Structure of the ADP bound form of subunit B at 2.7 Å resolution (KUMAR *et al*., 2008) (PDB 3DSR). The ADP molecule is shown as ball and stick. (B) A cartoon diagram of chain A of ADP bound subunit B structure with ADP molecule (ball and stick representation) shown. The P-loop sequence $_{150}$SASGLPHN$_{157}$ is highlighted in red color (KUMAR *et al*., 2008). The actual site of binding is shown by brown surface with nucleotide (brown line representation) docked inside. The P-loop region (S150-E158) is highlighted in red and the peptide G336 to R349 that is reported to covalently bind 8-N3-30-biotinyl-ATP (SCHÄFER *et al*., 2006b) is shown in magenta color.

A detailed summary of the data collection, phasing, and structure refinement statistics are given in Table 3.2.2. The bound ADP molecule that lies near the P-loop region of the central α/β domain has 50% occupancy which was confirmed during the structure refinement procedure. The electron density of the ADP molecule could be identified at 3σ cut-off in the ADP omit map. The occupancy level of the bound ADP molecule was varied while checking its thermal

parameters and the difference electron density peaks during refinement and the final occupancy was estimated. Figure 3.2.17 shows the amino acid residues that surround the ADP molecule within 5 Å region. It could be seen clearly that the ADP molecule has strong hydrogen bonding interaction with the chain A residues, while the chain B residues play more of a supporting role by way of stabilizing the ADP molecule through weak van der Waals interactions. The phosphate groups of the ADP molecule are well stabilized by hydrogen bonding interaction with the main chain atoms of the protein molecule. The oxygen atoms of the β-phosphate of the ADP molecule forms hydrogen bonding interaction with main chain carbonyl oxygen atom of S304(A) and P315(A). The α-phosphate is stabilized by hydrogen bonding interaction of its oxygen atom with the main chain amino nitrogen of L317(A) and main chain carbonyl oxygen atom of P315(A). Therefore, the P315(A) residue makes bifurcated hydrogen bonding interaction with both phosphate groups of the ADP molecule.

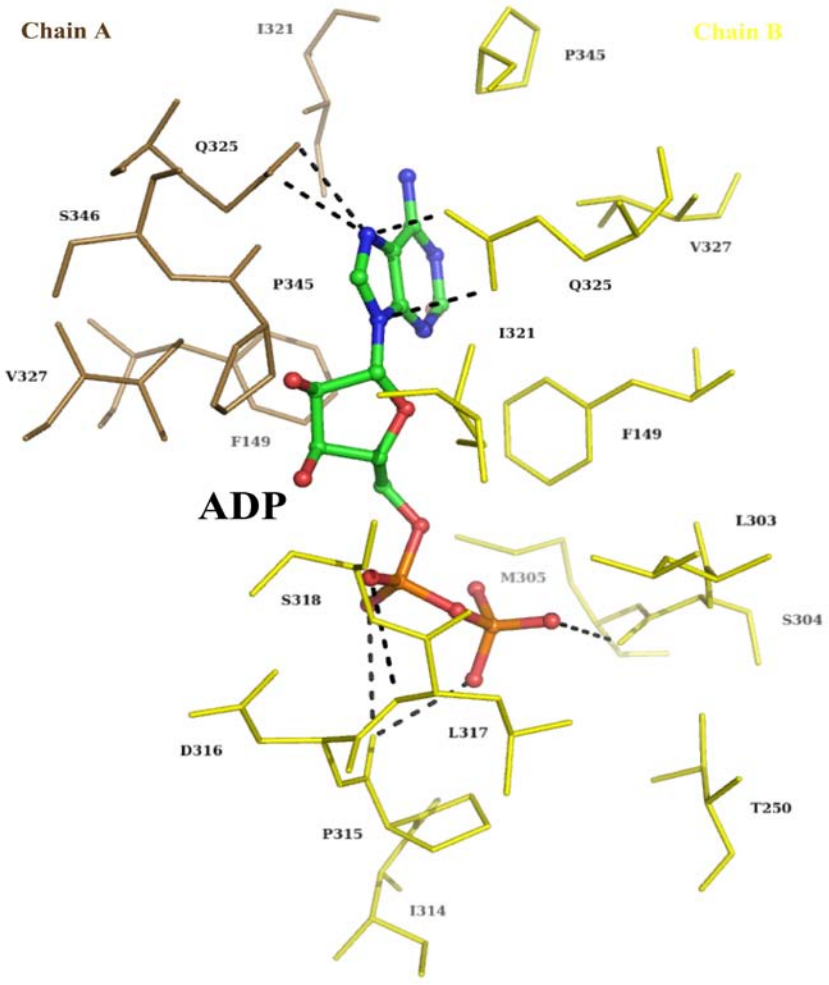

Figure 3.2.17. The amino-acid residues that surround the ADP molecule within a 5 Å radius (PDB 3EIU). The ADP molecule is shown in ball-and-stick representation and the amino-acid residues are represented as sticks. Chain A residues are shown in yellow and chain B residues in brown. The hydrogen-bonding interactions between the ADP molecule and the amino-acid residues are shown as dotted lines (KUMAR *et al*., 2008).

The ribose group of the ADP molecule is mainly stabilized by hydrophobic interaction with the side chain atoms of S318(A), V327(B), P345(B) and I321(A). The adenine ring is stabilized by the π...π stacking interaction with F149(B) and F149(A). In addition, the nitrogen atoms of the five membered ring in the adenine group makes a strong hydrogen bonding interaction with the side chain oxygen and nitrogen atoms of the Q325(A) and Q325(B) residues, whereas one of the nitrogen atoms of the six-membered ring of the adenine group has hydrogen bonding interaction with a water molecule. Furthermore, the residues V327(A), P345(A) and I321(B) confer van der Waals interaction to the adenine group of the ADP molecule. All these interactions strongly hold the ADP molecule in its binding position, located about 13 Å apart from the final nucleotide-binding site, made-up by the phosphate-binding loop (P-loop) and the adenine-binding pocket. Therefore, the ADP binding site has been termed as transient binding site (KUMAR *et al*., 2008).

3.2.13 Detection of ADP-binding due to Trp-fluorescence of subunit B mutant F149W

Intrinsic tryptophan fluorescence quenching experiments were performed with subunit B-WT and its newly created mutant F149W to ascertain ADP binding to these proteins. In the ADP bound structure of subunit B-WT, the F149 residue form a π...π interaction with the bound ADP molecule (Figure 3.2.17). Therefore, a mutant F149W was created to be used to confirm that the trapped transition nucleotide-binding site is crucial for ADP-binding. In this way, any nucleotide interacting with this residue could be identified directly by its intrinsic fluorescence. As shown in figure 3.2.18 the absorbance spectrum of the F149W mutant protein shows a maximum at 336 nm (*curve* ○). Addition of ADP (*curve* ◊) dropped the fluorescence intensity up to 18 % indicating that the tryptophan fluorescence spectrum of mutant F149W is sensitive to ADP binding.

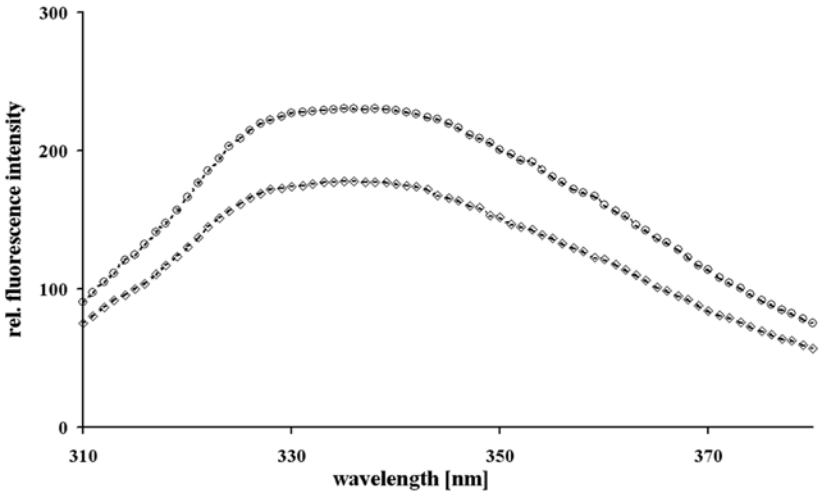

Figure 3.2.18. Fluorescence emission spectra of subunit B mutant F149W in the presence and absence of ADP. The fluorescence emission spectra (excitation wavelength of 295 nm with excitation and emission band passes of 5 nm) of mutant F149W were measured at 293 K. Fluorescence emission spectra of F149W mutant protein are shown in the absence (circles) and presence (diamonds) of 2 mM MgADP (KUMAR *et al*., 2008).

3.2.14 Structure comparison of ADP bound form with the nucleotide free B-subunit

The overall structure of the ADP-bound form is similar to the nucleotide free subunit B, the r. m. s. deviation being 0.782 Å for the backbone Cα atoms. Notable deviations occur near the N-terminal region and in the loop regions, R257-Y277 and M305-D316. Maximum deviations of 5.5 Å occur for the residue A274 in R257-Y277 region and 5.4 Å for P313 in M305-D316 region. These two regions are part of the loop region, above the P-loop, that would face the central stalk region in the intact A_1A_O ATP synthase. The latter region is also where the phosphate group of the ADP molecule binds and therefore could also be interpreted as being caused by ADP binding. Among the three domains of the B subunit, the N-terminal β-barrel (13-76) show an r. m. s. deviation of 0.563 Å, whereas the central nucleotide binding α-β domain (77-358) show deviation of 0.888 Å and the C-terminal α-helical bundle (359-460) has 0.238 Å deviation with the nucleotide free structure. When the N-terminal domains of both the structures are superimposed, their C-terminal domains are related by a rotation of 3.5°. The central α-β domain show slight deviation when compared with the C-terminal domain but significant movement is noted especially in the lower part of the domain where the adenine binding pocket is located. The region E323 to G358 shows marked movement. Interestingly, this region includes the peptide G336 to R349, reported to covalently bind 8-N_3-3′-biotinyl-ATP (SCHÄFER *et al.*, 2006b) and is the site for the adenine binding pocket. The C-terminal α-helical domain deviates most and it moves as a whole rigid body.

	B_{DP}
Data collection statistics	
Wavelength (Å)	1
Space group	$P2_12_12_1$
Unit cell parameters (Å)	
a =	74.21
b =	95.94
c =	130.38
α = β = γ (°)	90
Resolution range (Å)	50.0 - 2.70
Number of unique reflections	23211
I/σ^a	12.56 (2.7)
Completeness (%)	93.3 (78.5)
R merge[b] (%)	8.1 (45.8)
Multiplicity	3.7 (4.0)
Refinement statistics	
R factor[c] (%)	19.8
R free[d] (%)	26.7
Ramachandran statistics	
Most favored (%)	84.5
Additionally allowed (%)	14.7
Generously (%)	0.8
Disallowed (%)	0.0

	B_{DP}
R.M.S. deviations	
Bond lengths (Å)	0.01
Bond angles (°)	1.44
Mean atomic B values	
Overall	42.33
Wilson plot	51.6

[a] Values in parentheses refer to the corresponding values of the highest resolution shell (2.79 – 2.70).

[b] $R_{merge} = \Sigma\Sigma_i|I_h - I_{hi}|/\Sigma\Sigma_i I_h$, where I_h is the mean intensity for reflection h.

[c] R-factor = $\Sigma||F_O| - |F_C||/\Sigma|F_O|$, where F_O and F_C are measured and calculated structure factors, respectively.

[d] R-free = $\Sigma||F_O| - |F_C||/\Sigma|F_O|$, calculated from 5% of the reflections selected randomly and omitted during refinement.

Table 3.2.2. Statistics of crystallographic data collection and refinement for the B_{DP} structure of wild type subunit B.

3.2.15 Structure comparison of ADP bound form with the ATP bound transient-II state

In the case of ATP bound transient-II structure (KUMAR *et al*., 2009a), and the ADP bound structures of subunit B, the nucleotide molecules are bound near the P-loop region. Structural comparison of both the (Figure 3.2.19) yielded an r.m.s deviation of 0.79 Å indicating a significant structural similarity.

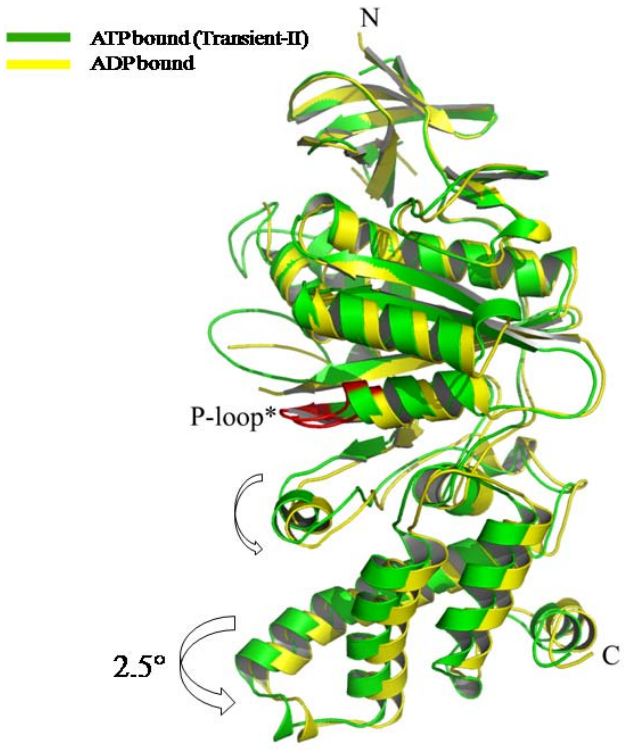

Figure 3.2.19. Structure comparison of ADP-bound (yellow, KUMAR *et al*., 2008; PDB 3DSR) and ATP bound transient-II state (KUMAR *et al*., 2008; PDB 3B2Q; green) of subunit B with respect to N-terminal domain superposition. The arrow represents the movement of the P-loop region, the peptide Gly336–Arg349 in the central α/β-domain and the C-terminal domain due to binding of the ADP molecule.

Larger than average deviation is found near the N-terminal region and for the loop regions Q258-Y277 (maximum deviation of 5.3 Å for the residue G274) and M305-D316 (maximum deviation of 5.6 Å occurs for the residue P313). The loop region M305-D316 is close to the nucleotide binding site in transient-II structure and therefore, the structural variation could be due to the binding of the ATP/ADP molecule. When the N-terminal domains of both the structures are superimposed (Figure 3.2.19), their C-terminal domains are found to be related by a rotation of 2.5° signifying the differential nucleotide binding in subunit B.

4. Discussion

4.1. Mode of nucleotide binding in subunit A

The availability of high resolution structures of the participating subunits in nucleotide bound forms is a prerequisite to get a deeper understanding of the mode of nucleotide binding in the A_1 headpiece and ATP synthesis of the A-ATP synthases. The first high resolution structure of the catalytic subunit A from *Pyrococcus horikoshii* OT3 was published in 2006 (MAEGAWA *et al*., 2006). The structure was determined at a resolution of 2.55 Å, where the N-terminal 1-60 amino acids could not be resolved due to high B-factor values in the region. The nucleotide-binding domain was also found disordered and the structure as described was devoid of nucleotides and water molecules, which plays a vital role in ligand binding and enzyme catalysis. Therefore, in this thesis, the crystal structures of the empty (A_E), AMP-PNP (A_{MP}) and ADP-bound (A_{DP})subunit A of the *P. horikoshii* OT3 A-ATP synthase have been determined to a resolutions of 2.47 Å and 2.4 Å, respectively. The nucleotides are found to bind to the P-loop region as expected in both the structures. These nucleotide bound structures of the catalytic subunit A provide a new understanding of the structural changes occurring in this subunit due to nucleotide-binding and during catalytic events. It also provides an excellent mean to identify those key amino acids which are involved in ATP synthesis, even though magnesium ion could not be identified in both the nucleotide bound structures. In the A_E structure, it was surprising to note that the phosphate analog SO_4^{2-} is bound via a water molecule to the P-loop residue, S238. The sulfate ion is located at a position between the β- and γ-phosphate of the AMP-PNP molecule. This has led us to mutate S238 to generate a S238A mutant and to solve its structure, which is a P-loop mutant, to a resolution of 2.4 Å. Although crystallized under identical conditions, no sulfate ion is present in the S238A mutant structure, indicating that the A_E structure may represent an intermediate state of the Pi-binding site. The importance of S238 in phosphate binding is emphasized by hydrogen bonding of S238 with α- and β-phosphates of ADP via a water molecule in the A_{DP} structure, and the bifurcated hydrogen bond with the γ-phosphate of AMP-PNP in the A_{MP} structure (Figure 4.1). The γ-phosphate of AMP-PNP is bridged by a water molecule to P235, which moves out of the active site, when ADP is bound, opening thereby the site for ADP + Pi binding (Figure 4.1). Thus the importance of the solvent molecules surrounding the catalytic centre is immense and for an in-depth understanding of the catalytic mechanism in the effect of protein residues on the bound nucleotide as well as their influence on the nearby solvent molecules and the interplay between nucleotide, solvent, and protein has to be interpreted (DITTRICH *et al*., 2003). When compared to the related rat liver mitochondrial F_1F_O ATP synthase, the P-loop residue P235 in subunit A is the structural equivalent of A158 of the catalytic subunit β which is proposed to be critical in the final events

of ATP synthesis, by moving into the active site and facilitating release of water and ATP formation (CHEN *et al*., 2006). Besides P235, conformational changes were also observed for the P-loop residues G234, K240 and T241. These observed structural deviations are in line with those of their functionally equivalent conserved lysine and threonine residues from the P-loop in β subunits of F-ATP synthases, which plays a role in Mg-ATP-binding and transition state formation, respectively (ABRAHAMS *et al*., 1994; SENIOR *et al*., 2000; KABALEESSWARAN *et al.*, 2006; SENIOR *et al.*, 2002).

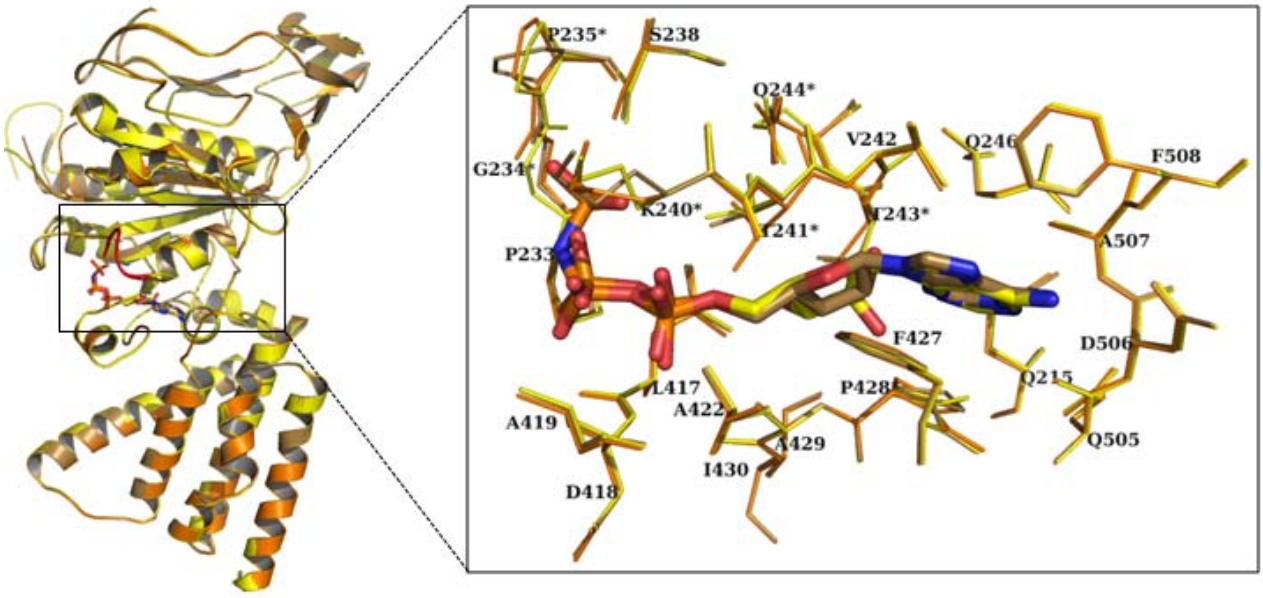

Figure 4.1. Structural comparison between the A_E (orange, PDB 3I72), and A_{MP} (yellow, PDB 3I4L) and A_{DP} forms (sand, PDB 3I73) of subunit A. The zoom in window shows the comparison of the P-loop regions highlighting side chain deviations for residues G234, P235, K240 and T241 due to nucleotide (stick) binding. Side chain variations for the nucleotide binding region indicating the conformational change (starred) in T243, Q244 and P428 residues in addition the P-loop region (KUMAR *et al*., 2009b).

The nucleotide binding sites and the corresponding residues marking the binding sites in the A subunit and the homologous catalytic β subunit from the F-ATP synthase are similar, yet there are pronounced differences in the P-loop arrangement. Superposition of the two subunits shows that the P-loop in subunit A is in a sort of strained conformation compared to the relaxed state of the same in the β subunit resulting in a different arrangement of the nucleotides inside the nucleotide-binding site (Figure 4.2A). Upon superposing the AMP-PNP bound $\tilde{\beta}$ subunits (β_{MP}) of bovine mitochondrial F_1-ATPases (1BMF; ABRAHAMS *et al.*, 1994) with the A_{MP} structure, it was observed that the central nucleotide binding α/β domain overlap well relative to the other two domains (Figure 4.2A). The superposition of these subunits demonstrates the subtle diversities in the orientation of the AMP-PNP inside the binding sites of both subunits. The adenine-, ribose, α and β-phosphate moieties form a horizontal axis below the P-loop of A_{MP}

followed by the kink of the γ-phosphate to align this γ-phosphate residue in the direction of the P-loop and thus enable the interaction with the S238 (Figure 4.2B). Upon comparison of the ADP-moiety of the AMP-PNP molecule in the β-subunit it was found oriented above the nucleotide in the A_{MP} structure by 35.86°, and thus bringing the β- and γ-phosphate in proximity to the conserved P-loop residues K240 and T241 and orienting these two phosphate residues above the P-loop (β subunit) (Figure 4.2B) (KUMAR *et al.*, 2009b).

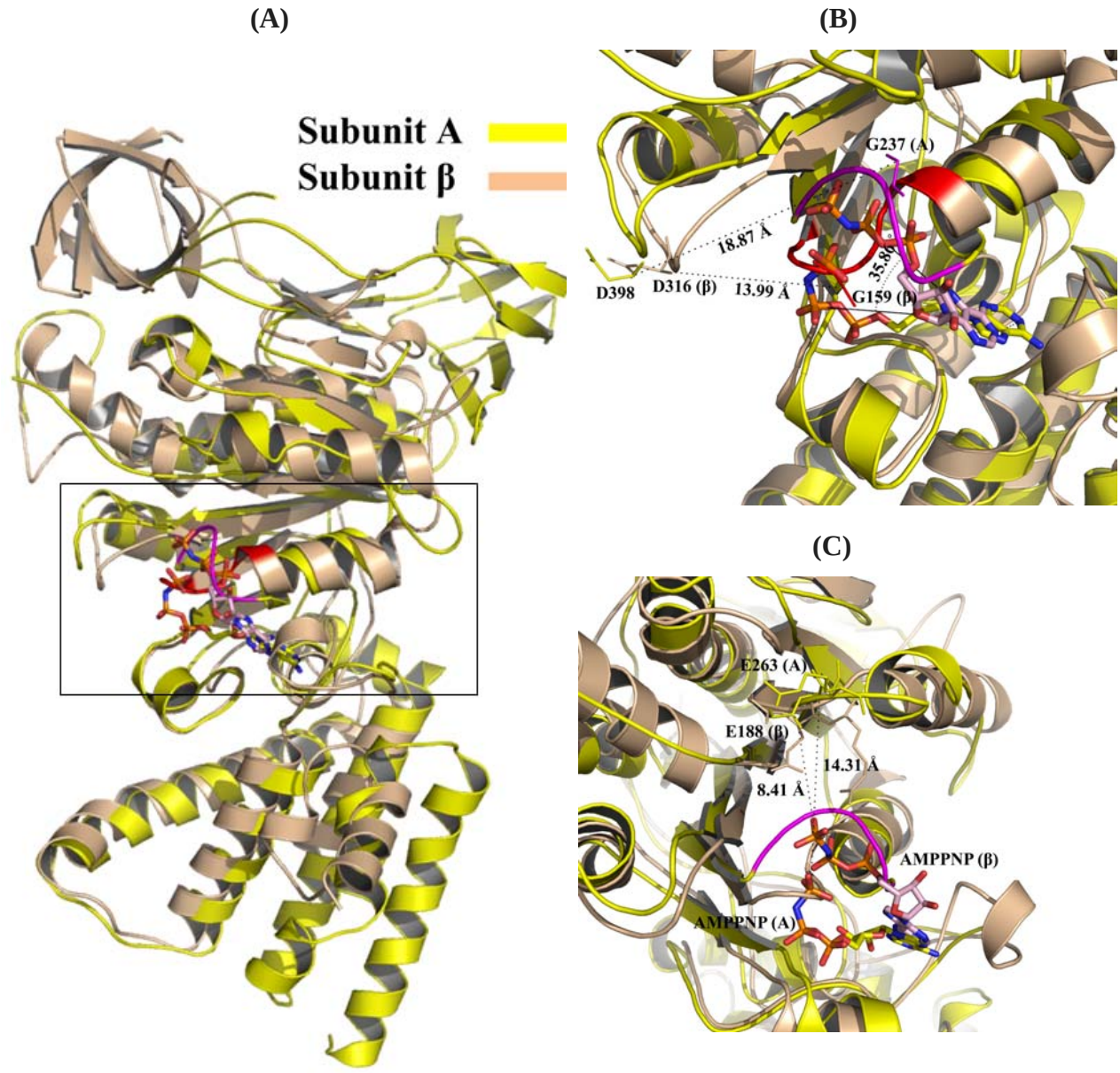

Figure 4.2. (A) Structural comparison of the bovine β_{MP} (wheat; 1BMF (ABRAHAMS *et al.*, 1994)) and the A_{MP} structure (yellow) (KUMAR *et al.*, 2009b). The P-loop is highlighted in magenta for A_{MP} and red for β_{MP}. The difference in the binding of the AMP-PNP molecules could be clearly seen. (B) The AMP-PNP binding region in the structural comparison of A_{MP} and β_{MP} structures. The angle and the slide difference of the bound AMPPNP molecules are highlighted (KUMAR *et al.*, 2009b). (C) Another view of the AMP-PNP binding region, showing the distance between the γ-phosphate and the A-E263 (β-E188) of the GER-loop in the structural comparison (KUMAR *et al.*, 2009b).

It was also found that the γ-phosphate in β_{MP} is significantly closer (8.41 Å) to the GER-formed loop above the P-loop compared to the distance of both loops in the A_{MP} structure (14.31 Å) (Figure 4.2C). This is important, since in subunit β of bovine F-ATP synthase the GER-loop residue E188 is involved in activating and aligning of a water molecule to make nucleophilic attack at the γ-phosphate to generate pentavalent transition intermediate (ABRAHAMS *et al*., 1994, SENIOR *et al*., 2000). The E188 is therefore believed to act as a mild base, enabling the formation and stabilization of the pentacoordinated transition state thus formed during catalysis (DITTRICH *et al*., 2003). Therefore, this comparative spatial arrangement of the bound nucleotides in A_{MP} and β_{MP} highlights the novel positioning of AMPPNP molecule in subunit A possibly due to characteristic P-loop arrangement in subunit A. It also suggests that the bound nucleotide molecule is weakly held in the binding site making it more solvent exposed. This finding could possibly provide an explaination for the not so strict specificity of the A-type ATP synthases to hydrolyze not only the main substrate ATP but also GTP and UTP with varied degree of activity (LINGL *et al*., 2003; CHEN and KONISKY, 1993). Therefore, it could possibly provide an explanation for the differential binding constants for Mg-ATP (2.38 μM) and Mg-ADP (1.50 μM). This differential binding preference of ADP to subunit A is contrary to the nucleotide binding pattern observed in homologous catalytic subunit β from F- ATP synthase and subunit B from A-ATP synthase. Both these subunits bind to nucleotides but with a preference for ATP- over ADP molecule (SCHÄFER *et al*., 2006b; KUMAR *et al*., 2009a). This is despite the fact that the P-loop sequences are not similar in these subunits but their P-loops are structurally equivalent.

In F-ATP synthases, the $\alpha_3\beta_3$ heapiece is the catalytic centre and the nucleotide binding sites are located at the interfaces of the alternating α and β subunits. The catalytic nucleotide binding sites are mostly located on the β subunits, with some contribution from the α subunits while the non-catalytic ones are mostly formed from α subunit residues with some contribution from the adjacent β subunits (ABRAHAMS *et al.*, 1994). There is no high resolution structure of the A_1 headpiece from the A-ATP synthase avialble so far. Therefore, to realize the importance of the amino acid residues from subunit A and B from A-ATP synthase, which are playing important role during nucleotide binding and catalytic events in the full complex, structural overlapping was planned with respective structural homolog subunits β and α of the $\alpha_3\beta_3\gamma$ sector of bovine F_1 ATPase (1BMF; ABRAHAMS *et al.*, 1994) and an A_3B_3 hexamer structure was constituted (Figure 4.3A and B). The subunit B (3B2Q; KUMAR *et al.*, 2009a) was overlapped with its structural homolog α subunit (ABRAHAMS *et al.*, 1994). Similarly, while overlapping subunit

A in its empty and nucleotide bound forms (A_E, A_{MP} and A_{DP}); it was carefully matched with the respective ligand bound forms of the homologous β subunit (β_E, β_{TP}, β_{DP}). In the A_3B_3 hexamer, the nucleotide binding sites occupies the A-B dimer interfaces and upon analysis of the binding sites for AMP-PNP (Figure 4.4A), ADP (Figure 4.4B) and the empty forms (Figure 4.4C); the R349 from subunit B is found to play an important role. Earlier results of photoaffinity labelling study using a photoaffinity ATP analogue, 8-N_3-3'-biotinyl-ATP on subunit B has showed that the azido group of the photoaffinity labeled ATP might be interacting with Y338 of the peptide G336-R349 of the subunit B (SCHÄFER *et al*., 2006b). Surprisingly, the residue R349 belongs to the same labelled peptide G336-R349. The R349 residue of the subunit B is homologous to R373 in subunit α of the bovine F-ATP synthase, described to stabilize the negative charge on the terminal phosphate in a penta-coordinated transition state during catalysis (ABRAHAMS *et al*., 1994; SENIOR *et al*., 2000). In the A_E-B interface, the residue R349 is free to interact, but in the A_{DP}-B interface it has steric clash with the P-loop residue S238 from subunit A. Similarly, in the A_{DP}-B interface the residue L347 from adjoining subunit B has steric clash with A-K240. These observations highlight the importance of the subunit B residues R349 and L347 in the nucleotide binding process.

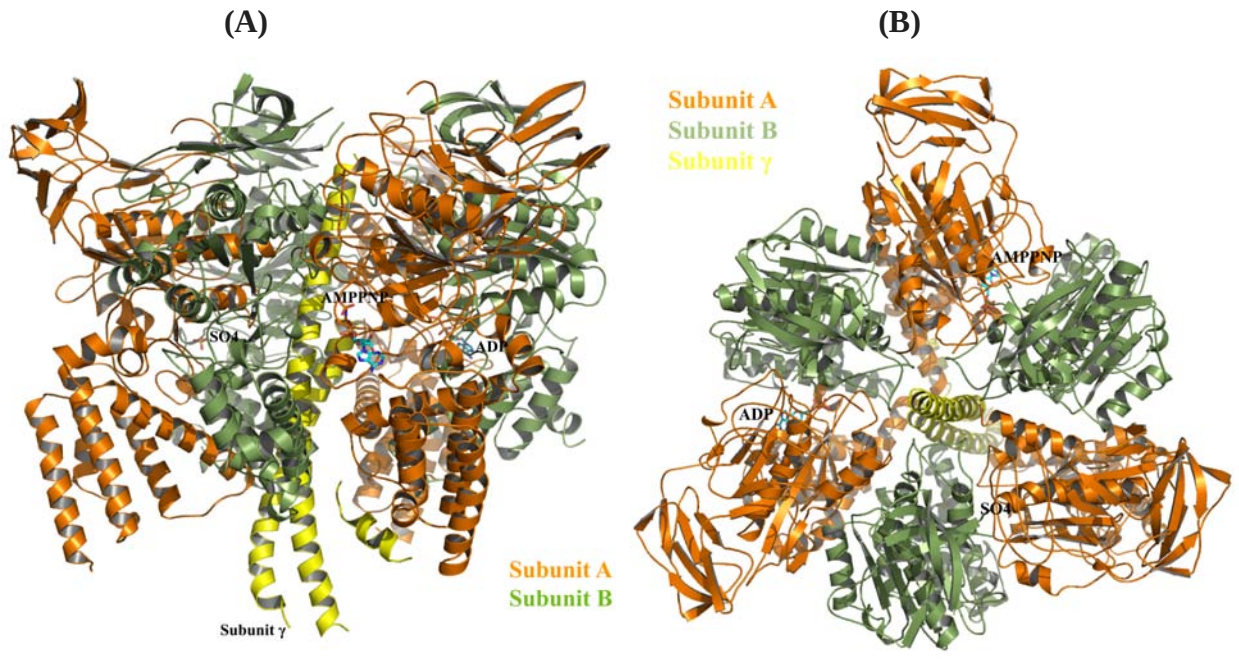

***Figure 4.3*. The hexamer structure of A_3B_3 ATPase, modified according to KUMAR *et al*., 2009b**. The hexamer was modelled by fitting the A subunit structures (orange; KUMAR *et al*., 2009b) and the *M. mazei* Gö1 B subunit (smudge; 3B2Q (KUMAR *et al*., 2009a)) on to the related β− and α subunits of the bovine mitochondrial F_1 ATPase (1BMF; ABRAHAMS *et al*., 1994), respectively. The γ subunit (yellow) of F_1 ATPase, which is the homolog to the D subunit of A_1 ATPases, is retained in the model. The nucleotides for the A subunit are rendered in stick representation. (A) Side view, (B) top view.

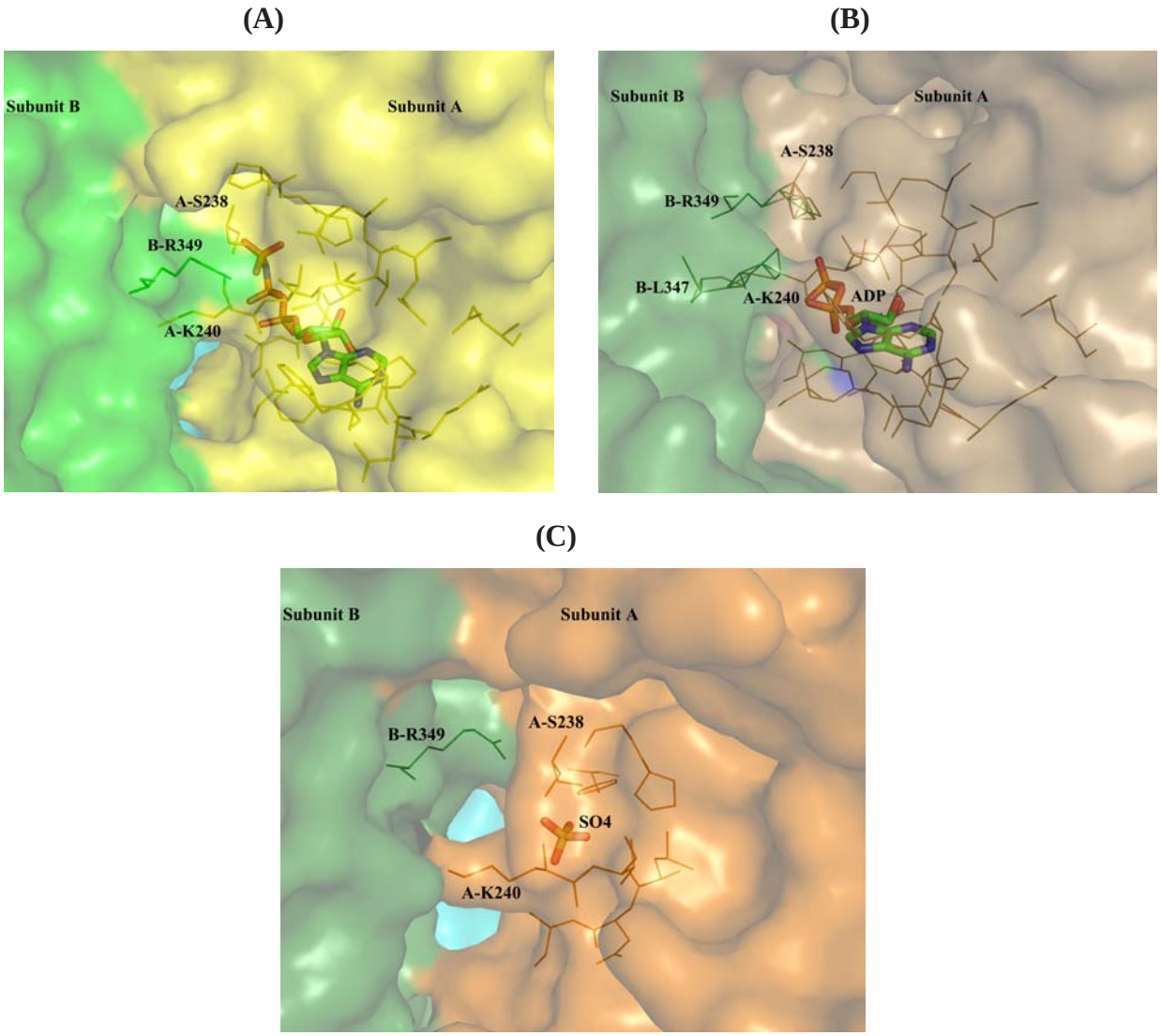

Figure 4.4. The structural interface near the P-loop region between the AMP-PNP bound (yellow) (A); ADP bound (sand) (B); and empty (C) forms of the A subunit with subunit B (green) in the hexamer model of A_1 ATPase (KUMAR *et al*., 2009b). The hexamer structure was modelled by fitting the respective A subunit structures and the *M. mazei* Gö1 subunit B (green; 3B2Q (KUMAR *et al*., 2009a)) on to the related β and α subunits of the bovine mitochondrial F_1 ATPase (1BMF; ABRAHAMS *et al*., 1994).

The availability of ADP and AMP-PNP bound structures of subunit A, and the reduced binding affinity of ADP and ATP in the mutant S238A determined using ITC, indicates that the amino acid S238 in the P-loop region is involved in the nucleotide binding in subunit A. The structural superposition of the S238A mutant and bovine β_E, shows that their P-loop regions are structurally very similar. This is a very significant observation which is indicative of the important role played by this residue during nucleotide binding and catalytic events. The interaction profile of the P-loop in A_E shows that the P-loop is held in characteristic strained conformation by the direct interactions of F236 with the side-chains of D331, the side-chain of P235 with the main chain of S238 and the indirect association of the side chain of D331 and E267 with G237 via a water molecule (Figure 4.5A). In the S238A mutant structure, the direct interaction of P235 and

S238 as well as the interactions of F236 with D331 and E244 are abolished; leading to the collapse of the loop to a relatively relaxed conformation as is seen in bovine β_E. This indicates that the alanine substitution in S238A has disrupted the interactions formed by the P-loop residues P235, F236 and S238.

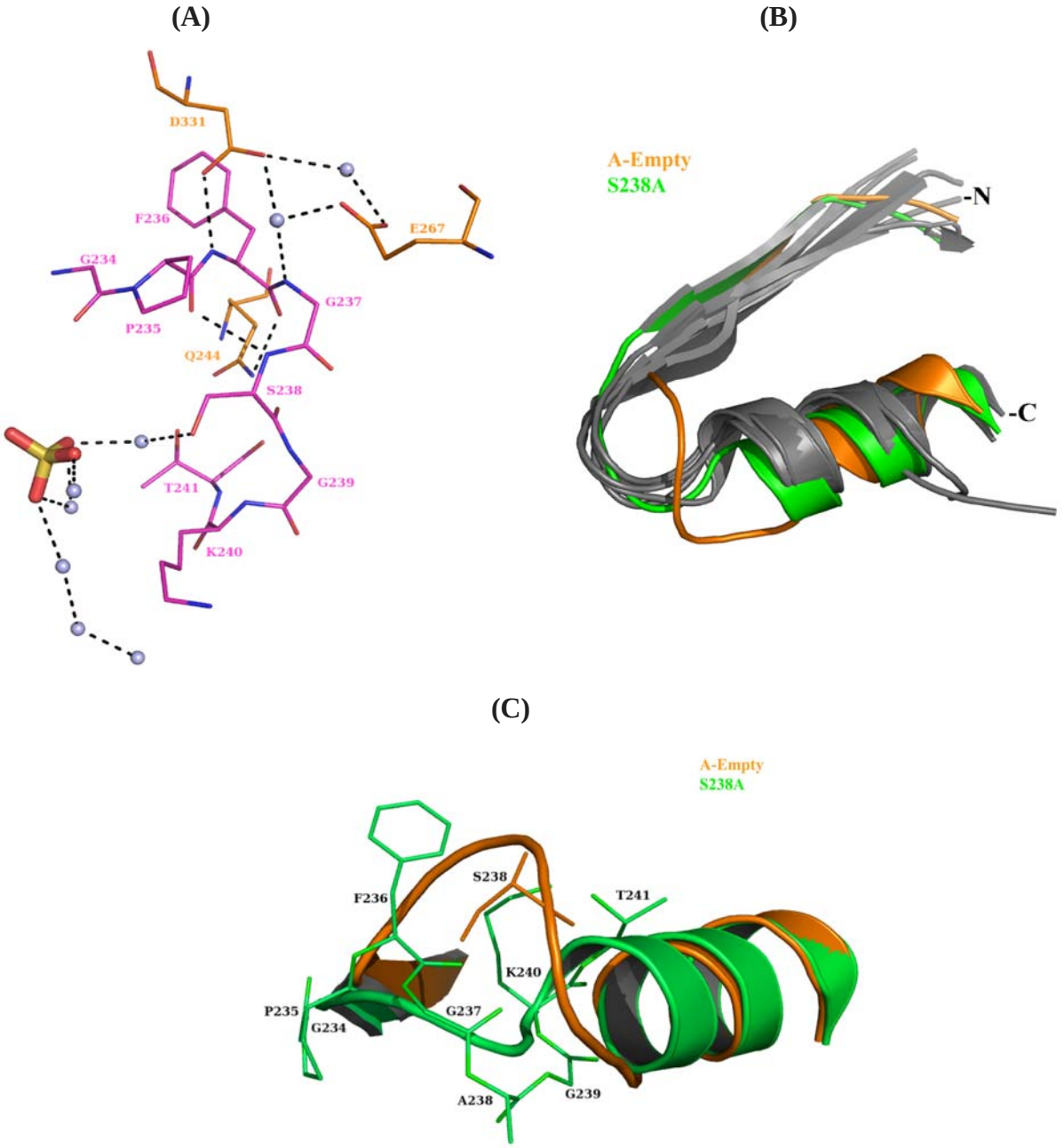

Figure 4.5. (A) The polar interaction profile of the P-loop region (magenta) in the empty form of the A subunit. The network of polar interaction (black dotted lines) stabilizing the P-loop is indicated. (B) The structural overlap of the β-loop-α motif of all the available P-loop structures (3KAR: Kinesin-like protein KAR2; 1D2N: N-Ethylmaleimide-sensitive fusion protein; 1FFH: signal recognition protein FFH; 1G6O: Traffic ATPase (+ ADP); 1BG2: Kinesin motor domain; A_E and S238A mutant of subunit A) having the primary sequence GXXGSGKT. (C) Overlap of the P-loops from empty and the S238A mutant of subunit A. The unique orientation of the empty P-loop could be visualized clearly.

All members (with few exceptions) of the superfamily of ATP/GTP-binding proteins possess the consensus sequence of GXXXXGKT(S) in the P-loop (SARASTE *et al.*, 1990). Upon superimposing the available P-loop structures with the consensus sequence of GXXGSGKT, it was observed that all P-loop structures, including the S238 mutant, overlapped quite well in the horizontal and relaxed orientation (Figure 4.5C). This state of the P-loops is comparable to the ones in α and β of F-ATP synthases, with the only exception of the arched P-loop of subunit A ($_{234}$GPFGSGKT$_{241}$), indicating its unique conformation. The structural comparison of these P-loops shows that the characteristic strained P-loop arrangement in the A subunit of A-ATP synthases is the result of the interactions of the three P-loop residues, P235, F236 and S238.

The ATP synthase family can be divided into three major subfamilies: the F-ATP synthases, the vacuolar V-type ATPases and the archaeal A-type ATP synthases. All the three members of the family are evolutionarily related and based on sequence, structural and functional attributes, it is believed that the three subfamilies have originated from a common ancestor during the course of evolution (NELSON, 1992; HILARIO and GOGARTEN, 1998; CROSS and MÜLLER, 2004). The divergences during evolution has happened by changes in their structure and function of the constituent subunits (CROSS and TAIZ, 1990; GRÜBER and MÜLLER, 2003; CROSS and MÜLLER, 2004). Two such major changes are discerningly apparent. First being the numerical change in the number of proteolipid subunits of the ion transporting domain. It has been observed that the V-ATPases have developed a proton transporting membrane embedded proteolipid oligomer with just half the normal number of ion-translocating groups, which prevents ATP synthesis but still allow ion pumping process. In similar line, it should be possible to switch between ATP synthesis or ATP hydrolysis in F/A-ATP synthases by varying the present number of ion-translocating groups (MÜLLER *et al.*, 2003). The second major change which brought about the reversal from ATPase to ATP synthase was probably achieved by the duplication of the gene encoding the nucleotide-binding catalytic subunit. This duplication then followed by a loss of catalytic capacity of one of the subunit by a single point mutation of a catalytically essential residue (e.g. E188Q in the GER-loop of the catalytic β subunit to form non-catalytic α subunit) (ABRAHAMS *et al.*, 1994). The crystallographic structures in the present thesis show that the alterations in the three critical residues in the P-loops of catalytic A (GPFGSGKT) and β subunit (GGAGVGKT) cause the conformational rearrangement of the strained P-loop in subunit A to a relaxed form as in β. This evolutionary switch in amino acid sequence and conformation of P-loops has led to an altered nucleotide-binding, -specificity and accessibility, causing catalytic variation in the energy producers A- and F-ATP synthase. Upon

comparision of the A subunit P-loop sequences of the representative organisms from the F-ATP synthases, the vacuolar V-ATPases and the archaeal A-ATP synthases, it was observed that the P-loop sequence of A subunits of A-ATP synthases (GPFGSGKT) differs only by the Phe and Ser residues (KUMAR *et al*., 2009b). These residues are substituted by an Ala- and Cys residue in V-ATPase subunit A (GAFGCGKT). Previous studies have shown that the conserved cysteine in V-ATPases is accessible to sulfhydryl reagents, leading to inhibition of activity in this class of the ATPases (FENG and FORGAC, 1992). The subunit A structures (A_E, A_{MP} and A_{DP}) presented in this thesis highlight the important interactions furnished by the S238 residue, which is acting as a functional equivalent of the Cys residue from V-ATPases. Hence, suggests that the conserved Cys residue might be able to bind to phosphate moiety in V-ATPases. The Phe residue responsible for maintaining the strained conformation of the P-loop in subunit A A-ATP synthases, is also found to be conserved across P-loop sequences in V-ATPases. On contrary, the substituted alanine residue in the P-loop of the V-ATPases, might not be able to confer the Pro-Ser like interactions as has been observed in A-ATP synthases. This might have led to characteristic V-ATPase specific P-loop arrangement. Therefore, the P-loop architecture is specific to the kind of pump which harbors it and has evolved during the course of evolution to serve the purpose of ATP synthesis and hydrolysis.

It is well established from the available crystal structures of the F_1 ATPases that during catalytic events in $\alpha_3\beta_3$ sector, the αβ pairs are in three different conformations (ABRAHAMS *et al*., 1994). This is attributed to the asymmetric contacts of the shaft subunit (γ) which it makes with one of the αβ pair at any given point of time. Hence, the rotating central stalk subunit γ in F-ATP synthases is an essential component to indirectly couple the proton motive force across the membrane to ATP formation (or hydrolysis) in the catalytic subunits of the $\alpha_3\beta_3$ headpiece (GIBBONS *et al*., 2000). The C-terminal α-helical coiled coil region in the γ subunit modulates the nucleotide affinities of catalytic sites in β subunits (KABALEESWARAN *et al*., 2006). The C-terminal helix of γ, which traverse the entire length of the cavity of $\alpha_3\beta_3$, forms a catch of hydrogen bonds with the loop (D316-D319) of the nucleotide-binding domain located above the P-loop of β_E (Figure 4.6). The distance of both loops is 22.76 Å in β_E. Further movement of γ abolishes the catch and brings both loops closer in the β_{MP} (13.99 Å (Figure 4.2B) and β_{DP} structure (13.96 Å). By comparison, the distances between the homologue D397-E399-loop and the P-loops in A_E (19.02 Å, A_{DP} (19.48 Å and A_{MP} (18.87 Å) do not alter significantly. In this context it is of interest that the C-terminal helix of γ is shorter in the homologue central stalk subunit D of A-ATP synthases. Cross sections of the previously determined 3D-reconstruction of

the A_1 ATPase from *Methanosarcina mazei* Gö1 shows that the central subunit D does penetrate into the A_3B_3 hexamer, ending already at the middle part of the cavity (COSKUN *et al*., 2004a), like the central subunit in V-ATPases ((Figure 4.6) (RADERMACHER *et al*., 2001; GRÜBER and MARSHANSKY, 2008)). Subunit D can be cross-linked to subunit A in a nucleotide-dependent manner, involving both N- and C-terminal segments of subunit D and regions in middle and lower part of the A subunit structure (COSKUN *et al*., 2002). Sequence alignment of subunit D and subunit γ from A-/F-ATP synthases of representative organisms shows that indeed the C-terminal part of subunit D is shorter than subunit γ by around 26 amino acids. This finding implies that the coupling processes between the central D subunit and the catalytic A_3B_3 hexamer occurs in the lower half of the cavity of the A_3B_3 subcomplex. It also states that the coupling between the central stalk subunit and catalytic subunit A and β of A- and F-ATP synthases undergo via different concerted mechanisms (KUMAR *et al*., 2009b). Though, following some general principles, there are significant differences in the coupling mechanism adopted by this family of biological motors.

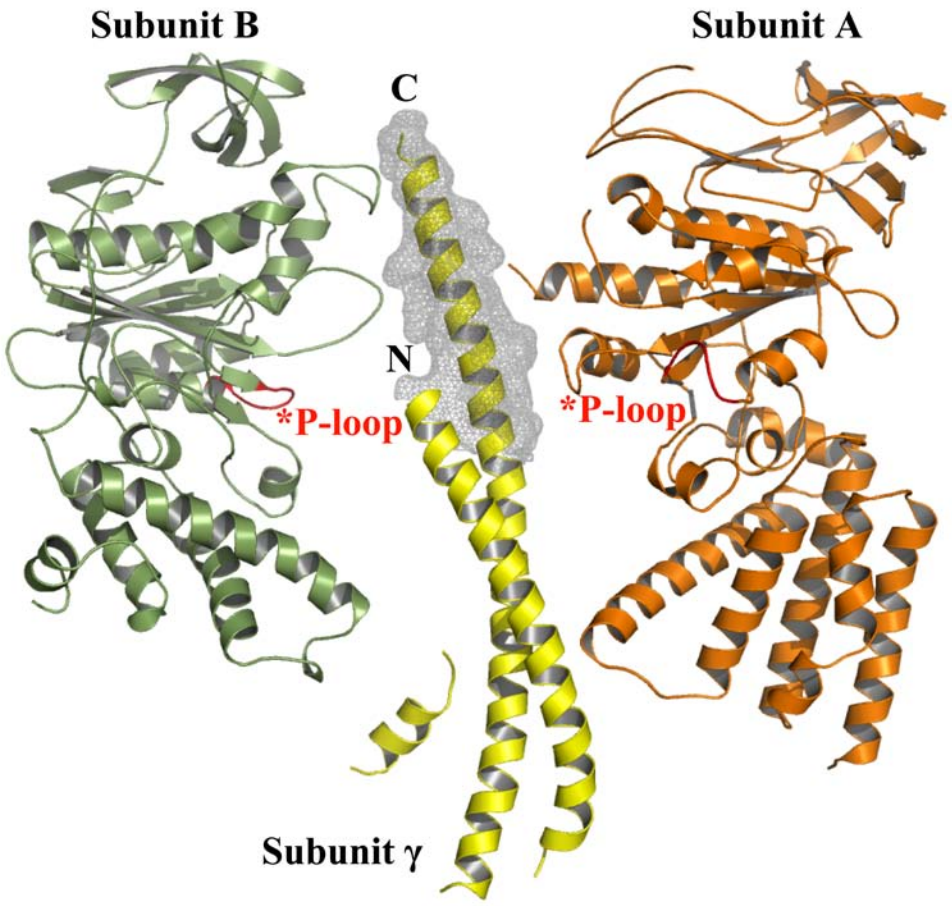

Figure 4.6. The subunit A (orange) and B (green) with the gamma subunit (yellow) in the hexamer model of the A_1 ATPase, modified according to KUMAR *et al*., 2009b; highlighting the missing C-terminal 26 amino acids (mesh representation) in the D subunit of A-ATP synthases.

4.2. Mode of nucleotide binding in subunit B

4.2.1 Nucleotide binding in subunit B

The crystal structure of subunit B from the A_1A_O ATP synthase of *M. mazei* Gö1 was solved in 2006 (SCHÄFER *et al*., 2006b). Until then it was proposed that subunit B has a non-catalytic role in ATP synthesis/hydrolysis processes. The very first evidences for the nucleotide binding capability of subunit B came from initial photoaffinity labelling experiments and fluorescence correlation spectroscopic experiments, which showed that subunit B from *M. mazei* Gö1 binds to nucleotides but with a weak affinity (K_d = 1.6 mM) compared to that of subunit A (SCHÄFER *et al*., 2006b). In these FCS experiments a bulky fluorophore BODIPY-FL-ATP was used for the measurements. In order to locate the nucleotide binding site and to investigate the role of individual amino acids in the nucleotide binding events, individual amino acids were mutated in a systematic way to generate mutants of subunit B. Ten different point mutants (F149W, L154C, L154S, P155G, H156K, I185E, Y338R, Y338W, A373W and R416W) and one double mutant (H156K/R416W) in the P-loop region and adenine binding site of subunit B were successfully generated (KUMAR *et al*., 2009a). The residues R416 and Y338 mark the adenine binding region of the nucleotide binding pocket in subunit B which are predicted to undergo π - π stacking and cation - π interactions, respectively with the incoming nucleotide. L154, P155 and H156 belong to the P-loop region which binds the phosphate group of ATP molecule. It was observed that unlike the P-loop mutants; L154, P155G, H156K and I185E, only Y338W and R416W mutants of subunit B were soluble and could be purified for further spectroscopic and crystallization experiments. Since, tryptophan can be used as an optical probe in spectroscopic experiments it was considered to be one of best candidates to substitute these key amino acids. The tryptophan fluorescence quenching experiments with R416W mutant of subunit B showed a significant dampening of the fluorescence signal upon addition of 2 mM Mg-ATP or Mg-ADP (KUMAR *et al*., 2009a). This indicated that the mutated residue (R416) is in close vicinity to the nucleotide binding site. In the tryptophan fluorescence spectrum, there was a significant shift observed in the λmax values, relative to the wavelength position of the wild-type spectrum with a λmax at 333 nm, the mutant spectrum shifted to 340 nm (red shift) (KUMAR *et al*., 2009a). The red shift observed in the fluorescence spectrum of R416W mutant shows that the microenvironment of a tryptophan residue has changed from non-polar to a polar environment. In order to investigate the effect of the mutation on nucleotide binding, FCS experiments were performed using wild type subunit B and R416W mutant of subunit B (KUMAR *et al*., 2009a). In the present study, in order to rule out the possibility of the negative effect of a bulky group attached to the nucleotide analogues, a different class of fluorophores (EDA-ATP ATTO-647N and EDA-ADP ATTO-647N analogues) were used which are smaller than BODIPY-FL-ATP.

The results showed binding constants of 22 ± 3μM and 38 ± 3 μM for Mg-ATP ATTO-647N for wild type subunit B and R416W mutant, respectively (KUMAR *et al*., 2009a). This indicated that the wild type subunit B binds slightly stronger to Mg-ATP ATTO-647N which might be caused by the reorientation of amino acid E158, resulting from the abolished salt bridge between E158 and the substituted R416 residue. The K_d values determined from intrinsic tryptophan measurements of R416W were in line with the FCS experiments (KUMAR *et al*., 2009a). The determined K_d values were found to be different for Mg-ATP (28 ± 2 μM) and Mg-ADP binding (41 ± 2 μM) (KUMAR *et al*., 2009a). This observation is quite unusual for a protein considered to be non-catalytic in function. The differential affinities of subunit B for Mg-ATP and Mg-ADP clearly indicate that it might not be a nucleotide binding/non-catalytic subunit only. The possibility of subunit B having a regulatory or even catalytic function during ATP synthesis or hydrolysis processes demanded further experiments. Incidentally, no such differences have been observed in the binding pattern of Mg-ATP and Mg-ADP in non-catalytic α subunit (homologue of subunit B) (WEBER *et al*., 1993), while differences were pronounced in catalytic β subunit from F_1F_O ATP synthase (WEBER *et al*., 1993). These results are in line with the nucleotide dependent cross-linking experiments performed using A_3B_3DF complex of A_1 and intact A_1A_O ATP synthase, where it was observed that the formation of B-F complex is reduced in the presence of Mg-ATP while addition of Mg-ADP showed no effect on B-F complex formation (COSKUN *et al*., 2004b). On contrary, it was found out that there was increased B-F complex formation in the presence of a non hydrolysable analogue of nucleotide (Mg-AMPPNP) (SCHÄFER *et al*., 2006a), indicating that coupling movement of shaft subunit F in the whole complex is dependent on the nucleotide bound to subunit B.

4.2.2 ATP-bound transient structures of R416W mutant of subunit B

In order to understand the catalytic mechanism during ATP synthesis/hydrolysis, one of the objectives of this thesis was to obtain the nucleotide bound form of subunit B. In the present thesis, a protocol for co-crystallization has been developed which helped in getting an ATP bound structure of R416W mutant of subunit B at 2.1 Å resolution (Figure 4.7A) (KUMAR *et al*., 2009a). In the ATP bound structure of the R416W mutant the nucleotide is located near to the phosphate binding P-loop region but not precisely into the predicted binding site. Hence, we believe that the present localization of ATP in the structure is possibly a trapped transition position (termed as transient-II) while on its way to the actual binding site made-up by the phosphate-binding loop (P-loop) and the adenine-binding pocket (KUMAR *et al*., 2009a; SCHÄFER *et al*., 2006b). The adenine ring of the bound ATP molecule is found to make a π - π interaction with the F149 residue, which precedes the P-loop sequence ($_{150}$SASGLPHN$_{158}$).

Intrinsic tryptophan fluorescence quenching experiments using subunit B-WT and its newly created mutant F149W showed that the tryptophan fluorescence spectrum of mutant is sensitive to ATP binding, thus confirming that the trapped transition nucleotide-binding site is important for ATP-binding. The understanding of the possible mode of entry by nucleotides to their respective binding sites in intact ATP synthases and the intermediate steps in catalytic reactions are still unresolved questions. In order to gain an insight into the reaction mechanisms, inhibition studies followed by high resolution structural characterization is one of the available approach. The catalytic F_1 domain of the F_1F_O ATP synthase enzyme has been studied by X-ray crystallography in a variety of inhibited states. There are reports of drug inhibited forms of the related bovine mitochondrial F-ATP synthase, where independent inhibitory sites have been identified by high-resolution structural studies (ORRIS *et al*., 1998; ABRAHAMS *et al*., 1996). While analyzing such drug inhibited structures from F_1F_O ATP synthase it was recognized that such kind of studies can be further extended to archaeal A_1A_O ATP synthases, to gain insight into the catalytic pathway of ATP hydrolysis and to elucidate binding sites and mechanisms of action of several inhibitors in this class of ATP synthases. Therefore, structural comparison of the ATP bound form of the R416W mutant B-subunit with the crystal structures of catalytic β-subunit of the bovine mitochondrial F-ATP synthase in complex with an antibiotic peptide, efrapeptin (ABRAHAMS *et al*., 1996), and with 4-chloro-7-nitrobenzofurazan (NBD-Cl) (ORRIS *et al*., 1998) were carried out. NBD-Cl is a covalent inhibitor for the F-ATP synthase which bind to the –OH group of a tyrosine residue in the central nucleotide-binding domain of the nucleotide-free β subunit (β_E) and the binding site is about 13 Å away from the P-loop (Figure 4.7). Efrapeptin is a non-covalent antibiotic inhibitor of the mitochondrial F-ATP synthase. It binds to F-ATP synthase with very high affinity of the order of 10^{-8} M. This bound peptide inhibitor makes contacts with the γ-, two adjacent α- and the so-called empty β subunit (β_E) of the catalytic F_1 domain of the enzyme. A structural superposition was performed for the residues that are within 5 Å distance from the inhibitors NDB-Cl and efrapeptin with their structural equivalent residues from the nucleotide bound (ATP) form of the R416W mutant B-subunit (KUMAR *et al*., 2009a). Almost all residues, except L317, that are found surrounding the intermediate ATP binding region are also found in the efrapeptin binding region in β_E subunit. It has been reported that the binding of efrapeptin to the β_E subunit affected the side chains of β_E-F326, β_E-D352 and β_E-R356, the structural equivalent for these residues in B-subunit are S318, P345 and R349. From this structural comparison study of the ATP bound R416W mutant of subunit B and efrapeptin inhibited β_E subunit of F_1F_O ATP synthase it can be clearly seen that the intermediate ATP binding site of mutant R416 is located at the inhibitory

site of efrapeptin. Similarly, the NBD-Cl binding pocket is also close to this transient binding site. This observation again supports the reliability of the transient binding site (Figure 4.7B). In order to study the inhibitory effect of efrapeptin C (synthetic efrapeptin), A_3B_3 and the $A_3B(R416W)_3$ subcomplexes were reconstituted from subunit A and B from *M. mazei* Gö1. The incubation of the A_3B_3 and the $A_3B(R416W)_3$ subcomplexes with efrapeptin C led to loss of hydrolytic rate, which shows that the efrapeptin C inhibits the ATP hydrolytic activity in A-ATP synthase. Hence, the present structural comparison is in line with the efrapeptin C mediated inhibition of ATP hydrolytic activity of the reconstituted A_3B_3 and the $A_3B(R416W)_3$ (KUMAR *at al*., 2009a)

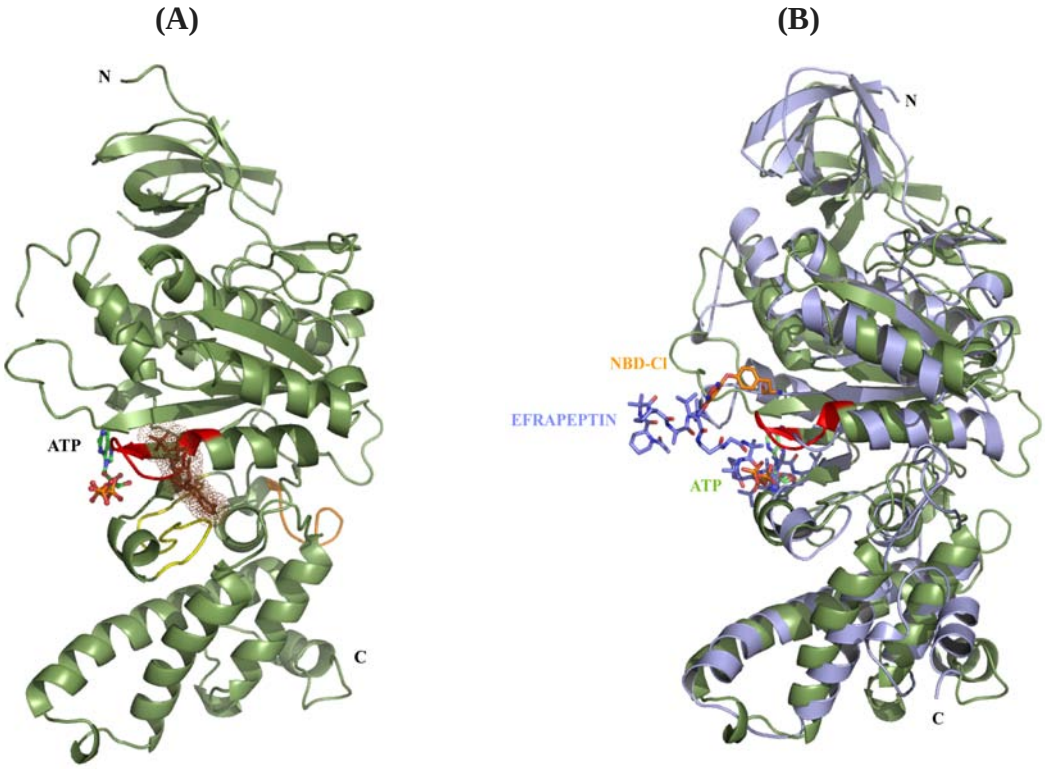

Figure 4.7. (A) Structure of the transient-II with ATP bound near the P-loop region (red). The actual nucleotide binding site is shown as brown dotted surface. (B) Superposition of the X-ray structure of NBD-Cl (ORRIS *et al*., 1998; 1NBM) and efrapetin bound β_E of the bovine F-ATP synthase (ABRAHAMS *et al*., 1996; 1EFR, *light blue*) with the ATP bound R416W mutant of B from *M. mazei* Gö1 (*green*) (KUMAR *et al*., 2009a) shows the similar binding sites for the ATP and inhibitor molecules. The NBD-Cl (*orange*), efrapetin (*green*) and ATP (*green*) molecules are shown in stick representation. The figues are modified according to (KUMAR *et al*., 2009a).

Following the same strategy of co-crystallization, the R416W mutant of subunit B successfully co-crystallized with ATP molecule bound at another transient site. The structure of nucleotide bound R416W mutant of subunit B was determined to 3.4 Å resolution (Figure 4.8A) (MANIMEKALAI *et al*., 2009). In this structure the ATP molecule is bound near the helix-turn-helix motif of the C-terminal domain of chain A. We term this structure as transient-I structure. The difference between the previously solved nucleotide bound structure (3B2Q, KUMAR *et al*.,

2009a) and the present one is that the ATP is bound at different positions. In the case of transient-II structure (KUMAR *et al*., 2009a), the ATP is bound near the P-loop region, whereas in the transient-I structure, it is bound near the helix-turn-helix motif in the C-terminal domain of the protein. Structural comparison of both the transient structures (Figure 4.8A) yielded an r.m.s deviation of 0.788 Å. Larger than average deviation is found near the N-terminal region and for the loop region G307-D316 (maximum deviation of 3.506 Å occurs for the residue G307). The loop region G307-D316 is close to the ATP binding site in transient-II structure and therefore, the structural variation could be due to the binding of the ATP molecule. When the N-terminal domains of both the transient structures are superimposed (Figure 4.8A), their C-terminal domains are found to be related by a rotation of 6°.

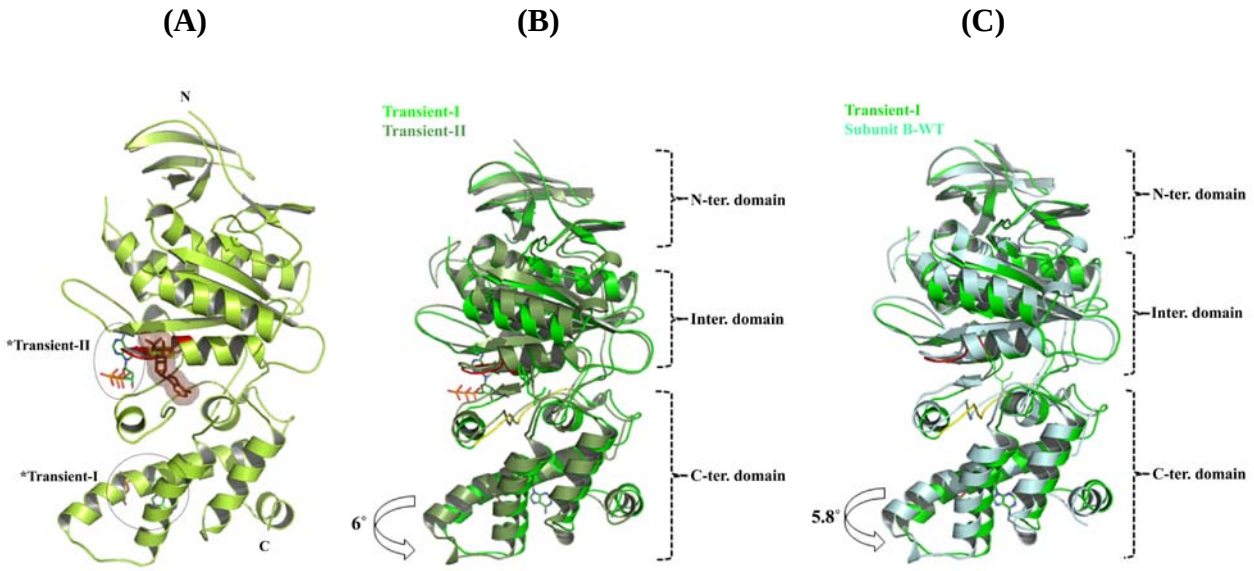

Figure 4.8. (A) A cartoon representation of R416W mutant of subunit B, highlighting the locations of the bound ATP in transient-I and transient-II structures. Bound ATP molecules are shown as in line representation and the predicted nucleotide binding site is highlighted as surface representation (brown). (B) N-terminal domain superposition of the nucleotide-bound transient-I (green, MANIMEKALAI *et al*., 2009) and transient-II (smudge; KUMAR *et al*., 2009a) of R416W mutant of subunit B. The ATP molecules are represented as stick. The arrow marks the movement of the P-loop region and the C-terminal domain due to the binding of ATP molecule. (B) N-terminal domain superposition of the transient-I (green) and wild type (2C61; cyan) subunit B. The ATP molecule of transient-I structure is shown in stick representation. The figures are modified according to KUMAR *et al*., 2009a.

Similar to transient-II structure, the empty form of the wild type subunit B (2C61) structure has an r.m.s. deviation of 1.129 Å with the transient-I structure, where notable differences occur in region G307-D316 with maximum deviation of 7.786 Å was observed for the residue D309 (Figure 4.8B). Upon N-terminal superposition, the C-terminal domains are rotated by 5.8° (Figure 4.8B). Therefore, it could be concluded that the binding of ATP molecule in transient-I structure led to a conformation change on the C-terminal domain by rotating it by around 6°. This is in line with the studies on the related F_1F_O ATP synthases, where the C-terminal domain

of β subunit adopts different conformations depending upon whether it is in nucleotide free or bound form state (MENZ *et al.*, 2001). The nucleotide free form (β_E) show a mobility of about 33° rotation when compared with the nucleotide bound form (β_{DP}). The binding site of ATP molecule at transient-I position is significant because it is located near a site where the central stalk subunit γ interact with the β_E-subunit in the thermoalkaliphilic *Bacillus* sp. TA2.A1 F_1 sector (STOCKER *et al*., 2007) (Figure 4.9). The main interactions are via salt bridges between residues β_E-D372 and β_E-D375 located in the helix-turn-helix motif of the C-terminal domain of β_E subunit with γ-R9 and γ-R10 of the N-terminal helix of the γ subunit (Figure 4.9). These electrostatic interactions pull the γ subunit during catalytic events in the $\alpha_3\beta_3$ sector.

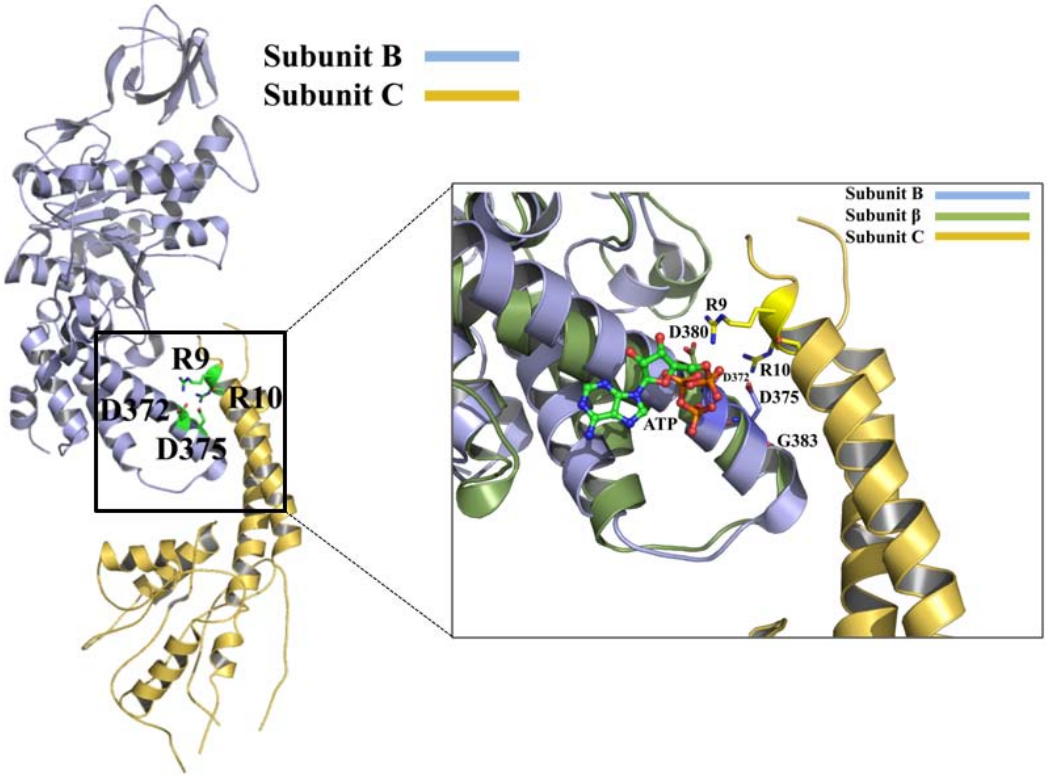

Figure 4.9. Structure of the subunit β_E (light blue) and the C-subunit (light orange) in the thermoalkaliphilic Bacillus sp. TA2.A1 F_1-ATPase (PDB 2QE7, STOCKER *et al*., 2007). The βE-D372 and βE-D375 residues that makes salt bridge interaction with C-R9 and C-R10 are shown in stick representation. Zoom in window shows the structural superposition of transient-I B-subunit (smudge) with the β_E subunit (light blue). The ATP molecule (ball and stick representation) is found to interact to similar position, where the C subunit (light blue) makes salt bridge interaction with β_E subunit. The structurally equivalent counterpart of β_E D372 and β_E D375 residues in transient-I structure, D380 and G383, are indicated in stick representation. The figure is modified according to MANIMEKALAI *et al*. 2009.

The structural overlapping of the transient-I structure to the β_E subunit in the hexamer of F_1-ATPase (thermoalkaliphilic *Bacillus* sp. TA2.A1) showed that D380 and G383 are the structurally equivalent residues in the transient-I (Figure 4.9). The residue D380 interacts with the β-phosphate of the ATP molecule in the transient-I structure, but it was observed that in the

reconstituted model, the residue γ-R9 has steric clash with the B-D380. Similarly, upon overlapping of the transient-II with the β_E structure into the hexamer, it showed steric clashes with the N-terminal residues, γ-M4 and γ-R5. These observations led us to conclude that in the empty state the C-terminal domain of subunit B and the γ homologue, subunit D, are closely held via the salt bridge interaction. Once the ATP enters, as in transient-I structure, the C-terminal domain rotates, allowing the ATP molecule to penetrate inside the hexamer leading to the disturption of the salt bridges and hence, rotates the D subunit. Again, when the ATP molecule moves in towards the transient-II position the D subunit rotates and moves to the other side to accommodate it until it reaches the actual binding pocket which is the P-loop region. Therefore, the presented three-dimensional structure of the transient binding position I of ATP inside subunit B of the methanogenic A-ATP synthase adds structural information towards an understanding of nucleotide-binding mechanism inside the A_3B_3 headpiece.

4.2.3 Structure of wild type subunit B in complex with ADP

The recently established protocol for the co-crystallization of subunit B mutant in the presence of nucleotides has been successfully employed to obtain the wild type subunit B in complex with ADP. The structure of this complex was solved at a resolution of 2.7 Å. Similar to the transient-II structure, in the present structure, the bound ADP molecule lies near the P-loop region. Apart from all relevant interactions required for the stabilization, the adenine ring is stabilized by the π–π stacking interaction with F149(B) and the T-shaped π–π interaction with F149(A). These interactions strongly hold the ADP molecule in its binding position, located about 13 Å apart from the final nucleotide-binding site, made-up by the phosphate-binding loop (P-loop) and the adenine-binding pocket (SCHÄFER *et al*., 2006b) (Figure 4.10). The tryptophan fluorescence quenching data showed that the trytophan fluorescence spectrum of mutant F149W is sensitive to ADP binding and therefore, the trapped nucleotide binding position found in the present structure can be called an ADP transition binding state similar to the transient-II. The overall structure of the ADP-bound form is similar to the nucleotide free subunit B (2C61), the r. m. s. deviation being 0.782 Å for the backbone Cα atoms. Notable deviations occur near the N -terminal region and in the loop regions, R257-Y277 and M305-D316. Maximum deviations of 5.5 Å occur for the residue A274 in R257-Y277 region and 5.4 Å for P313 in M305-D316 region. These two regions are part of the loop region, above the P-loop, that would face the central stalk region in the intact A_1A_O ATP synthase. The latter region is also where the phosphate group of the ADP molecule binds and therefore could also be interpreted as being caused by ADP binding.

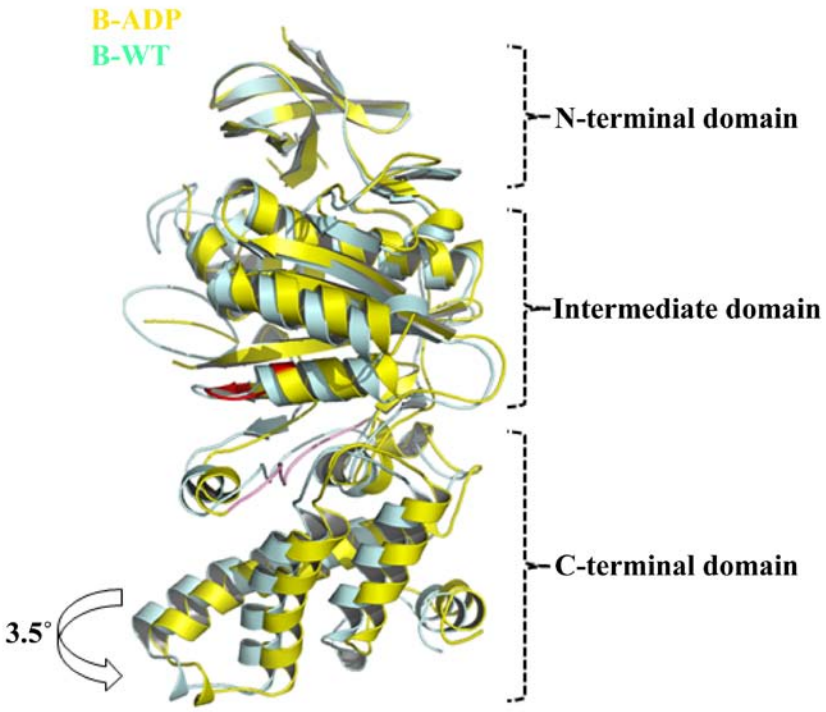

Figure 4.10. Structure comparison of ADP-bound (yellow, KUMAR *et al*., 2008) and nucleotide-free (SCHÄFER *et al*., 2006; PDB 2C61; cyan) subunit B with respect to N-terminal domain superposition. The arrow represents the movement of the P-loop region, the peptide Gly336–Arg349 in the central α/β-domain and the C-terminal domain due to binding of the ADP molecule. The figure has been modified according to KUMAR *et al*., 2008.

When the N-terminal domains of both the structures are superimposed, their C-terminal domains are related by a rotation of 3.5°. As could be seen from figure 4.10 the central α-β domain show slight deviation when compared with the C-terminal domain but significant movement is noted especially in the lower part of the domain where the adenine binding pocket is located. The region E323 to G358 shows marked movement. Interestingly, this region includes the peptide G336 to R349, reported to covalently bind 8-N_3-3′-biotinyl-ATP (SCHÄFER *et al*., 2006b) and is the site for the adenine binding pocket. The C-terminal α-helical domain deviates most and it moves as a whole rigid body. The transition binding position of ADP in the present structure compares well with one of the inhibitory sites of the F_1F_O ATP synthase where the antibiotic, efrapeptin C binds. The binding of efrapeptin happens in the helix G (residues 321-324) and strands 3 and 7 of the β-sheet (residues 151-155 and 302-309, respectively) in the central nucleotide binding domain of β_E. When this domain is superimposed for both the ADP bound subunit B and β_E structures the residues F149(A), S304(A), M305(A), I321(A), Q325(A), V327(A) and P345(A), which are found to interact with ADP in B subunit, have also interaction with efrapeptin. Out of the three residues in β_E subunit, β_E-F326, β_E-D352 and β_E-R356, whose side chain orientation is reported to affect the efrapeptin binding, two have structural equivalent residues in the B subunit in the ADP binding region, I321(A) and P345(A) respectively.

Therefore, in this context it can be concluded, that the mechanism of efrapeptine inhibition might be caused by its occupation to the transition binding position of ADP and finally by hindering the substrate to enter in its regulatory/catalytic binding site. This finding will also give insight into the nucleotide-binding mode of the ADP/ATP-binding subunits of the related energy transducer, V-ATPase, and the prokaryotic and eukaryotic energy producer, F-ATP synthases. It should be noted that in the intact A_1A_O ATP synthase from methanogens, subunit B is in close contact with the catalytic subunit A and the interface region between the subunit A and B is the nucleotide binding site. Subunit D (A_1A_O ATP synthase) is a homologue of the γ subunit (F_1F_O ATP synthase) which penetrates in the A_3:B_3 pseudohexamer of the A_1 head piece. In order to ascertain the confidence in the present transition position (intermediate state) of the bound ATP in the R416W mutant structure, we have constructed a model by fitting the X-ray structures of subunit A (MAEGAWA *et al*., 2006), B (mutant R416W) of A-ATP synthases (KUMAR *et al*., 2009a), together with the subunit D homologue, subunit γ of F-ATP synthases (ABRAHAMS *et al*., 1994), into the electron density map of the A-ATP synthase, as described recently (SCHÄFER *et al*., 2006b; GAYEN *et al*., 2007). Larger than average deviation occur in regions Q258-Y277 and P306-Y320, wherein the maximum deviation occur for N264 (2.7 Å) for the Q258-Y277 region and P315 (4.5 Å) for the P306-Y320 region. These two regions are part of the loop region that would face the central stalk region in the intact complex. The present observation is in accordance with the view that in order to perform the normal rotatory function, subunits D needs to have a flexible interaction with the amino acids in this area.

4.3 A model for the entry route for nucleotides in intact A_1A_O complex

The transient-I and transient-II structures have given us an opportunity in hand to propose a model for the possible entry route of ATP into A_1A_O ATP synthase. In the reconstituted $A_3B(R416W)_3\gamma$ complex, the trapped nucleotide of the R416W mutant is facing the cavity volume. This arrangements prompts to propose a model of ATP movement explaining the possible entry of ATP through the channel formed by the C-terminal domains of subunits A and B and moving up through the large solvent cavity of the A_3B_3 hexamer to the intermediate position determined in the present structures of the R416W mutant (KUMAR *et al*., 2009a; MANIMEKALAI *et al*., 2008) (Figure 4.11A-B). The entry point of nucleotide is the C-terminal cavity region, as in transient-I structure, followed by the rotation of the C-terminal domain allowing the ATP molecule to penetrate inside the hexamer and simultaneous disturption of the salt bridges between B and D. When the ATP molecule moves in towards the transient-II position, the D subunit rotates and moves to the opposite side to accommodate it until it reaches

the actual binding pocket. The proposal fits well with the nucleotide dependent cross-linking experiments, performed using A_3B_3DF complex of A_1, which indicates that the nucleotide-dependent alterations of the central stalk subunits C, D, and F and the close proximity of these subunits to the major nucleotide binding subunits A and/or B might provide coupling between the catalytic site events via subunit D (homologue of subunit γ) of the central CDF stalk domain. Hence, provide the physical and structural linkage between the A_3B_3 headpiece and the ion-conducting A_O domain (COSKUN *et al*., 2004b).

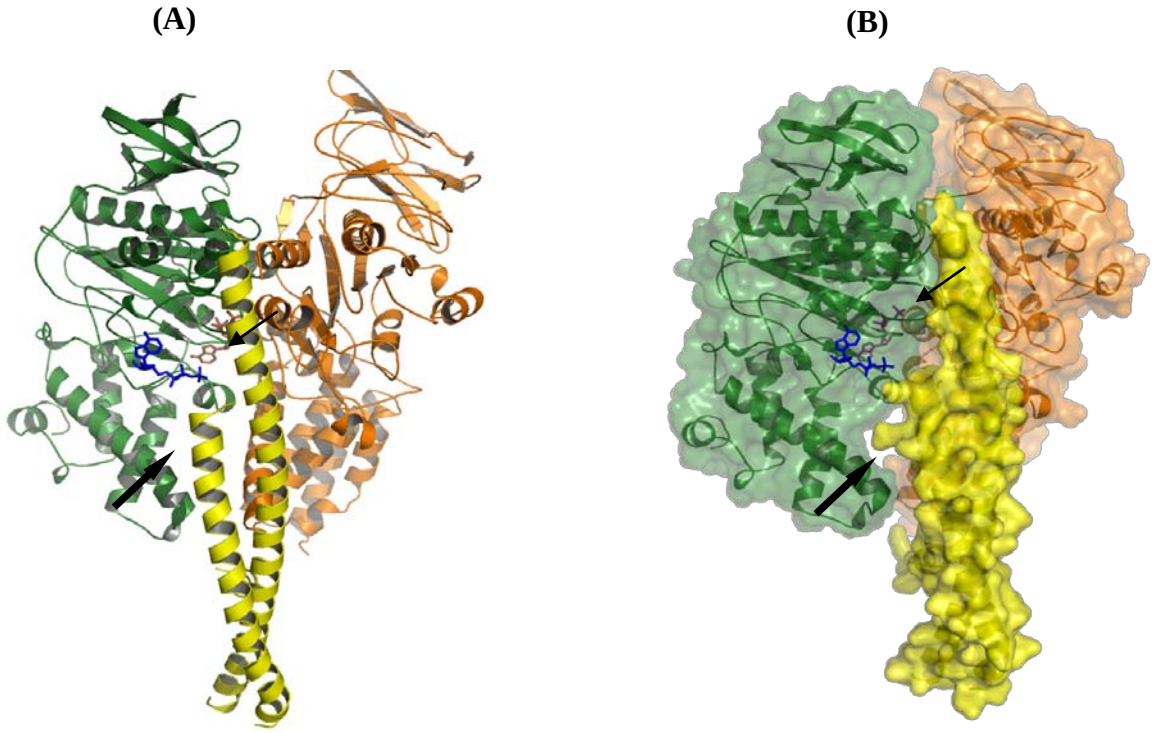

Figure 4.11. Cross sectional view of the cartoon (A) and surface representation (B) of the hexamer model showing the transient-II position of ATP molecule (blue-stick representation). The ATP molecule bound to the actual ATP binding site in P-loop region for the related F_1 ATPase complex is shown in magenta color, pointed by an arrow head (KUMAR *et al*., 2009a). The thick arrow head points at the solvent cavity in the A_3B_3 hexamer located near the C-terminal domain of the B subunit. The figure has been modified according to KUMAR *et al*., 2009a.

5. Conclusion

5.1. Conclusions

Little knowledge is available for the A-ATP synthase class of enzymes due to lack of a high resolution structure for the entire complex. Low resolution electron micrographs described so far reveal that the A-ATP synthases are composed of ion conducting pore channel complex (A_O) and a catalytic headpiece (A_1), consisting of nucleotide binding subunits A and B (COSKUN *et al*., 2004b; BERNAL and STOCK, 2004). The subunits A and B are homologous to subunits β and α of the extensively studied F-ATP synthases and are believed to be catalytic and non-catalytic/regulatory subunits, respectively (GRÜBER and MARSHANSKY, 2008). The availability of high resolution structures of nucleotide bound forms of subunits A and B is a prerequisite to understand the mode of nucleotide binding and subsequent catalytic events leading to ATP synthesis in the A_1 headpiece and of the A-ATP synthases. In the thesis presented, the crystal structures of subunit A of the *P. horikoshii* OT3 A-ATP synthase have been determined in complex with a phosphate analog-, AMP-PNP- and ADP to a resolutions of 2.47 Å and 2.4 Å, respectively. These structures highlighted the structural and functional significance of the residues, forming the adenine binding pocket and phosphate binding P-loop region. The interaction profile of the P-loop residues, G234, P235, F236 and S238 highlighted the structural role, played by them in maintaining the characteristic strained conformation of the P-loop in subunit A compared to the relatively relaxed conformation found in the α and β subunits of the related F-ATP synthase. The structure of S238A was determined at a resolution of 2.4 Å resolution. The P-loop in the empty form of S238A mutant is structurally equivalent to the ones in α and β of F-ATP synthases, highlighting the structural role played by this residue in maintaining the P-loop architecture. Similarly, the structural deviation profile shows the functional importance of K240 and T241, like the threonine and lysine residues of the catalytic β subunit, which are also believed to stabilize the transition state during catalysis.

The comparative spatial arrangement of the bound nucleotides in A_{MP} and β_{MP} highlights the novel positioning of AMPPNP molecule in subunit A possibly due to its characteristically strained P-loop arrangement, suggesting that the bound nucleotide molecule is weakly held in the binding site, and hence making it more solvent exposed. This finding provides an explanation for the not so strict specificity of the A-ATP synthases to hydrolyze not only the main substrate ATP but also GTP and UTP with varied degree of activity. Hence, provide an explanation for the differential binding constants for Mg-ATP (2.38 μM) and Mg-ADP (1.50 μM). This preferential binding preference of ADP to subunit A is contrary to the nucleotide binding pattern observed in homologous catalytic subunit β from F-ATP synthase and subunit B from A-ATP synthase. Both these subunits bind to nucleotides but with a preference for ATP- over ADP molecule. This is

despite the fact that the P-loop sequences are not similar in these subunits but their P-loops are structurally equivalent. This is in line with the observations from the comparative sequence alignment of the P-loop sequences across members of the A-/F- ATP synthases and V-ATPases.

The crystal structure of subunit B from the A_1A_O ATP synthase of *M. mazei* Gö1 was solved in 2006 (SCHÄFER *et al*., 2006b). The very first evidences for the nucleotide binding capability of subunit B came from initial photoaffinity labeling experiments and fluorescence correlation spectroscopic experiments, which showed that subunit B from *M. mazei* Gö1 binds to nucleotide analogues but with a weak affinity compared to subunit A (SCHÄFER *et al*., 2006b). Primary sequence and structural alignment studies with subunits α and β, revealed that the residues R416 and Y338 mark the adenine binding region of the nucleotide binding pocket in subunit B which are predicted to undergo π - π stacking and cation - π interactions, respectively with the incoming nucleotide. The tryptophan fluorescence quenching experiments with R416W mutant of subunit B showed a significant dampening of the fluorescence signal upon addition of Mg-ATP or Mg-ADP. This indicated that the mutated residue (R416) is in close vicinity to the nucleotide binding site. Subsequent FCS experiments using relatively small sized nucleotide analogues showed that the wild type subunit B binds slightly stronger to Mg-ATP ATTO-647N, which might be caused by the reorientation of amino acid E158, resulting from the abolished salt bridge between E158 and the substituted R416 residue. The K_d values determined from intrinsic tryptophan measurements of R416W were in line with the FCS experiments. This observation is quite unusual for a protein considered to be non-catalytic in function. The differential affinities of subunit B for Mg-ATP and Mg-ADP clearly indicate that it might not be a nucleotide binding/non-catalytic subunit only. In order to answer the question, a nucleotide bound form of subunit B was highly desired. Hence, in the present thesis, the recently developed protocol for co-crystallization helped in getting two ATP bound structures of R416W mutant of subunit B with ATP located at different positions. In transient-I structure the ATP molecule is bound near the helix-turn-helix motif of the C-terminal domain of chain A, while in transient-II structure, the ATP is bound near the P-loop region. The significance of the transient nucleotide binding sites was ascertained by the ATP dependent sensitivity of tryptophan fluorescence spectrum for subunit B mutants F149W and A373W. The superposition of the N-terminal domains of the transient forms with R416W empty structure of subunit B highlighted the structural change of about 6º at the C-terminal domain in nucleotide bound transient structures, a conformational change conferred due to ATP binding.

These transient structures mimic the trapped positions of the nucleotides while on its way to the actual site of catalysis. A model has been proposed for the possible entry route of ATP into A_1A_O ATP synthase which is in compliance with the previous nucleotide dependent cross-linking experiments, performed using A_3B_3DF complex of A_1 (COSKUN *et al*., 2004b).

5.2. Future plan and experimental strategies

5.2.1. Characterization of the nucleotide binding site in subunit A through mutational studies

In the ADP and AMPPNP bound structures of subunit A from *P. horikoshii* OT3, apart from S238A, the other P-loop residues, G234 and P235, play an important role in maintaining the characteristic strained conformation of the P-loop. Similarly, the structural deviation profile has highlighted the functional importance and of K240, T241 and T243, like the threonine and lysine residues of the catalytic β subunit, these residues are also expected to participate in nucleotide binding and/or stabilization of the transition state during catalysis. The nucleotide bound structures revealed the interactions conferred by the residues, F427, P428 and F508 to the bound nucleotide. These residues stabilize the adenine moiety of the incoming nucleotide inside the binding pocket. A systematic mutational analysis followed by spectroscopic, thermodynamic and structural characterization of these amino acids will pave a way for the in-depth understanding about the nucleotide binding kinetics and interactions conferred by the individual amino acids.

5.2.2. Characterization of the nucleotide binding sites in subunit B through mutational studies

In the P-loop region of subunit B ($_{150}$SASGLHN$_{157}$) from *M. mazei* Gö1, the residues H156 and N157 are the structural equivalent of K240 and T241 from the catalytic subunit A. Both the residues are expected to participate in nucleotide binding and stabilization of the transition state during catalysis. An alanine scan of these P-loop residues will give a hint about the role played in nucleotide binding and subsequent catalytic events. Earlier results of photoaffinity labelling study on subunit B have shown that the azido group of the labeled ATP might be interacting with Y338 of the peptide Gly336-Arg349 of the subunit B (SCHÄFER *et al*., 2006b). The residue Y338 form a part of the adenine binding site of the nucleotide binding pocket. The newly constructed Y338W mutant has shown pronounced binding with Mg-ATP and Mg-ADP. The dissociation constants for nucleotide binding will be determined using intrinsic tryptophan fluorescence spectroscopy and ITC. In order to gain insight into the structural alterations as a result of the mutation, crystallization of Y338W mutant will be tried simultaneously. In the ATP bound structure of R416W mutant of subunit B, F149 confers π – π stacking interactions to the adenine part of the ATP molecule and hence stabilizing it. Intrinsic tryptophan fluorescence quenching results have shown nucleotide binding to the F149W mutant protein. Structure

determination in ligand bound form followed by thermodynamic analysis will provide a thorough insight into the nucleotide binding in subunit B.

5.2.3. Characterization of the nucleotide binding in the A_3B_3 subcomplex

In an intact A_1A_O ATP synthase, the A_3B_3 subcomplex is the site of catalytic events, where synthesis/hydrolysis of nucleotides takes place. The A-B dimer interface region between the subunits A and B is the nucleotide binding site, where catalytic sites are predicted to be predominantly in A subunits, with some contributions from side chains of the B subunits and conversely with the non-catalytic/regulatory sites. In order to investigate the direct effect of individual amino acids in the nucleotide binding and catalytic events, the ATP hydrolysis rates of the overexpressed and reconstituted mutant subcomplexes will be determined by enzyme activity assay and will be compared with the wild type subcomplex. Such a strategy will give an insight in the direction of understanding and assignment of a reasonable role to subunit A and B, in ATP synthesis/hydrolysis events.

6. References

Abrahams, J. P., S. K. Buchanan, M. J. van Raau, I. M. Fearnley, A. G. W. Leslie and J. E. Walker (1996). *The structure of bovine F_1-ATPase complexed with the peptide antibiotic efrapeptin*. Proc. Natl. Acad. Sci. USA **93**: 9420-9424.

Abrahams, J. P., A. G. W. Leslie, R. Lutter and J. E. Walker (1994). *Structure at 2.8 Å resolution of F_1-ATPase from bovine heart mitochondria*. Nature **370**: 621-628.

Bernal, R. A. and D. Stock (2004). *Three-dimensional structure of the intact Thermus thermophilus H^+-ATPase/synthase by electron microscopy*. Structure **12**: 1789-1798.

Bianchet, M. A., J. Hullihen, P. L. Pedersen and M. L. Amzel (1998). *The 2.8-Å structure of rat liver F_1-ATPase: Configuration of a critical intermediate in ATP synthesis/hydrolysis.* Proc. Natl. Acad. Sci. USA **95**: 11065-11070.

Böttcher, B., I. Bertsche, R. Reuter and P. Gräber (2000). *Direct visualisation of conformational changes in EF_OF_1 by electron microscopy*. J. Mol. Biol. **296**: 449-457.

Boyer, P. D. (1993) *The binding change mechanism for ATP synthase – some probabilities and possibilities.* Biochim. Biophys. Acta **1140**: 215–250.

Brunger, A. T., P. D. Adams, G. M. Clore, W. L. Delano, P. Gros and R. W. Grosse-Kunstleve (1998). *Crystallography and NMR system (CNS): a new software system for macromolecular structure determination*. Acta Cryst. **D54**: 905-921.

Cann, I. K., S. Ishino, M. Yuasa, H. Daiyasu, H. Toh and Y. Ishino (2001). *Biochemical analysis of replication factor C from the hyperthermophilic archaeon Pyrococcus furiosus*. J. Bacteriol. **183**: 2614-2623.

Capaldi, R. A. and R. Aggeler (2002). *Mechanism of the F_1F_O-type ATP synthase, a biological rotary motor*. Trends Biochem. Sci. **27**: 154-160.

Chen, C., A. K. Saxena, W. N. Simcoke, D. N. Garboczi, P. L. Pedersen and Y. H. Ko (2006). *Mitochondrial ATP synthase: Crystal structure of the catalytic F_1 unit in a vanadate-indiced transition-like state implications for mechanism.* J. Biol. Chem. **281**: 13777-13783.

Chen, W. and J. Konisky (1993). *Characterization of a membrane-associated ATPase from Methanococcus voltae, a methanogenic member of the Archaea*. J. Bacteriol. **175**: 5677-5682.

Collaborative Computational Project, Number 4 (1994). *The CCP4 suite: programs for protein crystallography*. Acta Cryst. **D50**: 760-763.

Coskun, Ü., Y. L. Chaban, A. Lingl, V. Müller, W. Keegstra, E. J. Boekema and G. Grüber (2004b). *Structure and subunit arrangement of the A-type ATP synthase complex from the archaeon Methanococcus jannaschii visualized by electron microscopy*. J. Biol. Chem. **279**: 38644-38648.

Coskun, Ü., G. Grüber, M. H. J. Koch, J. Godovac-Zimmermann, T. Lemker and V. Müller (2002). *Cross-talk in the A_1-ATPase from Methanosarcina mazei Gö1 Due to Nucleotide Binding*. J. Biol. Chem. **277**: 17327-17333.

Coskun, Ü., M. Radermacher, V. Müller, T. Ruiz and G. Grüber (2004). *Three-dimensional Organization of the Archaeal A_1-ATPase from Methanosarcina mazei Gö1*. J. Biol. Chem. **279**: 22759-22764.

Coskun, Ü., V. F. Rizzo, M. H. J. Koch and G. Grüber (2004). *Ligand-Dependent Structural Changes in the V_1 ATPase from Manduca sexta*. J. Bioenerg. Biomembr. **36**: 249-256.

Coskun, Ü., Y. L. Chaban, A. Lingl, V. Müller, W. Keegstra, E. J. Boekema and G. Grüber (2004). *Structure and Subunit Arrangement of the A-type ATP Synthase Complex from the Archaeon Methanococcus jannaschii Visualized by Electron Microscopy*. J. Biol. Chem. **279**: 38644-38648.

Cross, R. L. and V. Müller (2004). *The evolution of A-, F-, and V-type ATP synthases and ATPases: reversals in function and changes in the H^+/ATP stoichiometry*. FEBS Lett. **576**: 1-4.

Cross, R. L. and L. Taiz (1990). *Gene duplication as a means for altering H^+/ATP ratios during the evolution of F_OF_1 ATPases and synthases.* FEBS Lett. **259**: 22227-22229.

DeLano, W. L. (2002). *The PyMol Molecular Graphics System, DeLano Scientific, Palo Alto, CA, USA.*

Deppenmeier, U. and V. Müller (2006). *Life close to the thermodynamic limit: How methanogenic archaea conserve Energy*. Results Probl. Cell Differ. **45**:123-152.

Deppenmeier, U. (2002). *Redox-driven proton translocation in methanogenic Archaea*. Cell. Mol. Life Sci. **59**: 1513-1533.

Deppenmeier, U. (2002). *The unique biochemistry of methanogenesis*. Prog. Nucl. Acid Re. **71**: 223-283.

Diepholz, M., M. Börsch and B. Böttcher (2008). *Structural organization of the V-ATPase and its implications for regulatory assembly and disassembly*. Biochem. Soc. Trans. **36**: 1027-1031.

Diez, M., B. Zimmermann, M. Börsch, M. Konig, E. Schweinberger, S. Steigmüller, R. Reuter, S. Felekyan, V. Kudryavtsev, C. A. Seidel, P. and Gräber (2004). *Protonpowered subunit rotation in single membrane-bound F0F1-ATP synthase.* Nat. Struct. Mol. Biol. **11**: 135–141.

Duncan, T. M., V. V. Bulygin, Y. Zhou, M. L. Hutcheon and R. L. Cross (1995). *Rotation of subunits during catalysis by Escherichia coli F1-ATPase.* Proc. Natl. Acad. Sci. USA **92**: 10964–10968.

Emsley, P. and K. Cowtan (2004). *Coot: Model-Building Tools for Molecular Graphics*. Acta Cryst. **D60**: 2126-2132.

Feng, Y. and M. Forgac (1994). *Inhibition of vacuolar H^+-ATPse by disulfide bond formation between cysteine 254 and cysteine 532 in subunit A.* J. Biol. Chem. **269**: 13224-12230.

Ferry, J. G. (1993). *Methanogenesis: Ecology, Physiology, Biochemistry & Genetics.* Chapman and Hall Inc., London.

Gibbons, C., M. G. Montgomery, A. G. W. Leslie and J. E. Walker (2000). *The structure of the central stalk in bovine F_1-ATPase at 2.4 Å resolution*. Nat. Struct. Mol. Biol **7**: 1055-1061.
Gledhill, J. R. and J. E. Walker (2006). *Inhibitors of the catalytic domain of mitochondrial ATP synthase*. Biochem. Soc. Trans. **34**: 989-992.

Grüber, G. (2003). *Introduction: A Close Look at the Vacuolar ATPase*. J. Bioenerg. Biomembr. **35**: 277-280.

Grüber, G. and V. Marshansky (2008). *New insights into structure-function relationships between archeal ATP synthase and vacuolar type ATPase.* BioEssays **30**: 1096-1109.

Grüber, G., D. I. Svergun, Ü. Coskun, T. Lemker, M. H. J. Koch, H. Schagger and V. Müller (2001). *Structural Insights into the A_1 ATPase from the Archaeon, Methanosarcina mazei Gö1*. Biochemistry **40**: 1890-1896.

Grüber, G., J. Godovac-Zimmermann, T. A. Link, U. Coskun, V. F. Rizzo, C. Betz and S. M. Bailer (2002). *Expression, purification, and characterization of subunit E, an essential subunit of the vacuolar ATPase*. Biochem. Biophys. Res. Comm. **298**: 383-391.

Hausrath, A. C., G. Grüber, B. W. Matthews and R. A. Capaldi (1999). *Structural features of the γ subunit of the Escherichia coli F_1 ATPase revealed by a 4.4-Å resolution map obtained by x-ray crystallography*. Proc. Natl. Acad. Sci. USA **96**: 13697-13702.

Hausrath, A. C., R. A. Capaldi and B. W. Matthews (2001). *The Conformation of the Epsilon and Gamma Subunits within the Escherichia coli F_1 ATPase*. J. Biol. Chem. **276**: 47227-47232.

Heinonen, J. K. and R. J. Lahti (1981). *A new and convenient colorimetric determination of inorganic orthophosphate and its application to the assay of inorganic pyrophosphatase*. Anal. Biochem. **113**:313–317.

Hilario, E. and J. P. Gogarten (1998). *The prokaryote-to-eucaryote transition reflected in the evolution of the V/F/A-ATPase catalytic and proteolipid subunits*. J. Mol. Evol. **46**: 703-715.

Ho, S. N., H. D. Hunt, R. M. Horton, J. K. Pullen and L. R. Pease (1989). *Site directed mutagenesis by overlap extension using polymerase chain reaction*. Gene **77**: 51-59.

Hosaka, T., T. Murata, Y. Kakinuma and I. Yamato (2004). *Identification of nucleotide binding sites in V-type Na+-ATPase from Enterococcus hirae*. Biosci. Biotechnol. Biochem. **68**: 293-299.

Imamura, H., S. Funamoto, M. Yoshida and K. Yokoyama (2006). *Reconstitution in vitro of V_1 complex of Thermus thermophilus V-ATPase revealed that ATP binding to the A subunit is crucial for V_1 formation*. J. Biol. Chem. **281**: 38582-38591.

Inatomi, K. I., S. Eya, M. Maeda and M. Futai (1989). *Amino acid sequence of the alpha and beta subunits of Methanosarcina barkeri ATPase deduced from cloned genes. Similarity to subunits of eukaryotic vacuolar and F_OF_1-ATPases*. J. Biol. Chem. **264**: 10954-10959.

Iwata, M., H. Imamura, E. Stambouli, C. Ikeda, M. Tamakoshi, K. Nagata, H. Makyio, B. Hankamer, J. Barber, M. Yoshida, K. Yokoyama and S. Iwata (2004). *Crystal structure of a central stalk subunit C and reversible association/dissociation of vacuole-type ATPase*. Proc. Natl. Acad. Sci. USA **101**: 59-64.

Jost, M., S. Weigelt, T. Huber, Z. Majer, J. C. Greie, K. Altendorf and N. Sewald (2007). *Synthesis, and structural and biological studies of efrapeptin C analogues*. Chem. & Biodiversity **4**:1170-1182.

Kabaleeswaran, V., N. Puri, J. E. Walker, A. G. W. Leslie and D. M. Mueller (2006). *Novel features of the rotary catalytic mechanism revealed in the structure of yeast F_1 ATPase*. EMBO J. **25**: 5433-5442.

Kaibara, C., T. Matsui, T. Hisabori and M. Yoshida (1996). *Structural asymmetry of F_1-ATPase caused by the gamma subunit generates a high affinity nucleotide binding site*. J. Biol. Chem. **271**: 2433-2438.

Karrasch, S. and J. E. Walker (1999). *Novel features in the structure of bovine ATP synthase*. J. Mol. Biol. **290**: 379-384.

Kasho, V. N., W. S. Allison and P. D. Boyer (1993). *Study of the mechanism of MF_1 ATPase inhibition by fluorosulfonylbenzoyl inosine, quinacrine mustard, and efrapeptin using intermediate ^{18}O exchange as a probe*. Archives Biochem. Biophys. **300**: 293-301.

Krissinel, E. and K. Henrick (2004). *Secondary-structure matching (SSM), a new tool for fast protein structure alignment in three dimensions*. Acta Cryst. **D60**: 2256-2268.

Kumar, A., M. S. S. Manimekalai and G. Grüber (2008). *Structure of the nucleotide binding subunit B of the energy producer A_1A_O ATP synthase in complex with adenosine diphosphate*. Acta Cryst. **D64**: 1110–1115.

Kumar, A., M. S. S. Manimekalai, A. M. Balakrishna, C. Hunke, S. Weigelt, N. Sewald and G. Grüber (2009). *Spectroscopic and crystallographic studies of the mutant R416W give insight into the nucleotide binding traits of subunit B of the A_1Ao ATP synthase*. Proteins: Struct. Funct. Bioinf. **75**: 807-819.

Kumar, A., M. S. S. Manimekalai, A. M. Balakrishna, J. Jeyakanthan and G. Grüber (2009b). *Nucleotide binding states of subunit A of A-ATP synthase and the implication of P-loop switch in evolution.* J. Mol. Biol., **396**, 301-320.

Laemmli, U. K. (1970). *Cleavage of structural proteins during the assembly of the head of bacteriophage T4*. Nature **227**: 680-685.

Laskowski, R. A., M. W. MacArthur, D. S. Moss and J. M. Thornton (1993). *PROCHECK: a program to check the stereochemical quality of protein structures*. J Appl Cryst **26**: 283-291.

Lewalter, K. and V. Müller (2006). *Bioenergetics of archaea: Ancient energy conserving mechanisms developed in the early history of life*. Biochim. Biophys. Acta Bioenergetics **1757**: 437-445.

Lingl, A., H. Huber, K. O. Stetter, F. Mayer, J. Kellermann and V. Müller (2003). *Isolation of a complete A_1A_O ATP synthase comprising nine subunits from the hyperthermophile Methanococcus jannaschii*. Extremophiles **7**: 249-257.

Löbau, S., J. Weber, S. Wilke-Mounts and A. E. Senior (1997). *F_1-ATPase, roles of three catalytic site residues*. J. Biol. Chem. **272**: 3648-3656.

Maegawa, Y., H. Morita, M. Yao, N. Watanabe and I. Tanaka (2004). *Crystallization and*

preliminary X-ray diffraction study of the catalytic subunit of archael H^+-transporting ATP synthase from Pyrococcus horikoshii OT3. Acta Cryst. **D60**: 1484–1486.

Maegawa, Y., H. Morita, D. Iyaguchi, M. Yao, N. Watanabe and I. Tanaka (2006). *Structure of the catalytic nucleotide-binding subunit A of A-type ATP synthase from Pyrococcus horikoshii reveals a novel domain related to the peripheral stalk*. Acta Cryst. **D62**: 483-488.

Manimekalai, M. S. S., A. Kumar, A. M. Balakrishna and G. Grüber (2009). *A second transient position of ATP on its trail to the nucleotide-binding site of subunit B of the motor protein A_1A_O ATP synthase*. J. Struc. Biol. **166**: 38-45.

McCoy, A. J., R. W. Grosse-Kunstleve, P. D. Adams, M. D. Winn, L. C. Storoni and R. J. Read (2007). *Phaser crystallographic software*. J. Appl. Cryst. **40**: 658-674.

Menz, R. I., J. E. Walker and A. G. W. Leslie (2001). *Structure of Bovine Mitochondrial F1-ATPase with Nucleotide Bound to All Three Catalytic Sites: Implications for the Mechanism of Rotary Catalysis*. Cell **106**: 331-341.

Mitchell, P. (1961). *Coupling of phophorylation to electron and hydrogen transfer by a chemi-osmotic type of mechanism.* Nature **191**: 144–148.

Müller, V. and G. Grüber (2003). *ATP synthases: structure, function and evolution of unique energy converters*. Cell. Mol. Life Sci. **60**: 474-494.

Müller, V., A. Lingl, K. Lewalter and M. Fritz (2005). *ATP Synthases With Novel Rotor Subunits: New Insights into Structure, Function and Evolution of ATPases*. J. Bioenerg. Biomembr. **37**: 455-460.

Murata, T., Y. Yoshikawa, T. Hosaka, K. Takase, Y. Kakinuma, I. Yamato and T. Kikuchi (2002). *Nucleotide-Binding sites in V-Type Na^+-ATPase from Enterococcus hirae*. J. Biochem. **132**: 789-794.

Murata, T., I. Yamato, Y. Kakinuma, A. G. W. Leslie and J. E. Walker (2005). *Structure of the Rotor of the V-Type Na+-ATPase from Enterococcus hirae*. Science **308**: 654-659.

Murshudov, G. N., A. A. Vagin and E. J. Dodson (1997). *Refinement of macromolecular structures by the maximum-likelihood method*. Acta Cryst. **D53**: 240-255.

Nelson, N. (1992). *Evolution of organellar proton-ATPases*. Biochim. Biophys. Acta **1100**: 109-124.

Nelson, H., S. Mandiyan and N. Nelson (1989). *A conserved gene encoding the 57-kD a subunit of the yeast vacuolar H+- ATPase*. J. Biol. Chem. **264**: 1775-1778.

Nielsen, K. J., J. M. Hill, M. A. Anderson and D. J. Craik (1996). *Synthesis and Structure Determination by NMR of a Putative Vacuolar Targeting Peptide and Model of a Proteinase Inhibitor from Nicotiana alata*. Biochemistry **35**: 369-378.

Nishio, K., A. Iwamoto-Kihara, A. Yamamoto, Y. Wada and M. Futai (2002). *Subunit rotation of ATP synthase embedded in membranes: a or b subunit rotation relative to the c subunit ring.* Proc. Natl. Acad. Sci. USA **99**: 13448–13452.

Noji, H., R. Yasuda, M. Yoshida and K. Kinosita (1997). *Direct observation of the rotation of F1-ATPase.* Nature **386**: 299–302.

Omote, H., M. Maeda and M. Futai (1992). *Effects of mutations of conserved Lys-155 and Thr-156 residues in the phosphate-binding glycine-rich sequence of the F_1-ATPase beta subunit of Escherichia coli*. J. Biol. Chem. **267**: 20571-20576.

Orris, G. L., A. G. W. Leslie, K. Braig and J. E. Walker (1998). *Bovine F_1-ATPase covalently inhibited with 4-chloro-7-nitrobenzofurazan: the structure provides further support for a rotary catalytic mechanism*. Structure **6**: 831-837.

Otwinowski, Z. and W. Minor (1997). *Processing of X-ray diffraction data collected in oscillation mode*. Methods Enzymol. **276**: 307-326.

Radermacher, M., T. Ruiz, H. Wieczorek and G. Grüber (2001). *The structure of the V_1-ATPase determined by three-dimensional electron microscopy of single particles*. J. Struct. Biol. **135**: 26-37.

Rudolf, K. T., K. Anne-Kristin, S. Henning, B. Wolfgang and H. Reiner (2008). *Methanogenic archaea: ecologically relevant differences in energy conservation*. Nat. Rev. Microbiol. **6**: 579-591.

Sabbert, D., S. Engelbrecht and W. Junge (1996). *Intersubunit rotation in active F-ATPase.* Nature **381**: 623–626.

Saraste, M., P. R. Sibbald and A. Wittinghofer (1990). *The P-loop-a common motif in ATP- and GTP binding proteins*. Trends. Biochem. Sci **15**: 430–434.

Schäfer, G. (1992). *Meyering-Vos M. F-type or V-type? The chimeric nature of the archaebacterial ATP synthase*. Biochim. Biophys. Acta **1101**: 232-235.

Schäfer, I., M. Rössle, G. Biuković, V. Müller and G. Grüber (2006a). *Structural and functional analysis of the coupling subunit F in solution and topological arrangement of the stalk domains of the methanogenic A_1A_O ATPsynthase*. J. Bioenerg. Biomembr. **38**: 83-92.

Schäfer, G., M. Engelhard and V. Müller (1999). *Bioenergetics of the Archaea*. Microbiol. Mol. Biol. Rev. **63**: 570-620.

Schäfer, I. B., S. M. Bailer, M. G. Düser, M. Börsch, R. A. Bernal, D. Stock and G. Grüber (2006b). *Crystal Structure of the Archaeal A_1A_O ATP Synthase Subunit B from Methanosarcina mazei Gö1: Implications of Nucleotide-binding Differences in the Major A_1A_O Subunits A and B.* J. Mol. Biol. **358**: 725-740.

Scheurich, P., H. J. Schäfer and K. Dose (1979). *8-Azido-adenosine 5'-triphosphate as a photoaffinity label for bacterial F_1 ATPase*. Eur. J. Biochem. **88**: 253-257.

Senior, A. E., S. Nadanaciva and J. Weber (2000). *Rate acceleration of ATP hydrolysis by F(1)F(o)-ATP synthase*. J. Exp. Biol. **203**: 35-40.

Senior, A. E., S. Nadanaciva and J. Weber (2002). *The molecular mechanism of ATP synthesis by F_1F_O-ATP synthase*. Biochom. Biophys. Acta **1553**: 188-211.

Senior, A. E., A. Muharemagic and S. Wilke-Mounts (2006). *Assembly of the Stator in Escherichia coli ATP Synthase. Complexation of α Subunit with Other F_1 Subunits Is Prerequisite for δ Subunit Binding to the N-Terminal Region of α.* Biochemistry **45**: 15893-15902.

Shirakihara, Y., A. G. W. Leslie, J. P. Abrahams, J. E. Walker, T. Ueda, Y. Sekimoto, M. Kambara, K. Saika, Y. Kagawa and M. Yoshida (1997). *The crystal structure of the nucleotide-free α_3:β_3 subcomplex of F_1-ATPase from the thermophilic Bacillus PS3 is a symmetric trimer*. Structure **5**:825–836.

Stewart, M., H. M. Kent and A. J. McCoy (1998). *The structure of the Q69L mutant of GDP-ran shows a major conformational change in the switch II loop that accounts for its failure to bind nuclear transport factor 2 (NTF2).* J. Mol. Biol. **284**: 1517-1527.

Stock, D., C. Gibbons, I. Arechaga, A. G. W. Leslie and J. E. Walker (2000). *The rotary mechanism of ATP synthase*. Curr. Opin. Struc. Biol. **10**: 672-679.

Stocker, A., S. Keis, J. Vonck, G. M. Cook and P. Dimroth (2007). *The structural basis for unidirectional rotation of thermoalkaliphilic F_1-ATPase*. Structure **15**: 904-914.

Vagin, A. and A. Taplyakov (1997). *MOLREP: and automated program for molecular replacement*. J. Appl. Cryst **30**: 1022-1025.

Vasilyeva, E., Q. Liu, K. J. MacLeod, J. D. Baleja and M. Forgac (2000). *Cysteine Scanning Mutagenesis of the Nancatalytic Nucleotide Binding Site of the Yeast V-ATPase*. J. Biol. Chem. **275**: 255-260.

Von Ballmoos, C., A. Wiedenmann and P. Dimroth (2009). *Essentials for ATP synthesis by F_1F_0 ATP synthases*. Annu. Rev. Biochem. **78**: 649-672.

Vonck, J., K. Y. Pisa, N. Morgner, B. Brutschy and V. Müller (2009). *Three-dimensional Structure of A1A0 ATP Synthase from the Hyperthermophilic Archaeon Pyrococcus furiosus by Electron Microscopy*. J. Biol. Chem. **284**: 10110-10119.

Vonck, J., T. K. von Nidda, T. Meier, U. Matthey, D. J. Mills, W. Kühlbrandt and P. Dimroth (2002). *Molecular Architecture of the Undecameric Rotor of a Bacterial Na+-ATP Synthase*. J. Mol. Biol. **321**: 307-316.

Walker, J. E. and V. K. Dickson (2006). *The peripheral stalk of the mitochondrial ATP synthase*. Biochim. Biophys. Acta Bioenergetics **1757**: 286-296.

Walker, J. E., M. Saraste, M. J. Runswick, and N. J. Gay (1982). *Distantly related sequences in the alpha- and beta-subunits of ATP synthase, myosin, kinases and other ATP-requiring enzymes and a common nucleotide binding fold*. EMBO J. **1**: 945–951.

Weber, J. and A. E. Senior (1996). *F_1F_O-ATP synthase: development of direct optical probes of the catalytic mechanism*. Biochim. Biophys. Acta **1319**:19-58.

Weber, J., A. Muharemagic, S. Wilke-Mounts.and A. E. Senior (2003). *F1F0-ATP synthase: Binding of d subunit to a 22-residue peptide mimicking the N-terminal region of a subunit.* J. Biol. Chem. **278**: 13623–13626.

Weber, J., S. Wilke-Mounts, E. Grell and A. E. Senior (1994). *Tryptophan fluorescence provides a direct probe of nucleotide binding in the noncatalytic sites of Escherichia coli F_1-ATPase*. J. Biol. Chem. **269**:11261-11268.

Weber, J., S. Wilke-Mounts, R. S. F. Lee, E. Grell and A. E. Senior (1993). *Specific placement of tryptophan in the catalytic sites of Escherichia coli F_1-ATPase provides a direct probe of nucleotide binding: Maximal ATP hydrolysis occurs with three sites occupied*. J. Biol. Chem. **268**: 20126-20133.

Weber, J. (2006). *ATP synthase: Subunit-subunit interactions in the stator stalk*. Biochim. Biophys. Acta - Bioenergetics **1757**: 1162-1170.

Wilkens, S. and R. A. Capaldi (1998). *Electron microscopic evidence of two stalks linking the F_1 and F_O parts of the Escherichia coli ATP synthase*. Biochim. Biophys. Acta Bioenergetics **1365**: 93-97.

Wilkens, S., D. Borchardt, J. Weber and A. E. Senior (2005). *Structural Characterization of the Interaction of the δ and α Subunits of the Escherichia coli F_1F_O-ATP Synthase by NMR Spectroscopy*. Biochemistry **44**: 11786-11794.

Wilkens, S., F. W. Dahlquist, L. P. McIntosh, L. W. Donaldson and R. A. Capaldi (1995). *Structural features of the ε subunit of the Escherichia coli ATP synthase determined by NMR spectroscopy*. Nat. Struc. Mol. Biol. **2**: 961-967.

Wilkens, S., S. Dunn, J. Chandler, F. Dahlquist and R. Capaldi (1997). *Solution structure of the N-terminal domain of the delta subunit of the E. coli ATPsynthase*. Nat. Struc. Biol. **4**: 198-201.

Woese, C. R., O. Kandler and M. L. Whellis (1990). *Towards a natural system of organisms: Proposal for the domains Archaea, Bacteria and Eucarya.* Proc. Natl. Acad. Sci. USA **87**: 4576–4579.

Yokoyama, K., E. Muneyuki, T. Amano, S. Mizutani, M. Yoshida, M. Ishida and S. Ohkuma (1998). *V-ATPase of Thermus thermophilus is inactivated during ATP hydrolysis but can synthesize ATP*. J. Biol. Chem. **273**: 20504-20510.

Zhou, Y., T. M. Duncan and R. L. Cross (1997). *Subunit rotation in Escherichia coli F0F1-ATP synthase during oxidative phosphorylation.* Proc. Natl. Acad. Sci. USA **94**: 10583–10587.

Appendix

APPENDIX: A

	A_E	A_{MP}	S238A
Data collection statistics			
Wavelength (Å)	1.0	1.0	1.0
Space group	$P4_32_12$	$P4_32_12$	$P4_32_12$
Unit cell parameters (Å)			
a = b =	128.25	128.39	128.21
c =	104.68	105.02	105.83
α = β = γ (°)	90	90	90
Resolution range (Å)	30.0 - 2.47	30.0 – 2.40	30.0 – 2.40
Solvent content (%)	62.41	62.42	62.61
Number of unique reflections	31567	34762	33166
I/σ[a]	28.68 (3.98)	32.12 (4.17)	26.6 (5.32)
Completeness (%)	99.6 (99.7)	99.7 (100.0)	100 (99.9)
R merge[b] (%)	5.7 (46.4)	6.8 (45.9)	8.0 (39.0)
Multiplicity	7.0 (7.2)	14.4 (14.1)	12.2 (12.1)
Refinement statistics			
R factor[c] (%)	21.7	21.9	23.4
R free[d] (%)	25.3	24.9	28.5
Number of amino acid residues	514	521	512
Number of water molecules	310	353	267
Number of MPD molecules	3	3	3
Number of Acetate molecules	1	1	-
Number of TRIS molecules	1	1	1
Ramachandran statistics			
Most favored (%)	88.4	87.9	87.2
Additionally allowed (%)	10.5	10.1	11.6
Generously (%)	1.1	2.0	1.1
Disallowed (%)	0.0	0.0	0.0
R.M.S. deviations			
Bond lengths (Å)	0.013	0.02	0.018
Bond angles (°)	1.49	1.62	1.78
Mean atomic B values			
Protein atoms	55.32	64.47	55.88
Nucelotide	-	72.55	-
Overall	54.24	64.48	55.88
Wilson plot	55.32	59.52	55.91

[a] Values in parentheses refer to the corresponding values of the highest resolution shell (A_E – 2.56-2.47; A_{MP} – 2.49-2.40; and S238A – 2.49-2.40 Å).

[b] $R_{merge} = \Sigma\Sigma_i|I_h - I_{hi}|/\Sigma\Sigma_i I_h$, where I_h is the mean intensity for reflection h.

[c] R-factor = $\Sigma||F_O| - |F_C||/\Sigma|F_O|$, where F_O and F_C are measured and calculated structure factors, respectively.

[d] R-free = $\Sigma||F_O| - |F_C||/\Sigma|F_O|$, calculated from 5% of the reflections selected randomly and omitted during refinement.

Table A. Statistics of crystallographic data collection and refinement for the A_E, A_{MP} and S238A structures of subunit A.

APPENDIX: B

	B_{TPI}
Data collection statistics	
Wavelength (Å)	1.0
Space group	$P2_12_12_1$
Unit cell parameters (Å)	
a =	75.69
b =	96.87
c =	139.63
α = β = γ (°)	90
Resolution range (Å)	50.0 – 3.4
Solvent content (%)	45.48
Number of unique reflections	11433
I/σ[a]	8.49 (1.94)
Completeness (%)	91.0 (85.7)
R merge[b] (%)	16.7 (47.3)
Multiplicity	3.5 (2.4)
Refinement statistics	
R factor[c] (%)	24.59
R free[d] (%)	31.54
Number of amino acid residues	844
Ramachandran statistics	
Most favored (%)	84.2
Additionally allowed (%)	15.1
Generously (%)	0.7
Disallowed (%)	0.0
R.M.S. deviations	
Bond lengths (Å)	0.006
Bond angles (°)	0.997
Mean atomic B values	
Protein atoms	70.78
ATP molecule	79.23
AES molecule	73.79
Overall	72.18

[a] Values in parentheses refer to the corresponding values of the highest resolution shell.

[b] $R_{merge} = \Sigma\Sigma_i|I_h - I_{hi}|/\Sigma\Sigma_i I_h$, where I_h is the mean intensity for reflection h.

[c] R-factor $= \Sigma||F_O| - |F_C||/\Sigma|F_O|$, where F_O and F_C are measured and calculated structure factors, respectively.

[d] R-free $= \Sigma||F_O| - |F_C||/\Sigma|F_O|$, calculated from 5% of the reflections selected randomly and omitted during refinement.

Table B. Statistics of crystallographic data collection and refinement for the B_{TP} (transient-I) structure of subunit B.

Author's publications related to this study

1. **Kumar, A.**, Manimekalai, M. S. S. and Grüber, G. (2008) Structure of the nucleotide binding subunit B of the energy producer A_1A_O ATP synthase in complex with adenosine diphosphate. *Acta Cryst. D***64**, 1110–1115
   PDB: 3DSR

2. **Kumar, A.**, Manimekalai, M. S. S., Balakrishna, A. M., Hunke, C., Weigelt, S., Sewald, N. and Grüber, G. (2009) Spectroscopic and crystallographic studies of the mutant R416W give insight into the nucleotide binding traits of subunit B of the A_1A_O ATP synthase. *PROTEINS: Structure, Function and Bioinformatics* **75**, 807-819 (cover page article)
   PDBs: 3B2Q, 2RKW

3. Manimekalai, M. S. S., **Kumar, A.**, Balakrishna, A. M. and Grüber, G. **(**2009) A second transient position of ATP on its trail to the nucleotide-binding site of subunit B of the motor protein A_1A_O ATP synthase. *J. Struct. Biol.* **166**, 39-45
   Pdb: 3EIU

4. **Kumar, A.**, Manimekalai, M. S. S., Balakrishna, A. M., Jeyakanthan J. and Grüber, G. Nucleotide binding states of subunit A of A-ATP synthase and the implication of P-loop switch in evolution. *J. Mol. Biol.*, **396**, 301-320.
   PDBs: 3I72, 3I4L, 3I73, 3IKJ

5. **Kumar, A.**, Jeyakanthan J. and Grüber, G. Understanding the role of conserved P-loop residues Lys240 and Thr241 of subunit A of the A_1A_O ATP synthase using isothermal titration calorimetry. (*in prep.*)

Conference publications

1. Manimekalai, M. S. S., **Kumar, A.**, Balakrishna, A. M., and Grüber, G. (2009) Structural characterization of the nucleotide binding ability of subunit A of the A_1A_O ATP synthase. *Acta Cryst. A* **65**, s 169

2. Grüber, G., Manimekalai, M. S. S., **Kumar, A.**, Balakrishna, A. M., and Gayen, S. (2009) Structural insight into the motor protein A_1A_O ATP synthase and implications in coupling events. *Acta Cryst. A* **65**, s 36

Invited talks

1. 2nd Asia-Oceania Forum for Synchrotron Radiation Research (2nd AOFSRR), (NSRRC), Hsinchu, Taiwan, 1st-2nd Nov. 2007
   Title: "High resolution structures of the empty and the nucleotide intermediate state of the subunit B mutant R416W of the A_1A_O ATP synthase"

2. 3rd Korea-Singapore International Conference on Bioscience & Biotechnology 2008 on 15th-16th Dec. 2008
   Title: "How ATP/ADP enters into the nucleotide-binding pocket of subunit B of the A_1A_O ATP synthase"

Posters

1. Joint Third AOHUPO and Fourth Structural Biology and Functional Genomics Conference, NUS, Singapore from 4th-7th Dec. 2006
   Title: "Insight into the binding mode of subunit B of the methanogenic A_1A_O ATP synthase"

2. 2nd Asia-Oceania Forum for Synchrotron Radiation Research (2nd AOFSRR), (NSRRC), Hsinchu, Taiwan, 1st-2nd Nov. 2007
   Title: "High resolution structures of the empty and the nucleotide intermediate state of the subunit B mutant R416W of the A_1A_O ATP synthase"

3. Joint 5th Structural Biology and Functional Genomics and 1st Biological Physics International Conference, NUS, Singapore from 9th-11th Dec. 2008
   Title: "Structure of the nucleotide binding subunit B of the A_1A_O ATP synthase in complex with ADP"

Awards

Received "Young scientist presentation certificate" from the Director of National Synchrotron Radiation Research Center (NSRRC) during 2nd Asia-Oceania Forum for Synchrotron Radiation Research, held during 1st-2nd Nov 2007. A financial support of USD 400/- was awarded by the organizing committee.